max planck institute of biochemistry

Technische Universität München

Physiological Response of Human Cells to Aneuploidy

Transcriptome Studies and Cellular Assays

By

Milena Dürrbaum

SUBMITTED IN FULFILLMENT OF THE REQUIREMENTS FOR THE DEGREE OF MASTER OF SCIENCE

Munich, 2012/10/16

Examined by

Prof. Dr. Ramon Angel Torres Ruiz
Chair of Genetic, TUM

Prof. Dr. Iris Antes
Theoretical Chemical Biology and Protein Modelling Group, TUM

Supervisor:

Zuzana Storchova, PhD
Maintenance of Genome Stability
Max Planck Institute of Biochemistry

Table of Content

Abstract

Aneuploidy, a karyotype deviating from a whole multiple of the haploid chromosome complement, is a common genetic variation in cancer cells. This unbalanced genome content evidently alters the cell physiology. The mechanisms by which aneuploidy promotes tumorigenesis and cancer development are poorly understood. To elucidate changes in response to aneuploidy, transcriptome analysis helps to survey gene expression changes on a large- scale basis.

In my master thesis I developed and conducted bioinformatics analysis of gene expression microarray data to investigate a transcriptional response to aneuploidy. In order to find a common pattern in the deregulated gene expression, I analyzed data from defined whole chromosome aneuploid cell lines of different cell types, as well as data from post- tetraploid cell lines with complex aneuploidy. I found a consistent pattern of pathways deregulated in their expression independent of the cell line and the type of aneuploidy. Annotated pathways for DNA and RNA metabolism were globally down- regulated. Whereas lysosome, membrane, Golgi apparatus and ER related pathways were up- regulated. I could show that these responses to aneuploidy do not correlate with the transcriptional response to inflammatory or nutrition stress. Further, investigations on single gene entries identified few genes commonly deregulated in aneuploid cell lines and therefore present a potential marker for aneuploidy.

Despite the remarkable similarities between the different aneuploid cell lines, I observed differences between whole chromosome aneuploid cell lines and post- tetraploid cell lines. In particular, cellular assays indicated that post- tetraploid cells display no enhanced level of autophagy as it has been reported for whole chromosome aneuploid cells. Additionally, I show that no accumulation of lipid deposits and altered mitochondria morphology can be observed in post- tetraploid cell lines. Moreover, I could confirm that although known to be chromosomally instable, these cells don´t show enhanced DNA damage. Finally, the transcriptome analysis revealed an interesting deregulation pattern for genes associated with the p53 dependent cell cycle arrest and apoptosis pathway. I found the expression of Mdm2, inhibiting p53 tumor suppressor function, but also p53 target genes up- regulated. These findings provide a first possible link how post- tetraploid attenuate the p53 pathway, which is the suggested cause for the proliferation defects commonly found in whole chromosome aneuploid cells.

1. Introduction

1.1. Aneuploidy is a Common Feature of Cancer

Cancer has become a major health challenge within the last century (World Health Statistics 2012). In addition to ageing of the population this can also be attributable to changes in environmental factors (Jemal et al. 2011). In fact, the world health organization reported 2012 cancer as the leading cause of death in economically developed countries and the second cause of death worldwide. Cancer, characterized by deregulated cell growth, is a large group of different malignant neoplasias affecting various parts of the human body. Despite diversity, one of the common features of cancer cells is the occurrence of aneuploidy (Rajagopalan and Lengauer 2004). Studies have shown that more than 90% of solid tumors and 75% of blood cancers are aneuploid (Weaver and Cleveland 2006; Albertson et al. 2003).

Aneuploidy is an unbalanced genomic state in which the karyotype deviates from a whole multiple number of the haploid chromosome complement (Storchova, ed. 2012). The gain or loss of single chromosomes due to chromosome segregation errors is referred to as a “whole chromosome aneuploidy", whereas rearrangements of chromosomal parts is described as “segmental aneuploidy”. Combination of both aneuploidy types is known as “complex” or “composite” aneuploidy. In contrast, polyploidy describes a state with whole multiples of a chromosome set which presents a balanced genomic state.

Although polyploidy, in particular tetraploidy, has been described for early stages of cancers, cancer cells rather harbor complex aneuploid karyotypes (Ganem et al. 2007). This complexity and variability of cancer genome is illustrated by the 61,846 (August 15, 2012) cases listed in the Mitelman database of chromosome aberrations and gene fusions in cancer (Mitelman et al. 2012). Interestingly, evolution of cancer cells appears to correlate with increase and complexity of aneuploidy (Albertson et al. 2003). Therefore, to investigate aneuploidy as a hallmark of cancer and its role in tumorigenesis and cancer progression is of a great interest.

1.2. Causes and Consequences of Aneuploidy

1.2.1. The Causes of Aneuploidy

Aneuploid cells can originate from improper chromosome segregation prior to cell division. First steps necessary for chromosome segregation occur already during S-phase where sister chromatids are linked to each other via the cohesin complex (Alberts 2002). In Prophase the microtubule nucleating from the microtubule organizing centers (centrosomes) attach to the sister chromatids, thus forming mitotic spindle. That is, microtubules emanating from opposite centrosomes attach to each sister kinetochore, which forms at the centromere of each chromosome. The correct kinetochore attachment and tension at the microtubule-kinetochore interface is monitored by the spindle assembly checkpoint

machinery (SAC). SAC delays the onset of anaphase until all chromosomes are correctly bi-orientated on the microtubule spindle. When SAC inhibition is relieved, the anaphase- promoting complex (APC) is activated by the subunit Cdc20 leading to ubiquitinylation of securin. Ubiquitin dependent degradation of securin activates the protease separase. Cleavage of the cohesin complexes by separase releases the linkage between the sister chromatids and leads to their immediate separation to the opposite spindle poles.

Mutations in genes associated with the chromosome segregation process and checkpoint pathways have been associated with increasing rate of gain and loss of chromosomes (Holland and Cleveland 2009; Gordon et al. 2012; Storchova, ed. 2012). For instance, mutations in the SAC proteins can compromise the SAC function and give rise to aneuploid daughter cells (Kops et al. 2005; Thompson et al. 2010). Similarly, a hyperactive APC can initiate chromosome segregation in presence of incorrectly chromosome attachment to the mitotic spindle (Siegel and Amon 2012). In addition, defective cohesion between the sister chromatids or their premature loss has been shown to promote aneuploidy. In aneuploid human colorectal cancers mutations in genes contributing to sister chromatid cohesion were identified (Barber et al. 2008). The importance of the cohesin function was also demonstrated experimentally, as inactivation of STAG2, which encodes for a cohesin subunit, in human cell lines lead to an increased aneuploidy (Solomon et al. 2011). Consistently, the overexpression of separase was shown to induce aneuploidy (Zhang et al. 2008). One of the major sources of aneuploidy results from merotelic attachment, in which a single kinetochore attaches to microtubules from both spindle poles (Cimini et al. 2001). Uncorrected merotelic attachment can result in lagging chromosomes and thus promotes aneuploidy. The condition of supernumary centrosomes is known to enhance the frequency of merotelic attachments and chromosome segregation errors (Ganem et al. 2009). Multiple centrosomes can lead to multipolar cell division, but more often observed is the clustering of the extra centrosomes (Gordon et al. 2012). Clustered centrosomes build a pseudo- bipolar spindle which enables normal cell division but also increases the frequency of merotelic attachments.

Complex aneuploidy results from various different types of segmental rearrangements resulting in deletion, insertion, inversion, duplication and translocation of chromosome parts and sequences. Copy number variations (CNV) of genomic elements, with a size greater than one kilobase, are often described in a variety of diseases including cancer (Colnaghi et al. 2011). CNV results from non-allelic homologous recombination between low copy number repeats upon DNA breakage. Another mechanism involved in CNV is the non –homologous end-joining (NHEJ) DNA double strand break repair pathway, which facilitates non- recurrent rearrangements variable in their size and breakpoints (Stankiewicz and Lupski 2010). More complex chromosomal rearrangements have been described involving mechanisms like the fork stalling template- switching mechanism, the microhomology mediated break induced repair mechanism and the breakage- fusion- bridge cycle (Colnaghi et al. 2011). These various mechanisms act on primary DNA damage, which can occur at

random sites due to nonspecific DNA damage, at specific hot spots or fragile sites (Alberts 2002). Segmental rearrangements can additionally occur on lagging chromosomes. Recently, it has been described that lagging chromosomes can be trapped during cytokinesis in the cleavage furrow, which results in damage of the lagging chromosomes and both daughter cells inherit parts of the chromosome (Janssen et al. 2011). Furthermore, lagging chromosomes might form micronuclei (Fenech et al. 2010). It has been shown that DNA replication in micronuclei is often defective due to compromised recruitment of DNA repair machinery components (Crasta et al. 2012). Reassembling of the micronuclei chromosomes with the chromosomes in the main nuclei can therefore lead to structural rearrangement and give rise to segmental aneuploid daughter cells after cell division. Notably, the above described mechanisms lead to a certain aneuploid state of the genome. This genomic state can be stable, but if the described genomic rearrangements persist above the basal rate, these cells are chromosomal instable. Chromosomal instability describes the rate of karyotype changes. CIN may give rise to aneuploid cells, but not all aneuploid cells exhibit CIN above the basal rate of genomic rearrangements (Gordon et al. 2012; Holland and Cleveland 2012).

1.2.2. Consequences of Aneuploidy

As a consequence of aneuploidy, the cell physiology is evidently altered. One of the major questions in studying the altered cell physiology is whether these effects are due to their specific copy number changes. Thus, it is interesting to assess whether aneuploid cells exhibit dosage compensation on transcriptional or translational level to counterbalance the gene copy number imbalances arising from aneuploidy. Several studies revealed a proportional correlation between gene copy number and the relative gene expression levels. A genome- wide microarray mRNA expression analysis of human fetal trisomy 21 cases provided evidence for mRNA expression proportional to DNA copy number changes in aneuploid cells (Mao et al. 2003). Similar results were published for model trisomic mouse embryonic fibroblasts (MEFs) and just recently in model human trisomic and tetrasomic cell lines (Williams et al. 2008; Stingele et al. 2012). Whether the genome proportional expression is also translated into a general change on proteome level is highly discussed. Proteome studies on human trisomic and tetrasomic cell lines provide evidence for dosage compensation on protein level, specifically in a stoichiometry manner for protein kinases and subunits of protein complexes (Stingele et al. 2012). As in the same study an activation of the autophagic pathway was shown, the correction of the protein imbalance in aneuploid cells was suggested via autophagy. The importance of autophagy was first indicated by published data on MEFs, where increased autophagy and occurrence of proteotoxic stress was shown (Tang et al. 2011). Evidence for proteotoxic stress was already provided before in yeast studies (Torres et al. 2007). Increased proteotoxic stress as a result of increased protein load on the cells protein quality control and proteolytic pathways could also explain the observed higher sensitivity of aneuploid cells towards drugs negatively affecting protein synthesis, folding and degradation.

Another phenotype frequently observed in aneuploid cells is elevated metabolic stress and energy demand (Williams et al. 2008; Li et al. 2010). The observed upregulation of metabolic pathway proteins in proteome studies of human aneuploid cell lines might be in accordance with these results (Stingele et al. 2012). The higher energy demand of aneuploid cells might also possibly lead to activation of autophagy in aneuploid cell lines, as nutrient deprivation is a known inducer of this pathway (Altman and Rathmell 2012).

A general frequently confirmed phenotype of aneuploidy is the growth impairment of aneuploid cells (Torres et al. 2007; Williams et al. 2008; Stingele et al. 2012, for review see: Siegel and Amon 2012; Gordon et al. 2012). One proposed mechanism leading to decreased proliferation is a metabolic and energy stress dependent ATM and p53 activation (Guo et al. 2010; Fang and Zhang 2011). Therein, the aneuploid stress responses trigger the production of reactive oxygen species (ROS) above a certain threshold, which in turn limits via ATM/ p53 activation the proliferation of aneuploid cells. Another mechanism independent of ROS, but p53 dependent that compromises proliferation of aneuploid cells in response to CIN is suggested (Thompson and Compton 2010). This is chromosome missegregation was observed to lead to p53 accumulation and growth impairment in diploid cells. In subsequent experiments it was shown, that p53 inhibition permits the propagation of the aneuploid cells resulted from chromosome segregation errors. In accordance, a weakened SAC function which also results in CIN was shown to cause a p53 response (Li et al. 2010). Interestingly, studies of trisomic MEFs imply that aneuploidy seems to interfere with proliferation also in a p53 independent manner (Tang et al. 2011). Although trisomic MEFs showed a growth defect, elevated levels of p53 were not detected. Inactivation of p53 in those cells, could not suppress the proliferation defect.

Aneuploidy has detrimental effects on organism development and it is the leading cause of spontaneous miscarriage and mental retardation in humans (Brown 2008; Hassold et al. 2007). Only autosomal trisomy of chromosome 13 (Edwards syndrome), 18 (Pateu syndrome) and 21 (Down syndrome) are viable (Hassold et al. 1996). But as these trisomies result in severe developmental defects and reduced life expectancy, only Down syndrome patients survive till adulthood. Aneuploidies of sex chromosomes are better tolerated, probably because few encoded genes on the Y chromosome and dosage compensation of the X chromosome (Prestel et al. 2010). A rare heritable syndrome, the mosaic variegated aneuploidy (MVA), is the result of loss of functions mutations in SAC components, which leads to increased random cellular aneuploidy (Hanks et al. 2004). Besides mental retardation and developmental defects, MVA patients show a predisposition to cancer, demonstrating the severe effects of aneuploidy in humans and its causative relation to cancer development (Hanks and Rahman 2005).

However, aneuploidy affects cellular growth and metabolism not only adversely. Some tissues in humans are naturally aneuploid. The percentage of aneuploid cerebral neuroblasts decline during development but seem to be still functional in mammalian brain (Rehen et al. 2001; Kingsbury et al.

2005). The differentiated neurons with single chromosome abnormalities don´t undergo any further cell division, thus it is suggested that the proliferation defects have a small impact on cell function (Pfau and Amon 2012). Also in the liver aneuploidy occurs as a response to ageing, regenerative challenge and adaption to toxic stress (Gupta 2000). Failure of cytokinesis leads to polyploidy hepatocytes which suggest an adaption to stresses, but the potential aneuploid progenies are discussed as a sign of less fitter aged cells (Pfau and Amon 2012).

To date the effects of aneuploidy on cell physiology have been well described on the phenotypic level. To further elucidate the molecular function and pathways of the general response of cells to aneuploidy is important to investigate its role in diseases and therefore of great research interest.

1.3. Aneuploidy and Tumorigenesis

Studies of the link between aneuploidy and tumorigenesis, manifested in the frequent occurrence of aneuploid cells in cancers, have revealed a complex interaction between the aneuploid state, the rate of karyotypic changes and tumorigenesis. Although aneuploid cells are commonly found in tumors and cancer cells exhibit many characteristics also described in aneuploids, the consequences of aneuploidy in cancer development are often context- dependent (Weaver et al. 2007; Weaver and Cleveland 2007). Prominent examples of aneuploidy serving as tumor suppressor are Down syndrome patients, who show besides an increased risk for leukemia a remarkable decrease in solid tumors (Satge et al. 1998). Tumor suppressor functions of aneuploidy have been also described in mouse models with reduced level of centromere protein E (CenpE) and mice trisomic for 50% of orthologous genes on chromosome 21 (Weaver et al. 2007; Sussan et al. 2008; Chen et al. 2012).

However, most of the extensively studied mouse models support the hypothesis that aneuploidy rather facilitates tumor formation (Ricke et al. 2008; Holland and Cleveland 2009).Further evidence is provided by the observation that patients with mosaic variegated aneuploidy (MVA), a syndrome resulted from mutation in the key SAC component BubR1, show a predisposition to cancer (Plaja et al. 2001; Callier et al. 2005). But SAC gene mutations are relatively rare in tumors and the majority of chromosomally unstable (CIN) cancer cells maintain robust SAC (Tighe et al. 2001), suggesting aneuploidy *per se* as a trigger of tumorigenesis without mitotic gene mutation requirement as a prerequisite for tumorigenesis. The potential route to tumor formation might be the genetic and protein imbalances caused by aneuploidy (Pfau and Amon 2012). Moreover, aneuploid phenotypes compromise proliferation in a p53-dependent manner (Thompson and Compton 2010), which presents the ATM/p53 pathway as a major limiting factor for tumorigenesis (Li et al. 2010). Genetic alterations in the p53 pathway might help to overcome the adverse effects of aneuploidy and benefit tumorigenesis. Likewise, the loss of other tumor suppressor genes, such as components of the retinoblastoma (Rb) tumor suppressor is proposed to drive aneuploidy-induced tumorigenesis upon Mad2 upregulation (Schvartzman et al. 2011). Finally, CIN may represent an adaptation to persistent

chromosome missegregation enabling the survival of aneuploid karyotypes, which in turn can facilitate tumorigenesis in aneuploid cells (McClelland et al. 2009). Several studies in mouse models observed elevated tumorigenesis through CIN, suggesting CIN as the essential driver of tumorigenesis (Baker et al. 2009; Dai et al. 2004; Iwanaga et al. 2007; Li et al. 2010; Sotillo et al. 2010). Under selective pressure karyotype diversity promotes phenotypic diversity and thus increase tumor fitness under adaptation to new environment conditions (Pfau and Amon 2012; Holland and Cleveland 2012). Together with the notion that aneuploidy itself promotes CIN (Holland and Cleveland 2012), aneuploidy, CIN and tumorigenic mutations may constitute to multiple routes and positive feedback loops driving tumorigenesis and cancer development. Thus, CIN, driving the variability and evolutionary potential of cells in different cancer microenvironments, seems to be the important factor in context of the role of aneuploidy in tumor development. Therefore, the CIN and the aneuploid cell physiology are attractive therapeutic targets. But in order to effectively target the functions and pathways promoting tumorigenesis, it is necessary to further elucidate the underlying molecular mechanisms.

The key aim of my master thesis is to identify the global response to aneuploidy. As transcriptome analysis allows to assess gene expression on a large scale basis, I analyzed microarray data of aneuploid cell lines originated via two distinct mechanisms. To this end, defined aneuploid cell lines with a known chromosome composition generated by single chromosome transfer served as a model system for investigations of whole chromosome aneuploidy. Further, aneuploid cells lines generated from offspring of tetraploid cells (so-called post-tetraploid cells) were used to assess the response to complex aneuploidy, which is observed in many cancer cells. Besides a global transcriptional response to aneuploidy, we aimed to investigate the cell physiology of the whole chromosome aneuploid and post-tetraploid cell lines. It has been proposed that tetraploidy, frequently found in early cancer stages, is an intermediate to the complex aneuploid cancer cells (Ganem et al. 2007; Storchova and Kuffer 2008). CIN mechanisms in tetraploid cells may lead to an adaption to the unstable karyotype and give rise to complex aneuploid cancer cells. Since post-tetraploid cells originate from unstable tetraploid cells, these cell lines model this hypothesis. Investigations in form of cellular assays could help to understand the physiology of these cells and moreover in which means they tolerate the complex aneuploid genomic state. Moreover, transcriptome studies in post- tetraploid cells might reveal specific altered expression of genes which can be linked to the adaptation of post-tetraploid cells to the unstable karyotype.

1.4. Transcriptome Analysis

1.4.1. Gene Expression Microarrays

Since the first simultaneously analyzed gene expression was published by Patrick O. Brown in 1995, microarray technology has developed into a powerful tool to study global gene expression

(Schena et al. 1995). Compared to standard techniques like Northern and Southern blot, the major technical advance is the ability to examine the expression of multiple genes in one experiment and nowadays even a whole genome (Emmert-Streib and Dehmer 2008; Hofmann 2006; Schena 1999). To measure the gene expression by using the microarray technology takes advantage from the hybridization of a specific mRNA to a complementary sequence of a cDNA or an oligonucleotide spotted on a glass slide. The complementary cDNA or oligonucleotides, called probes, are cross- linked on a surface. A RNA sample isolated from cells or tissues is labeled with fluorescent dyes. Once the sample reacts with the microarray, washing steps are followed by the detection of the fluorescent signal.

Microarrays differ in their platforms and probes spotted onto a solid support (Wang et al. 2012). Traditional microarrays utilized membranes, mostly nylon membranes. Nowadays, solid surfaces such as glass slides are more common. The advantages of this strategy are the covalent attachments of the samples, longer durability and lower background noise (Hofmann 2006). Further, the microarrays are classified according to the length of the probes, the manufacturing method and the number of samples that can be simultaneously profiled on the array (Tarca et al. 2006). Conventionally, microarrays are spotted using the PCR amplified cDNA targets chosen from a cDNA library of interest. cDNA probes are less sensitive to single base pair changes compared to oligonucleotides, which on one hand leads to a higher robustness to small changes but on the other hand it presents a detection limit for small changes. A clear disadvantage is the high cross reactivity for example within one gene family (Mah et al. 2004). Therefore, smaller oligonucleotide probes allow a much more sensitive and specific detection of gene expression.

Microarrays are conducted in a single- channel or multiple- channel experiments (Wang et al. 2012). Whereas in a single- channel analysis, one single sample is labeled with one fluorescent dye and hybridized with the microarray, in a two- channel analysis two samples are labeled with different dyes and hybridized on a single microarray chip. Two dye experiments results in a ratio of the expression between the two samples, usually experimental sample versus control sample. The single channel experiment data represents the absolute expression ratio of a specific gene.

The data used for my thesis were obtained from single channel oligonucleotide microarrays from Agilent technology. Agilent oligonucleotide microarrays use 60-mer oligonucleotides in contrast to the 25-mer oligonucleotides from Affymetrix. Whereas Affymetrix chips are more sensitive to sequence mismatches, Agilent microarrays provide a lager hybridization sequence compared to smaller oligonucleotide microarrays and is therefore more tolerant (Hofmann 2006). On the other hand, longer oligonucleotides are still more specific than cDNAs. Hence, Agilent oligonucleotide microarrays are described as a good compromise of specificity and sensitivity.

1.4.2. Microarray Preprocessing and Normalization

Preprocessing and normalization of microarray data is a crucial part of microarray experiments as it allows to separate meaningful biological variances from random errors and experimental bias (Kreil and Russell 2005, Stafford and Brun 2007; Quackenbush 2002; Tarca et al. 2006). The selection of an appropriate normalization method has a tremendous effect on precision, accuracy and correlation of the data. Although there are a large number of methods described in the literature, it is not trivial to choose the best method. Several variables starting with the experimental design, the microarray type, the hybridization method and importantly the biological problem which is examined has to be considered.

Prior to normalization, the signal intensities are usually preprocessed to enhance meaningful data characteristics and prepare the data for further analysis (Tarca et al. 2006; Duggan et al. 1999). Background correction of the overall signals adjusts for non-specific hybridization signals (Korn et al. 2004; Tarca et al. 2006). For estimation of the background signal, several methods are described. The direct vicinity of the probe or for high-density arrays, the intensity level of mismatch control probes can provide information for the non-specific hybridization signal, which has to be subtracted from the raw intensity signal. After background subtraction, the signals are often log transformed (Quackenbush 2002; Tarca et al. 2006; Kreil and Russell 2005). Raw intensity signals typically span a range from 0 to ∞ with an expression ratio for downregulation from 0 to 1 and for upregulation from 1 to ∞. As this distribution doesn´t treat up- and down- regulated signals equally, a log2 transformation produces a fair distribution with symmetrically log2 ratios with a continuous spectrum of signals (Quackenbush 2002). A further advantage of the log2 transformation is decoupling the random error from the actual signal intensity (Kreil and Russell 2005; Long 2001). For microarray, an increase in variances with increasing signal intensities can be observed which results in a multiplicative error. A log2 transformation of the signals turns the multiplicative error in an additive error.

In every microarray experiment, various experimental and systematic variations can occur (Yang et al. 2002; Stafford and Brun 2007; Bolstad et al. 2003). Thus, the normalization is performed to minimize the effect of variation on the real biological differences in gene expressions within array. A widely described source of systematic variation is a dye bias resulting from a consistent difference between two dyes in two-color microarray (Margaritis et al. 2009). As in this thesis only data from one-color microarray experiments were analyzed, dye bias can be neglected. But gene- or probe specific biases have been also described for one-channel microarray experiments (Hekstra et al. 2003; Schuster et al. 2007; Naef and Magnasco 2003). However, it seems to be difficult to account for these specific platform and experimental design biases by conventional normalization methods.

Two prominent examples for technical intra- array variations are known as spatial bias and intensity bias (Tarca et al. 2006; Quackenbush 2002; Bolstad et al. 2003). Spatial bias describes intensity differences due to the location of the probes on the array. Intensity bias presents variations in overall hybridization efficiency, washing stringency, printing of the array and non-linear interaction of probes on the array (Kreil and Russell 2005). These sources for experimental bias can be assessed

by quality control of internal hybridization controls for which the resulting intensity signal is known (Xiao et al. 2006). Most of the normalization methods correcting the data for spatial and intensity bias are based on loess or lowess method (Cleveland 1979; Cleveland and Devlin 1988). The algorithm detects systematic deviations in a ratio-intensity plot and normalizes the detected intensities for each hybridization by local weighted linear regression (van Iterson et al. 2012; Quackenbush 2002).

Expression levels observed in a microarray experiment are often compared to expression levels of other experiments. In multiple array or slide comparisons the spread of the intensity log ratios often differs. It is important to normalize for the inter- array and slide differences in variances and average relative expression levels in order to determine the biological relevant differences (Stafford and Brun 2007; Yang et al. 2002). Global normalization methods center the distribution of signal intensities to the same value by rescaling with a constant factor (Yang et al. 2002; Kreil and Russell 2005; Stafford and Brun 2007; Quackenbush 2002). For instance, median subtraction of all signal intensities of an array from each probe signal intensity is a commonly applied global normalization method (Upender et al. 2004; Quintana 2004). Quantile normalization is often applied to normalize the data in a global manner for different signal distributions (Bolstad et al. 2003). However, global normalization methods underlie the critical assumption that the true biological variance in the sample is small compared to the set of invariant genes in the sample. Hence, the median signal intensity should be influenced largely by invariant signal intensities across the different arrays (Kreil and Russell 2005). To test whether this criteria is met, the differences between the arrays and slides have to be assessed before normalization and comparison. In addition to classical global normalization, a large number of sophisticated algorithms have been published during the last years (Cheadle et al. 2003; van Iterson et al. 2012). Importantly, the applied normalization method has to be chosen carefully, as there is also the possibility to overfit the data. If the inter- and intra- array differences are substantially low, the gain of normalizing the data would be lost by introducing artificial variability (Yang et al. 2002; Cheadle et al. 2003).

1.4.3. Gene and Pathway Analysis on Microarray Expression Data

Identification of differentially expressed genes compared to a control conditions helps to interpret the biological meaning provided by the microarray experimental data. The log2 transformed ratios of a condition compared to the control conditions presents the log2 fold change in the expression of a specific gene (Quackenbush 2002). Differential expressed genes can be simply detected according to the fold change in expression. The most extensively used criterion is to simply choose a threshold fold change that defines the differentially expressed genes (Hofmann 2006). However, observed differences in expression can occur just by chance (Draghici 2002; Nadon and Shoemaker 2002; Sebastiani et al. 2003). Statistical hypothesis testing is therefore important for selection of differentially expressed genes. In a classical statistical testing approach, Students t- test is performed to calculate a significance level, the p- value, for each gene. Other statistical models including

ANOVA or linear regression models consider the variability between replicate microarray data. By testing each gene expression against its null hypothesis the problem of multiple testing arises. With the increasing number of hypothesis tested the number of false positives increases dramatically and small p-values can result by chance. Therefore, there is a number of procedures for correcting for multiple comparisons available (Farcomeni 2008; Hofmann 2006). One of the approaches to account for multiplicity is calculation of the false discovery rate (Benjamini and Hochberg 1995). The false discovery rate describes the expected proportion of false positives among the differentially expressed genes in the statistical testing.

Filtering the microarray data for a specific fold change and/ or significance results in a large list of differentially expressed genes involved in the studied biological conditions. One method to incorporate biological knowledge in those lists is a gene set enrichment analysis (Irizarry et al. 2009). Gene sets are a group of genes that form a group according to their function, cellular localization or involvement in a pathway. The biological information on each gene entry is organized in annotations, which are defined in gene annotation databases. Gene annotations are most commonly provided by the Gene Ontology project, which presents a database with structured, controlled vocabularies and classifications for molecular domains, genes and gene products (Gene Ontology Consortium 2004). Furthermore, the Kyoto Encyclopedia of Genes and Genomes (KEGG) is a useful knowledge base for systematic analysis of gene functions (Ogata et al. 1999). Enrichment analysis assess whether genes with a specific annotations are present in the filtered gene list in a higher percentage than in the normal gene population e.g. in the human genome. This can be also measured with statistical methods like X^2 or Fisher´s exact test. A useful tool for functional analysis of large gene list is the database for annotation, visualization and integrated discovery (DAVID) (Dennis, JR et al. 2003). Pathway enrichment as it is conducted with Perseus (1.2.6.16) software as part of the MaxQuant Software Package (Cox and Mann 2008) goes one step further than the gene enrichment analysis. The algorithm summarizes the same annotation terms with their enrichment factor and calculates a score for the overall deregulation of that annotation, thus providing a quantitative estimate of the level of pathway changes.

The investigation of the transcriptional response to aneuploidy in human cell lines will help to further understand the cause of the aneuploidy- induced phenotypes and the role of aneuploidy in tumorigenesis. Especially, the comparison of the transcriptome from different aneuploid cell types might be useful because it might reveal a more global response to aneuploidy.

2. Materials and Methods

2.1. Materials and Equipment

2.1.1. Chemicals

The following chemicals were used for experiments and purchased from the companies indicated. 4',6-diamidino-2-phenylindole, DAPI (Roth, Karlsruhe, Germany); β-Mercaptoethanol (Merck Biosciences, Darmstadt, Germany); Acetic acid (Sigma-Aldrich, Taufkirchen, Germany); Acrylamide ,30% w/v (SERVA Electrophoresis, Heidelberg, Germany); Ammoniumpersulfate, APS (Merck Biosciences, Darmstadt, Germany); Bafilomycin A1 (Sigma-Aldrich, Taufkirchen, Germany); Bromphenol blue (Merck, Biosciences, Darmstadt, Germany); Bovine serum albumine, BSA (Sigma-Aldrich, Taufkirchen, Germany); Dimethylsulfoxide, DMSO (SERVA Electrophoresis, Heidelberg, Germany); DMEM + GlutaMAX^{TM}-I (Invitrogen, Karlsruhe, Germany); Ethylene glycol tetraacetic acid**,** EGTA (Biomol); Ethanol (Sigma-Aldrich, Taufkirchen, Germany); Fetal bovine serum, FBS (Invitrogen, Karlsruhe, Germany); Formaldehyde (Applichem, Darmstadt, Germany); Formamide (Merck Biosciences, Darmstadt, Germany); Glycerol (Sigma-Aldrich, Taufkirchen, Germany); HCl (Merck Biosciences, Darmstadt, Germany); Isopropanol (Sigma-Aldrich, Taufkirchen, Germany); KCl (Roth, Karlsruhe, Germany); KH_2PO_4 (Merck Biosciences, Darmstadt, Germany); Methanol (Merck Biosciences, Darmstadt, Germany); $MgCl_2$ (Merck Biosciences, Darmstadt, Germany); NaCl (VWR); NaF (Sigma- Aldrich, Taufkirchen, Germany); Na_4HPO_4 (Merck Biosciences, Darmstadt, Germany); $Na_4P_2O_7$ (Sigma- Aldrich, Taufkirchen, Germany); N,N,N'-Tertramethylethylene diamine, TEMED (SERVA Electrophoresis, Heidelberg, Germany);NP-40 (Sigma-Aldrich, Taufkirchen, Germany); Opti-MEM I + GlutaMAX^{TM}-I (Invitrogen, Karlsruhe, Germany); Penicillin/ Steptomycin, Pen-Strep (PAA, Pasching, Austria); Phosphatase inhibitor (Roche Diagnostics, Mannheim, Germany); Polyvinylidene fluoride membrane, PVDF (Roche, Mannheim, Germany); Protein Assay (Bio-Rad Laboratories, Munich, Germany); Sodium azide (Merck Biosciences, Darmstadt, Germany); Sodium dodecyl sulfate, SDS (SERVA Electrophoresis, Heidelberg, Germany); tris-(hydroxymethyl)-aminomethane, TRIS (Sigma- Aldrich, Taufkirchen, Germany); Trisodium citrate (Sigma-Aldrich, Taufkirchen, Germany); Triton-X-100 (Roth, Karlsruhe, Germany); Trypsin-EDTA (PAA, Pasching, Austria); Tween20 (Applichem, Darmstadt, Germany); ECLplus™ kit proteins (GE Healthcare, Munich, Germany)

2.1.2. Buffers and Solutions

*Lower running gel (15%) pH 8.8:*7.5 ml 30% (w/v) Acrylamide; 3.75 ml Lower SDS- buffer pH 8.8; 3.75 ml H_2O; 150 µl APS; 15 µl TEMED

Upper stacking gel (7.5%) pH 6.8: 1.25 ml 30% (w/v) Acrylamide; 1.25 ml Upper SDS- buffer pH 6.8; 2.5 ml H_2O; 50 µl APS

Lower SDS buffer pH 8.8: 1.5 M Tris-HCl; 0.4% (w/v) SDS

Upper SDS buffer pH 6.8: 0.5 M Tris- HCl; 0.4% (w/v) SDS

RIPA buffer: 10% IPEGAL (NP-40); 10% Natriumdeoxycholate; 5 M NaCl; 0,5M EDTA; 1 M Tris, pH 7,5

*PTEMF fixation solution:*0.2% Triton X-100; 20mM Pipes pH 6.8; 1mM $MgCl_2$; 10 M EGTA; PBS(T), pH 7.5; 137 mM NaCl; 2.7 mM KCl; 10 mM Na4HPO4; 2.0 mM KH2PO4; (0.1% Tween-20)

2.1.3. Antibodies

Primary and secondary antibodies were purchased from the companies listed in Table 1.

Table 1: List of primary and secondary antibodies use for experiments.

Antigen	Cat. No.	Host	Application	Company/reference
gamma H2A.X	ab2893	Rabbit	IF 1:1000	Abcam, Cambridge, UK
PCNA	16d10	Rat	IF 1:3000	Chromotek, Planegg, Germany
RPA	Ab16850	Mouse	IF 1:200	Abcam, Cambridge, UK
LSM4		Chicken	IF 1:400	
Ubiquitin P4D1	3936	Mouse	WB 1:1000	Cell Signalling, Danvers, USA
LC3	M115-3	Mouse	WB	MBL/ Biozol, Eching, Germany
p62	610832	Mouse	WB 1:1000	BD Biosciences, Heidelberg, Germany
p62 (C-terminal)	GP62-C	Guinea pig	IF 1:1000	Progen, Heidelberg, Germany
α-Actinin	SC_17829	Mouse	WB 1:1000	Santa Cruz Biotechnology ,Heidelberg, Germany
Secondary Antibody				
Anti- chicken	703586155	Donkey	Alexa Fluor594	Dianova, Hamburg, Germany
Anti- mouse HRP	HAF007	Goat	HRP	RD Systems, Minneapolis, USA
Anti- mouse IgG	715605151	Donkey	Alexa Fluor647	Dianova, Hamburg, Germany
Anti- mouse IgG	715495159	Donkey	DyeLight649	Dianova, Hamburg, Germany
Anti- mouse IgG	715515150	Donkey	DyeLight594	Dianova, Hamburg, Germany
Anti- rabbit	711495152	Donkey	DyeLight649	Dianova, Hamburg, Germany
Anti- rat IgG	712585153	Donkey	Alexa Fluor594	Dianova, Hamburg, Germany
Anti- goat IgG	705605147	Donkey	Alexa Fluor649	Dianova, Hamburg, Germany
Anti- guinea pig	706495148	Donkey	DyeLight649	Dianova, Hamburg, Germany

2.1.4. Dyes

Following dyes were used For chemical staining of cellular structures (Table 2).

Table 2: List of chemical dyes used in experiments.

Product name	Cat. No.	Company/ Reference
MitoTracker® Deep Red FM	M22426	Invitrogen, Eugene, Oregon, USA
LysoTracker® Red Lysosomal Probe	PA-3015	Lonza, Walkersville, USA
HCS LipidTOX™ Red neutral Lipid Stains	H34476	Invitrogen, Eugene, Oregon, USA

2.1.5. Cell Lines

The diploid chromosomally stable human colorectal carcinoma cell line (HCT116) as well as the tetra- and trisomic cell lines HCT116 5/4 and HCT116 3/3 were kindly provided by Minoru Koi (Baylor University Medical Centre, Dallas, Texas, USA). The retinal pigment epithelial cell lines RPE1-hTERT (thereafter RPE1) and RPE1-hTERT H2B-GFP were a gift from Stephen Tylor (University of Manchester, UK). HCT116 H2B-GFP cell line was generated in the laboratory by Christian Kuffer by stable transfection of HCT116 with H2B-GFP. Corresponding aneuploid cell lines HCT116 H2B-GFP 5/4 were generated by microcell fusion by Silvia Stingele. RPE1-hTERT H2B-GFP 21/3 and RPE1-hTERT 5/3 12/3 were generated using the same protocol by Karolina Peplowska. Post- tetraploid cell lines HPT1, HPT2 and RPT1 were produced by Anastasia Kuznetsova. In brief, tetraploidy was induced in HCT116 H2B-GFP and RPE1-hTERT H2B-GFP cell lines by inhibition of cytokinesis through dihydrocytochalasin treatment. Subcloning was conducted by limited dilution on 96 well plates and after 6 weeks the DNA content was measured by flow cytometry. Evolved cell lines were generated by Silvia Stingele and Sarah Schunter by subculturing the cell lines for at least 50 passages.

2.1.6. Technical Equipment

Imaging was carried out with an inverted Zeiss Observer.Z1 microscope (Zeiss, Jena, Germany) equipped with the CSU-X1 spinning disk confocal head (Yokogawa, Herrsching, Germany), a LaserStack Launch (Intelligent Imaging Innovations, Denver, USA) and an X-CITE Fluorescent Illumination System (Lumen Dynamics Group Inc., Mississauga, Canada). Images were captured using a CoolSnap HQ camera (Roper Scientific, Ottobrunn, Germany) under the control of the Slidebook software (Intelligent Imaging Innovations, Denver, CO).

Other technical equipment used is: Electrophoresis Power Supply EPS 301 (GE Healthcare Biosciences, USA), Eppendorf centrifuge 5415R, 5417 C, Thermomixer comfort (Eppendorf, Hamburg, Germany), Fluoroscan Ascent FL (Labsystems, Kilsyth Victoria, Australia), Hera Cell, Hera Safe, Megafuge 3.0R (Thermo Fisher Scientific, Bonn, Germany), LaserStack Launch (Intelligent Imaging Innovations, Denver, USA), Mini-PROTEAN II electrophoresis system (Bio-Rad

Laboratories, Munich, Germany), MS-2000 stage (Applied Scientific Instrumentation, USA), MUPID ONE electrophoresis unit (Advance Co., Japan), Nanodrop ND-1000 spectrophotometer (PEQLAB, Erlangen, Germany), Rotina 420R centrifuge, Micro centrifuge SD220 VAC (Hettich, Tuttlingen, Germany), SmartSpec 3000 (Biorad, Munich, Germany), Vortex Genie 2 (Scientific industries, New York, USA), VWR Digital Heat Block (VWR, Darmstadt, Germany), X-CITE Fluorescent Illumination System (Lumen Dynamics Group Inc., Mississauga, Canada), X-ray film processor MI-5 (Medical Index, Bad Rappenau, Germany), Z2 Coulter Particle Count and Size Analyzer (Beckman Coulter, Munich, Germany), Zeiss Axio Observer Z1 inverted microscope (Zeiss, Jena, Germany).

2.1.7.Software Equipment

Imaging was carried out using the Slidebook 5.0 software (Intelligent Imaging Innovations, Denver, USA). Analysis of captures was performed with Cell Profiler (Jones et al. 2008). Statistical analysis of the imaging results as well as the microarray data normalization and analysis was conducted using R (R Development Core Team 2009) on the free open source integrated development environment R Studio. Commonly used R packages were “lattice” (Sarkar 2008), “genefilter” (R. Gentleman and V. Carey and W. Huber and F. Hahne), “fdrtool” (Strimmer 2008b) and “calibrate” (Graffelman and van Eeuwijk 2005). In addition, Perseus (1.2.6.16) as part of the MaxQuant Software Package (Cox and Mann 2008) was used for microarray analysis. Final graphs were made using GraphPad Prism 5 (GraphPad Software, La Jolla, USA) and Adobe Illustrator CS2 (Adobe Systems Incorporated, San Jose, USA).

2.2. Methods

2.2.1.Cell Culture

2.2.1.1. Cultivation

Cells were maintained in 10 cm dishes in Dulbecco´s modified eagle medium (DMEM) at 37°C and 5% CO_2. Culture medium was supplied with growth factors from 5% fetal calf serum (FCS) and 1% Penicillin/ Streptavidin to avoid bacterial growth and contaminations. Cell lines were subcultured at 70- 90% confluence for maximal 10 passages. To this end, the confluent cells were washed with 1x PBS and incubated for 5 minutes (min) at 37°C with 1x Trypsin- EDTA solution to detach the cells from the culture plates. The trypsinization was stopped by adding DMEM up to 10ml. Cells were seeded into the new culture plates in appropriate dilutions.

2.2.1.2. Cryopreservation of Cell Lines

Cell lines were stored in vials with 2 million cells/ ml in FCS, 10% DMSO. Cells were harvested in 10ml DMEM after 5 min incubation at 37°C in 1x Trypsin- EDTA solution. Cell concentration was measured with Beckman coulter particle counter. Cell suspension was centrifuged

at 1500 rpm for 4 min and cell pellet resuspended in FCS with 10% DMSO. Aliquots of 1ml were gradually cooled down in vials and stored at -80°C. For recovery, vials were thaw in the water bath. Cell suspension was diluted with DMEM up to 10ml and pelleted at 1500 rpm for 3 min. In DMEM resuspended cells were seeded on 10cm dishes for further cultivation.

2.2.1.3. Cell Lysis

Adherent cells were washed and treated with trypsin as described above. Cell suspension was centrifuged at 1500rpm for 4 min and the pellet was resuspended in 1ml 1x PBS. The suspension was transferred to an eppendorf tube and spun down. Optionally, the pellet was freezed at this step in liquid nitrogen. For cell lysis, the cell pellet was resuspended in 300µl RIPA Lysis buffer with protease inhibitors. After dissolving, the pellet was sonicated for 15 min in an ice cooled waterbath for mechanical cell disruption followed by centrifugation for 6 min at 13200 rpm, 4°C. Supernatant with soluble cell proteins was transferred to an ice cooled eppendorf tube. Cell lysates were freezed in liquid nitrogen and stored at -80°C. For short term storage at -20°C 20 µl of 4x Lämmli buffer (62.5mM Tris/HCl pH 6.8, 2% (w/v) SDS, 10% (v/v) glycerol, 5% (v/v) β-mercaptoethanol, 0.002% (w/v) bromphenole blue) were added to 60 µl of the lysate and boiled for 5 min at 95°C.

2.2.2. Protein Biochemistry

2.2.2.1. Bradford Assay

Bradford dye assay for determination of protein concentration was previously described (Bradford 1976). For protein quantification, 1µl protein sample and 850µl 1x Bradford solution were incubated for 5 min. The absorbance of 200µl triplicates were measured at 595nm. Applying Lambert Beer´s Law concentration of standard was calculated and in comparison with the standard curve sample concentration was obtained.

2.2.2.2. Sodium Dodecyl Sulphate-polyacrylamide Gel Electrophoresis (SDS-PAGE)

SDS-PAGE was performed as described by Lämmli (Laemmli 1970) with some modifications using a 15% resolving gel and a 7.5% stacking gel. 1x Lämmli buffer was added to cell lysates with a total protein concentration of 15µg to a total volume of 25µl. A voltage of 80V was applied for running the stacking gel in SDS- running buffer (25mM Tris/HCl, 200mM glycine, 0.1% (w/v) SDS) for 15 min. For separation, the probe in the resolving gel voltage was changed to 200V for approximately 1 hour (h). PrecisionPlus All Blue protein marker was used for molecular weight comparison.

2.2.2.3. Western Blotting

The standard western blot method is described elsewhere (Burnette 1981). In brief, proteins were transferred to a methanol activated polyvinylidene difluoride (PVDF) membrane from the SDS-

PAGE gel by a wet transfer system in transfer buffer (25mM Tris/ HCl, 1.44% (w/v) glycerol, 20% (v/v) methanol), by applying an electric field for 1h at 375mA. To prevent unspecific binding of the antibody, the blotted membrane was blocked with 5% skim milk in TBST for 0.5h at room temperature. After blocking, membrane was washed in TBST for 1 min. Incubation with the primary antibody was performed for 1h at 4°C. Before incubation with secondary antibody, membrane was washed 3 times to remove unspecific bound proteins with TBST. Secondary antibody incubation was performed at a room temperature for 0.5h, respectively, followed by three times washing of the membrane with TBST. Secondary antibody was detected applying the ECL Plus Western blotting detection Kit. Therefore, horseradish peroxidase conjugated to the secondary antibody catalyzed the chemiluminescence reaction resulting in a luminescence which was detected on ECL hyperfilm in different exposure times. For LC3 detection the western blot protocol had the following changes: blocking for 1h with 1% BSA in PBST, washing steps with PBST, primary antibody incubation overnight and secondary antibody incubation for 1h.

2.2.3. Cell Biology

2.2.3.1. Immunofluorescence Experiments

For immunofluorescence experiments, the cells were seeded on glass- bottomed 96- black well plates at a concentration of 30000 cells/ ml for HCT116 and 20000 cells/ ml for RPE1. Prior to the experiments the cells were treated depending on the type of experiment.

As a positive control for DNA damage and DNA replication stress, control wells for the RPA, PCNA and γH2AX immunofluorescence experiment was incubated with 1μM doxorubicin for 1h. After a recovery of 3h, cells were fixed and permeabilized with at -20°C precooled methanol for 5 min at 4°C. Fixed cells were washed three times with 1x PBS. To avoid unspecific protein- protein interactions, fixed cells were blocked with 5% FCS, 0.3% Triton in 1x PBS. To avoid cross reaction of the secondary anti- mouse antibody with the primary rat anti- PCNA antibody (Table 1), the immunostaining was carried out separately. Incubation with mouse anti- RPA was performed over night at 4°C. Cells were washed two times with 1x PBS, followed by a washing step with 1x PBS containing 400mmol NaCl to remove unspecific bound antibodies. Subsequently, the plate was incubated with the secondary anti- mouse antibody for 1h at RT. After washing with 1x PBS, incubation with a rat anti-PCNA antibody for 4h at 4°C was performed. Secondary anti- rat antibody incubation for 1h at room temperature was followed by three times 1x PBS washing. 1x PBS with.0.02% sodium azide was added to avoid bacterial growth before storage at 4°C

γH2AX and PCNA in immunofluorescence experiments were carried out as described for RPA and PCNA detection, except that the rabbit anti- γH2AX antibody and rat anti- PCNA antibody were incubated in the same solution over night at 4°C.

Immunofluorescence experiment on processing bodies using the detection of a marker protein LSM4 was carried out on both untreated and bafilomycin treated cells. Bafilomycin A1 treatment was

performed at a concentration of 50pmol, (stock concentration 50µmol in DMSO), for 16h. Cells were fixed with 3% PFA for 15 min at 4°C. Blocking and permeabilization of cells with 3% BSA, 0.2% Triton X-100 in 1x PBS was performed for 10 min at room temperature. Followed washing steps and antibody (chicken anti- LSM) treatments were performed as described above with the exception of the wash buffer, which contained 0.2% BS, 0.1% Tween-20.

p62 and Ub-p62 detection was performed on untreated, 16h bafilomycin treated and 30h bafilomycin treated cells. The cells were fixed for 10 min at a room temperature with PTMF buffer. As PTMF permeabilizes the cells, the following washing steps with PBST reduced the amount of unbound cytoplasmic p62. The fixed and permeabilzed cells were blocked for 30 minutes in 3% BSA in PBST. Following washing steps and antibody treatments were performed as described above.

2.2.3.2. Cell Organelles Staining

Mitochondria were stained in untreated, 16h and 30h bafilomycin treated cells in 96 well plates. Lysosomes were stained with LysoTracker dye only on untreated cells. The cells were incubated for 30 min at 37°C with 100nM LysoTracker and MitoTracker dye, respectively, prior to fixation. The MitoTracker dye passively diffuses across the plasma membrane and is oxidized by active mitochondria. After sequestation into the mitochondria, the chemical dye reacts with thiols on proteins and peptides, thereby labeling the mitochondria. cell membranes are permeable for LysoTracker dye that consists of a fluorophore linked to a weak base. It accumulates in compartments with low pH and is only partially protonated at neutral pH. Cells were fixed with 3% PFA in DMEM for 5 min at room temperature. After washing with 1x PBS, 1x PBS containing 0.02% sodium azide was added and plates stored at 4°C in the dark.

2.2.3.3. Lipid Droplet Staining

Staining of neutral lipids was carried out on untreated, 16h and 30h bafilomycin treated cells in 96 well plates. Cells were fixed with 3% PFA and stored as described above. Incubation with neutral lipid stain was performed 30 min before imaging with a dilution of 1:1000 in 1x PBS.

2.2.3.4. Imaging and Computational Image Analysis

Imaging was carried out on an inverted Zeiss Observer.Z1 microscope with 473 nm, 561 nm and 660nm argon lasers lines. Imaging devices were controlled and captures stored and processed with SlideBook 5.0 Software. Nuclei were identified by stably expressed H2B-GFP that was imaged with 473 nm argon laser at an exposure time of 100ms. Detection of the immunofluorescent proteins or stained cellular structures as described above was performed at an exposure time of 1500ms with the 561nm and 660 nm argon lasers, respectively. For the Cell Profiler analysis, the images were captured on single optical plane with a 40x magnification air objective.

Cell Profiler analysis was carried out on 16- bit TIFF files with separated files for each captured emitted wavelength. Nuclei were identified with the Otsu Global thresholding method. In cases were overall cellular signal was detectable, the cellular background signal was used to identify the cytoplasm. Therefore, MoG thresholding method in combination with the watershed- Image method to identify the secondary objects was applied. Depending on the experiment, high intense signals were identified as speckles or overall area in the nuclei or cytoplasm applying the RobustBackground PerObject thresholding method. In addition, the mean signal intensity per cell was measured. Subsequent statistical analysis was performed in R and Prism.

2.2.4. Transcriptomics- mRNA Expression Analysis

2.2.4.1. Oligonucleotide Microarray

Genome- wide expression profiling was conducted by IMGM laboratories GmbH (Martinsried, Germany) as previously described (Stingele et al. 2012). In brief, cDNA was hybridized on Agilent Whole Human Genome Oligo Microarrays (4x44K format) for HCT116 and HCT116 5/4 or Agilent SurePrint G3 Human GE Microarrays (8x60K) for the other cell lines according to a One-Color based hybridization protocol. The fluorescent signal intensities were detected with an Agilent DNA Microarray Scanner and the data was extracted using Feature Extraction 10.5.1 Software (Agilent Technologies). Raw data was background normalized. Agilent microarray Quality Control was performed by IMGM according to the company protocol.

2.2.4.2. Published Microarray Data

Microarray data of trisomic and diploid colorectal cancer cell lines (DLD1) was kindly provided by Thomas Ried (National Institutes of Health, Bethesda, Maryland, USA). Microarray experiments are described in the original publication (Upender et al. 2004). mRNA expression data of HCT116 cell lines grown under various stress conditions were obtained from NCBI's Gene Expression Omnibus (Edgar 2002). Expression data of HCT116 cell line grown under high and low glucose conditions were accessed through GEO Series accession number GSE31084 (http://www.ncbi.nlm.nih.gov/geo/query/acc.cgi?acc=GSE31084). Data of HCT116 transcriptome after stress treatment was accessed via the accession number GSE3176 (http://www.ncbi.nlm.nih.gov/geo/query/acc.cgi?acc=GSE3176). Human embryonic diploid and trisomic cells mRNA expression data was obtained from Omnibus database via the accession number GSE28076 (http://www.ncbi.nlm.nih.gov/geo/query/acc.cgi?acc=GSE28076).

2.2.4.3. Microarray Normalization

Bioinformatics analysis of the microarray data was performed using Perseus (1.2.6.16) as part of the MaxQuant Software Package (Cox and Mann 2008) and R on the free open source integrated development environment R Studio. The gBGSubSignal (green background subtracted Signal) from

background-normalized cDNA Microarray data was used for further normalization. To improve data distribution for further statistical analysis and to uncouple the multiplicative error from signal intensities, background subtracted raw intensities were log2 transformed (Kreil and Russell 2005; Long 2001).

Global normalization on log transformed raw data was performed by subtracting the median of the overall signal intensities for one experiment from each signal in this experiment. Probe sets for one gene were summarized by taking the median resulting in one intensity signal per gene. The median of replicative probes signal intensities was calculated for each cell line. To filter for the spiked-in control entries the dataset was compared to a Perseus generated Homo sapiens gene list.
For comparison of each aneuploidy cell line to the corresponding diploid (WT) cell line gene expression fold change ratios were calculated. These log2 ratios were obtained by subtracting the log2 ratio for each individual gene entry of the WT cell line from the log2 ratio of that individual gene entry of each aneuploid cell line.

$$\log_2 fold\ change = log2(\frac{aneuploid}{WT}) = log2(aneuploid) - log2\ (WT)$$

2.2.4.4. Gene Enrichment Analysis

In order to verify the statistical significance of the fold change in mRNA expression, a Student t-test was performed between the signal intensities of aneuploid and diploid cell line. To correct the test statistics for multiple comparisons, false discovery rate control of the p-values was applied. Both local and frequent FDR were calculated with the "fdrtool" package (Strimmer 2008a, 2008b). Significant fold change of expression ratios in comparison to WT cell line were determined with a local fdr cut off of 0.1. For further analysis a fold change cut off of approximately 1.4 fold change in mRNA expression was applied. Therefore, ratios on the $\log_2$ scale greater than 0.5 and smaller than -0.5 were filtered. To investigate the correlation between the cell lines, Spearman correlation coefficient was calculated in R using the "ClassDiscovery" package in the OOMPA library and "mclust" package. Correlation was visualized in a colored correlation matrix map in the "spatstat" package. Further visualization of the general gene expression filtered for 1.4 fold up- and down-regulated genes was obtained by creating heat maps with the heatmap.2 function in the "gplot" package (Gregory R. Warnes 2012). To investigate a global response to aneuploidy on gene level, data sets were filtered for those genes more than 1.4 fold up- or down- regulated in all HCT116 and RPE1 derived cell lines. The resulted gene lists were analyzed for their function and relation using the DAVID functional annotation tool (Dennis, JR et al. 2003), KEGG pathway and the NCBI Gene database.

2.2.4.5. Pathway Enrichment Analysis

Pathway enrichment analysis was conducted in Perseus using the 2D annotation enrichment tool. Thereby, enriched GO and KEGG annotations were identified by testing whether genes in an annotated category have a significant preference to be altered compared to the global fold change data distribution. Significance was tested by a t-test followed by a false discovery rate correction in the Benjamini Hochberg procedure. An FDR cut off of 0.02 was chosen. Expression values for significant enriched annotations were summarized in an annotation score from -1 to 1 to represent levels of up- or downregulation. Significant enriched annotations were summarized in larger, general categories for visualization purpose. 2D annotations enrichments of two cell lines were plotted with the help of the annotation score in a scatterplot and data points colored according to broader defined categories.

3. Results

3.1. Transcriptomics- mRNA Expression Analysis

3.1.1. Microarray Data Preprocessing and Normalization

3.1.1.1. Microarray Data Quality

Assessing the quality of microarray data is important to make decisions about the further processing and normalization methods applicable to the datasets. Quality parameters such as inter array reproducibility and accuracy, detection limit, spatial distribution bias, system sensitivity and dynamic range were analyzed by IMGM with the Agilent Feature Extraction Software. The quality requirements were fulfilled for each hybridization experiment. Hence, for the microarray data of the RPE1 and HCT116 derived cell lines no additional normalization was necessary to correct for an intensity or spatial bias.

Reproducibility between the replicates was investigated by correlation analysis of the three replicates of each cell line. For that purpose, overall log transformed signal intensities were plotted in a scatterplot. The obtained scatter plots (Figure 1) reveal a high correlation between the replicates of each cell line. The Spearman correlation coefficient was calculated using the "cor" function defined in the "stats" package. The coefficients for each pair of replicates ranged from 0.967 to 0.997, which proves a high positive correlation.

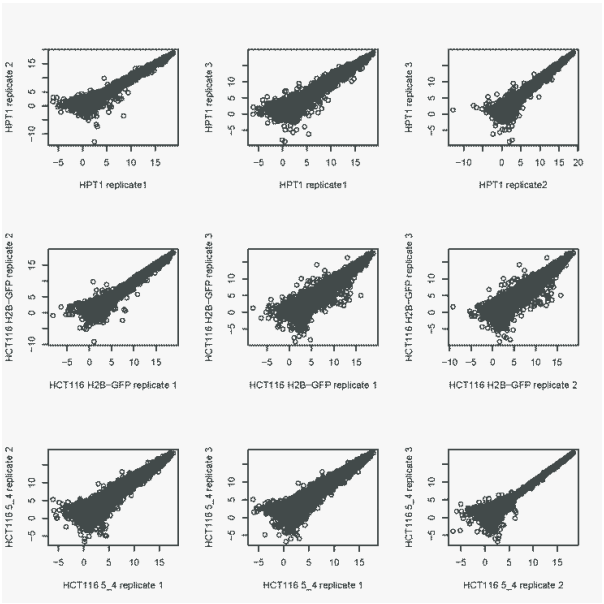

Figure 1: Representative scatter plots of log2 transformed signal intensities of oligonucleotide microarray experiment replicates.

To assess the intra array quality, raw data was plotted as box plots with 5% and 95% percentiles to analyze the overall distribution of the signal intensities (Figure 2).

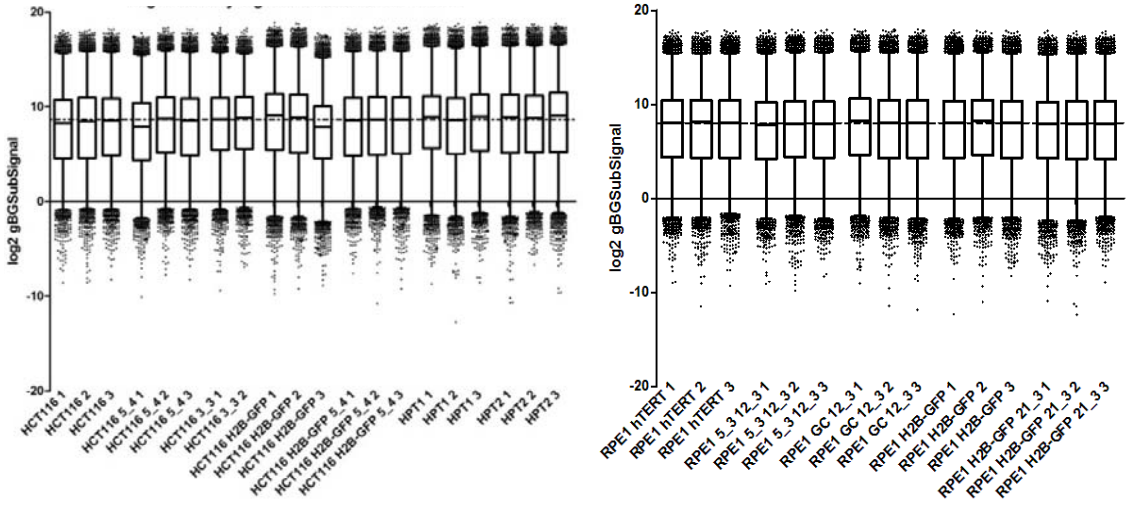

Figure 2: Box plots (5% and 95% percentiles) of log2 transformed signal intensity distribution. The averaged median is indicated by the dotted line. HCT116 and RPE1 derived cell lines are plotted with three replicates for each cell line different in ploidy.

The signal distribution of the raw data was observed to be fairly similar between the cell lines. However, the 25% and 75% percentiles showed a standard deviation of 0.34 and 0.31, respectively. The averaged median was 8.65, with a deviation of 0.325. These standard deviations are relatively high given that already small differences in gene expression are important for the subsequent analysis. Besides this deviation, a shift in the overall signal distribution in one replicate for the cell lines HCT116 H2B-GFP, HCT116 5/4 and HPT2 can be observed. Consequently, I decided to normalize the raw data prior to further analysis.

3.1.1.2. Microarray Data Normalization

To minimize the effect of technical and experimental variation on the meaningful biological differences in signal intensities, median normalization on the raw data was applied. Subtraction of the median of the overall intensity in one microarray experiment from each intensity value in that experiment resulted in a data distribution with a forced median of 0 (Figure 3). Since the median normalization method does not force an equal distribution including the quantiles, a deviation in the 25% and 75% percentiles of 0.278 and 0.098 could be still observed. A deviation is critical as already small changes in the gene expression were assessed. On the other hand, an overall forced equal distribution as it results from quantile normalization bears the possibility to overfit the data. As the deviation is relatively low, I decided to make a compromise to the normalization in order to limit the chance to introduce artifacts by over-normalization.

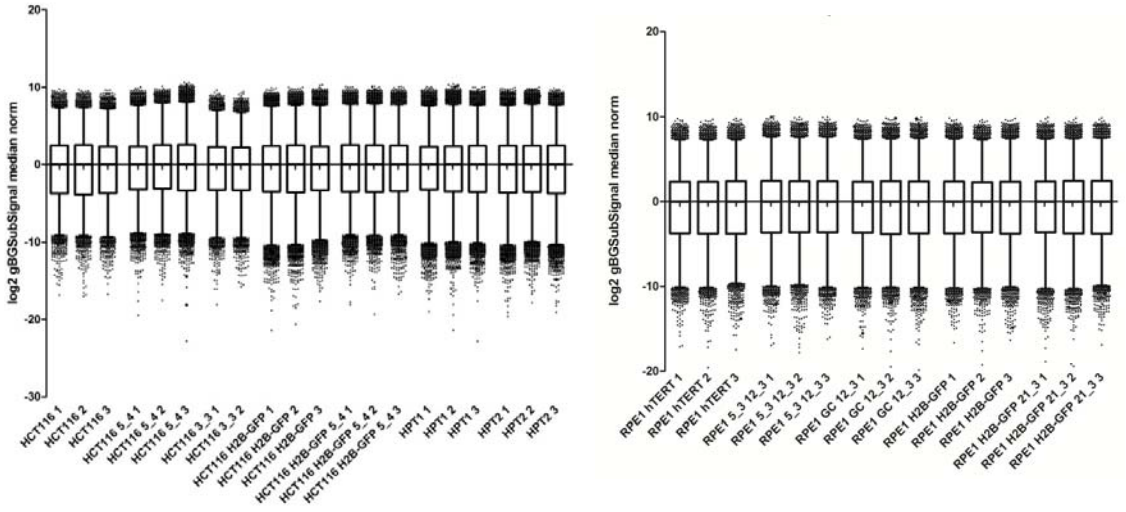

Figure 3: Box plots (5% and 95% percentiles) of log2 transformed and median normalized data for each replicate each HCT116 and RPE1 derived cell line.

To prepare the data for final analysis, probe sets were averaged and control genes eliminated. The replicative signal intensities for each cell line were averaged. Further, the log2 transformed and normalized signal intensity of the diploid cell line was subtracted from the corresponding log2 transformed and normalized signal intensity of the aneuploid cell line. This transformation resulted in log2 fold change ratios with the median of the overall distribution close to zero. The representative box plots of the log2 fold change ratios of HCT116 derived cell lines in Figure 4 indicate an overall similar distribution of the final normalized data. An exception is the distribution of HCT116 H2B-GFP 5/4, where the quantiles and percentiles are spread in a wider range compared to the other data distributions. This might indicate that HCT116 H2B-GFP 5/4 has a more genes strongly altered in their expression than the other cell lines.

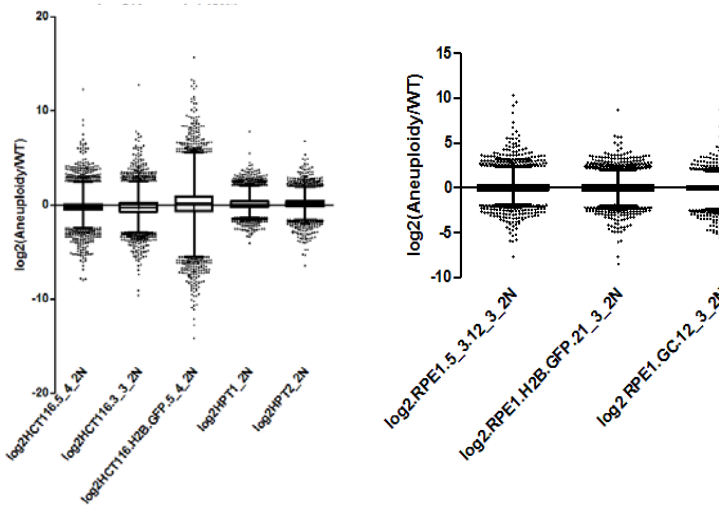

Figure 4: Box plots (5% and 95% percentiles) of log2 fold change ratios of each HCT116 and RPE1 derived aneuploid cell line to the corresponding diploid cell line.

3.1.1.3. Preprocessing and Normalization of published Data

In addition to the gene expression analysis of the RPE1 and HCT116 derived cell lines, I have analyzed previously published transcriptome data obtained from aneuploid human cells. Microarray raw data of DLD1-derived cell lines was log2 transformed. To assess the quality between replicates and different aneuploid cell lines, raw data were plotted as depicted in Figure 5.

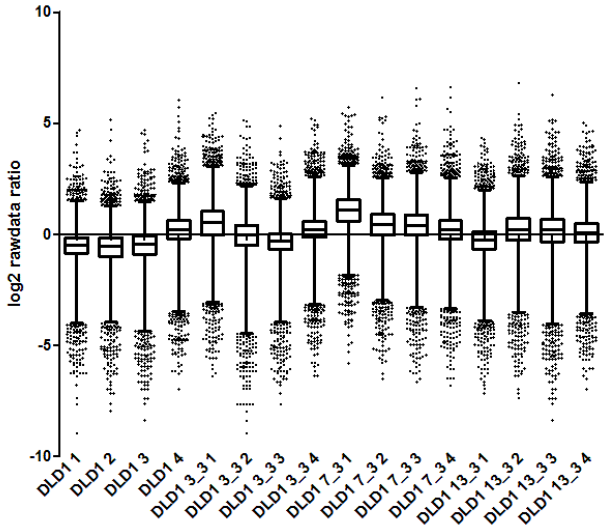

Figure 5: Box plots (5% and 95% percentiles) of DLD1 raw data showing the overall log2 transformed data distribution of four replicates each DLD1 derived aneuploid cell lines.

In comparison to the log2 raw data distribution of the data obtained from IMGM, there are more differences in the overall data distribution of both replicates and between the aneuploid cell lines derived from DLD1. The median ranges between -0.400 and 1.075. The 25% percentile and 75% percentile show a standard deviation of 0.394 and 0.458, respectively. To be consistent with the previous IMGM data normalization, I chose the median scale normalization as described above. By applying this method, I observed a more similar distribution with a forced median of zero (Figure 6).

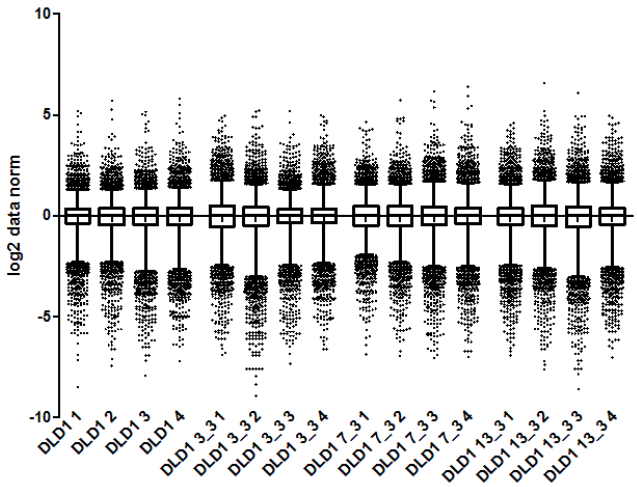

Figure 6: Box plots (5% and 95% percentiles) of DLD1 log2 and median normalized data of three replicates each DLD1 derived aneuploid cell line.

For the human embryonic (HE35) cell line, expression data of three clones for the trisomic HE35 and the diploid HE35data was available. For each clone three independent microarray experiments were performed (Nawata et al. 2011). I normalized the data with the above described method. To limit the amount of data, I later analyzed only one clone of the diploid HE35 and of the aneuploid HE35 with a trisomy in chromosome 8 in the 2D enrichment. In order to verify that the clones show no substantial differences in their data quality, I analyzed the correlation between the clones in a scatterplot analysis (Appendix Figure 42). Additionally, I performed a 2D enrichment analysis between the clones and could exclude biological differences.

mRNA expression data of HCT116 after treatment inducing cellular stress were published as log2 transformed and median normalized data of three replicates from two- color microarray experiments. Raw data plots showed an overall normalized data distribution. Hence, no further normalization was necessary. Replicates were summarized by the median expression value for each gene. Because the data were derived from two- color microarray experiments, the expression values already represented the expression fold change ratio to the diploid control expression.

3.1.2. Gene Expression Analysis

3.1.2.1. Correlation Analysis of Aneuploid Cell Lines

To assess the overall correlation of the gene expression in the analyzed, correlation analysis on single gene level was conducted. Therefore, Spearman correlation coefficient was calculated in R and visualized in a correlation matrix. In general, correlation ranges from 1 (strong correlation) to 0 (no correlation). As correlation analysis of RPE1 and HCT116 derived aneuploid cell lines resulted in a strong correlation from 1 to 0.965, the scale was adapted for a better visualization of small differences. Figure 7 shows the correlation matrix with a color code from blue to brown indicating

identical cell lines and a strong correlation of 0.965, respectively. The blue diagonal represents identical cell lines.

Strong correlation can be observed for the cell lines HPT1 and HPT2, as well as for the correlation between RPE1 12/3 5/3 and the evolved cell line RPE1 GC (12/3). Correlation of 0.98 indicated in white can be observed for HCT116 3/3 and HCT116 5/4, RPE1 12/3 5/3 and RPE1 H2B-GFP 21/3. The post- tetraploid cell lines are closest to the HCT116 H2B-GFP 5/4, followed by the RPE1 derived cell lines and with a weaker correlation to the HCT116 5/4 and HCT116 3/3. Whereas HCT116 H2B-GFP 5/4 is correlating with the RPE1 derived cell lines with a Spearman correlation of 0.975, the HCT116 3/3 and HCT116 5/4 show the weakest correlation to the RPE1 derived cell lines. However, judging from the scale of the Spearman correlation, all the aneuploid cell lines are closely related in their mRNA expression profiles.

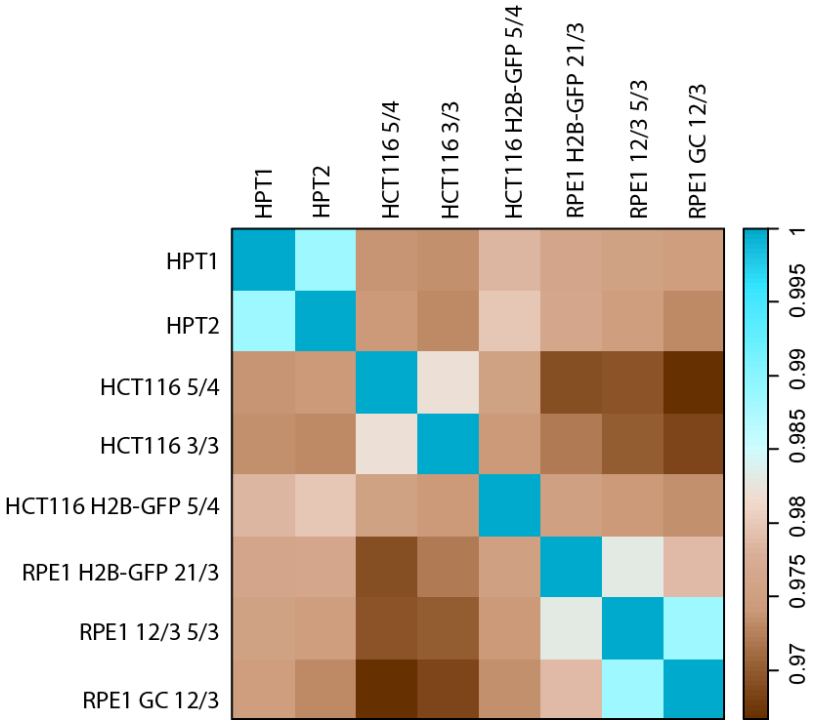

Figure 7: Correlation matrix map of the RPE1 and HCT116 derived aneuploid cell lines. Spearman correlation was calculated in R using the "ClassDiscovery" package (OOMPA library). The color code from blue to dark brown indicates the range of correlation from 1 (identical cell lines) to 0.965 (still strong correlation).

3.1.2.2. Significance Analysis of Fold Change Differences in mRNA Expression

Prior to the analysis of the mRNA expression data on the level of gene entries, I carried out the significance analysis of expression ratios. To this end, a t- test was performed in R between the replicate expression ratios of the aneuploid cell lines and the corresponding diploid cell lines. The resulting p- values were corrected for multiple comparisons by estimating the false discovery rate (FDR) in R with the "fdrtool" package. Figure 8 presents FDR frequency distributions of the cell lines HCT116 3/3, HPT1 and RPE1 12/3 5/3. FDR distributions are representative for the analyzed cell lines and show the differences in range and frequency of the FDR values between the cell lines

observed. As shown for HCT116 3/3, the HCT116 derived aneuploid cell lines gave a FDR distribution spread from 1 to 0.01. For a cut off of 0.1, indicated by the red line in the plot, approximately hundred genes are left for further analysis. However, for the post- tetraploid cell lines, the minimal FDR value was calculated as 0.056, with only a few or none genes for HPT2 left after setting a cut off of 0.1 In contrast, a large number of genes were observed with an FDR below 0.1 for the RPE1 derived cell lines.

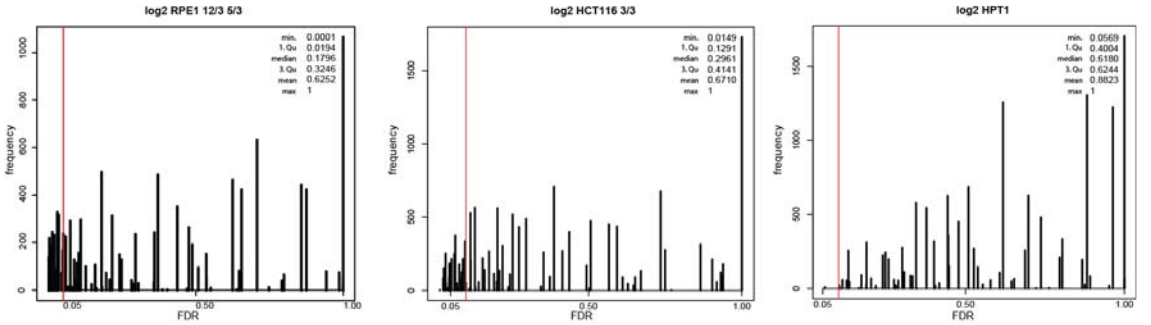

Figure 8: FDR frequency distribution plots for the cell lines RPE1 12/3 5/3, HCT116 3/3 and HPT1. The red line indicates a cut off of 0.1. Minimum, 1st quantile, median, 2nd quantile, mean and maximum are given in the legends of the plots.

The FDR frequency distributions were proven by another R packages, performing first a test for statistical significance and correcting the results for multiple comparisons by calculating the FDR. With the packages “fdr_ame”, “twilight” and “limma”, similar FDR values were obtained. In summary, particularly for the post- tetraploid cell lines the FDR values might indicate that we have to expect a high chance of false positive hits. This means, that genes showing significant differential expression are just by chance with a low p-value. The big differences in the FDR distributions between the cell lines made it difficult to define a cut off.

3.1.2.3. Fold Change Analysis of mRNA Expression

Due to the differences in FDR distributions between the cell lines, it was not possible to choose one FDR cut off which represents a similar significance criterion for all analyzed cell lines. Consequently, the analysis of mRNA expression on gene level was conducted on genes filtered for a fold change. I chose a fold change cut off of approximately 1.4 upregulation and downregulation. The data was filtered for log2 fold change ratios bigger than 0.5 and smaller than -0.5 and visualized in the heat maps (Figure 9). The heat maps of all up- or down- regulated gene expression levels indicate the similarities between the different HCT116 derived aneuploid cell lines. Dark red demonstrates strong upregulation, whereas dark blue illustrates strong downregulation. Interestingly, HCT116 H2B-GFP 5/4 contains a higher number of genes strongly down or up- regulated than the other HCT116 derived aneuploid cell lines. Comparing the datasets for more than 1.4 fold up- regulated gene expression of the HCT116 derived aneuploid cell lines, the high number of genes strongly up- regulated in HCT116 H2B-GFP 5/4 is followed by HCT116 5/4 and secondly by HCT116 3/3. The post- tetraploid cell lines HPT1 and HPT2 reveal only a few genes strongly deregulated. Hierarchical clustering mirrors

these observations by providing a close distance of HPT1 and HPT2, followed by HCT116 3/3 and HCT116 5/4, which in turn is the closest to the HCT116 H2B-GFP 5/4. In comparison to those findings, I observed a similar clustering of down- regulated genes, with the exception that instead of HCT116 5/4, HCT116 3/3 is closely related to HCT116 H2B-GFP 5/4, whereas HCT116 5/4 shows only a small number of down- regulated genes. Here, HCT116 5/4 is closer to HPT2, followed by HPT1, HCT116 3/3 and HCT 116 H2B-GFP 5/4.

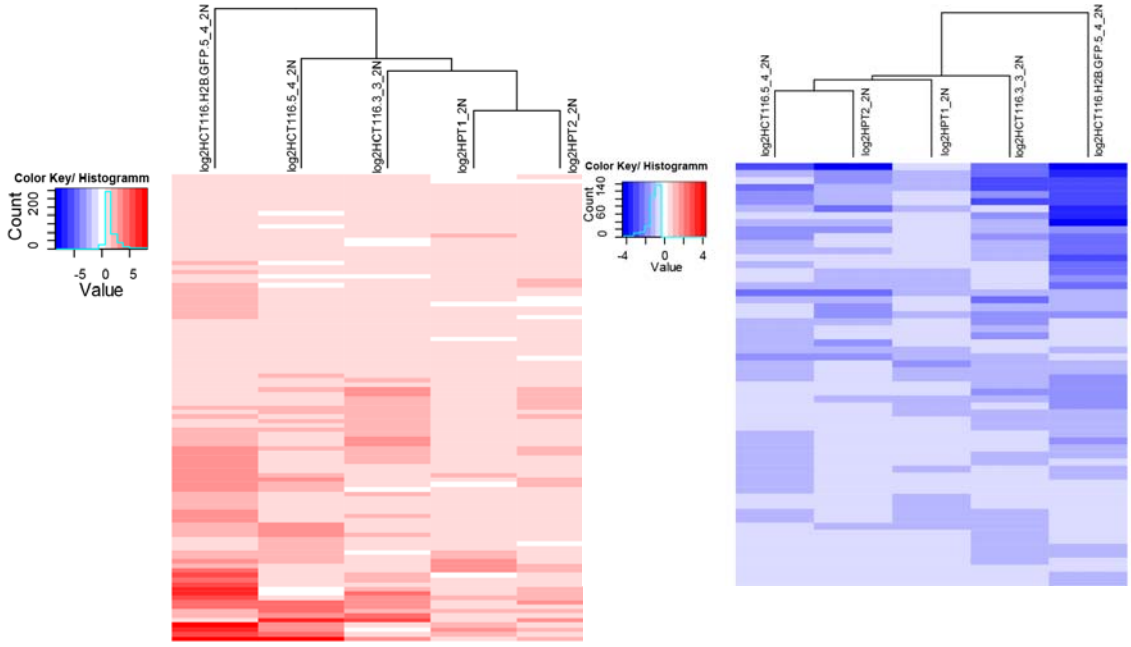

Figure 9: Heat map of HCT116 derived aneuploid cell lines filtered for gene expression greater than 1.4 fold up- regulated (left) and smaller than 1.4 fold down- regulated (right).

The heat map summary of the gene expression filtered for more than 1.4 fold up- or downregulation reveals a similar trend of strong deregulation for RPE1 12/3 5/3 and RPE1 H2B-GFP 21/3 (Figure 10). Upregulation of gene expression is indicated by red and can be observed in the lower gene cluster of the left plot. Downregulation of gene expression seems also similarly clustered, indicated by a blue color key.

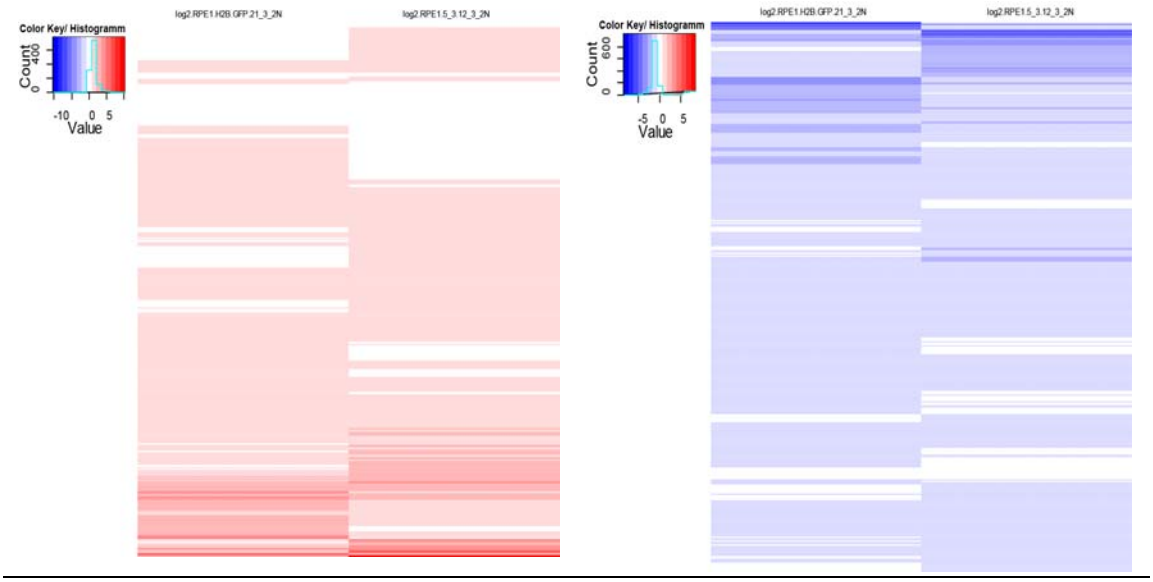

Figure 10: Heat map of RPE1 12/3 5/3 and RPE1 H2B-GFP 21/3 filtered for gene expression greater than 1.4 fold change up- regulated (left) and smaller than 1.4 fold down- regulated (right) compared to the diploid cell line.

Taken together, overall trend of up- and down- regulated genes is similar in the HCT116 and RPE1 derived cell lines. Strong up- or downregulation can be observed in the same genes over the cell lines. HCT116 H2B-GFP 5/4 shows more strongly up- and down- regulated genes. This is in line with the observation in chapter 4.1.1.2 (Figure 4) that the spread of the fold change values is larger in this cell line than in other cell lines.

To have a general overview of the chromosomes which are deregulated in their expression, I analyzed the percentage of expression from each chromosome for each cell line (Figure 11). Capitalized "D" indicates the down- regulated gene expression and the corresponding chromosome distribution and "U" indicates the up- regulated gene expression. As expected the percentage of up- regulated gene expression for the extra chromosomes in the whole chromosome aneuploid cell lines is bigger than for the other chromosomes. In all cell lines the chromosomes 1 and 19 are notably deregulated in their expression. The expression of the chromosomes 20, 21, 22 and Y possess only a small percentage of the differential expressed genes. But this might be also explained by the smaller size of those chromosomes. Interestingly, for HPT1 is the down- regulated gene expression with a high percentage from chromosome 7.

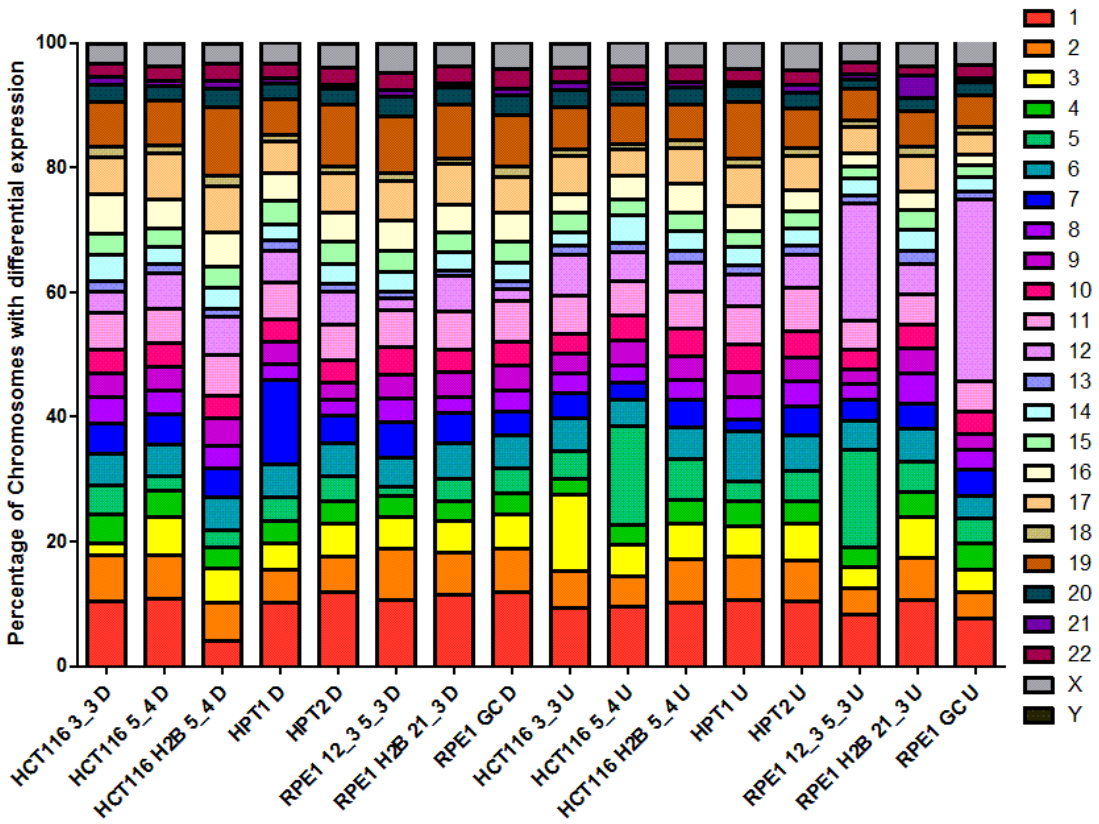

Figure 11: Percentage of chromosomes for which a differential expression was observed. Capitalized "D" indicates the down- regulated gene expression for this cell line and "U" the up- regulated gene expression.

3.1.2.4. Gene Enrichment Analysis

For closer investigation of strongly up- and down- regulated genes, I generated data subset consisting only of those genes that were present in all of the cell lines. The lists with the overlapping genes were submitted to the DAVID functional annotation tool in order to elucidate the functional importance and relationships in and between clusters of highly up- or down- regulated expression of genes.

Filtering of the mRNA expression data for genes that are more than 1.4 fold up- or down-regulated and present in all analyzed HCT116 and RPE1 derived aneuploid cell lines resulted in 5 down- regulated gene entries (Table 3) and 18 up- regulated gene entries (Table 4). As 5 gene entries don´t allow a functional clustering, these genes are only briefly described here. XYLB, translated into the xylulose kinase like protein, is encoded on chromosome 3. The annotated function lies in the energy metabolism (Tamari et al. 1998). The lysyl oxidase (LOX) proteins are involved in cross-linking collagen fibers and in epithelial mesenchymal transition (Nishioka et al. 2012). In previous studies it was hypothesized that LOX proteins promote tumor cell invasion and metastasis. MYB and NFIB are both genes encoding for transcription factors known as proto-oncogenes. Fusion of these genes was associated with abolished negative MYB feedback loop leading to enhanced activation of MYB target genes (Stenman et al. 2010). EEPD1 encodes for a protein with an endonuclease and

exonuclease activity. The function of this specific protein is related to DNA repair and DNA binding. C9orf100 is also known as Rho guanine nucleotide exchange factor protein (GEF). GEFs are important activators of Rho GTPases and associated with tumorigenesis and metastasis.

Table 3: Genes for which the expression is more than 1.4 fold down- regulated in all RPE1 and HCT116 derived cell lines aneuploid cell lines compared to the diploid cell lines

Gene name	Protein name
XYLB	Xylulose kinase like protein
LOXL3	Lysyl oxidase homolog 3
MYB/NFIB fusion	MYB/NFIB fusion protein variant 2; Transcriptional activator Myb; Proto-oncogene c-Myb
EEPD1	Endonuclease/exonuclease/phosphatase family domain-containing protein 1
C9orf100	Vav-like protein C9orf100

Genes which expression was found to be more than 1.4 fold up- regulated were analyzed via functional annotation clustering in DAVID. The genes could be clustered in three clusters: extracellular region, transmembrane and cell/plasma membrane. KEGG Pathway analysis of the genes resulted in the association with the complement and coagulation cascades (PLAUR, BDKR) and metabolic pathways as the top two hits. It seems that on single gene entries only few genes are similarly highly up- and down- regulated in aneuploid cells derived from the different cell lines. Thus, it is difficult to identify a direct link between the genes and possibly deregulated pathways as a response to aneuploidy.

Table 4: Genes for which the expression is more than 1.4 fold up- regulated in all RPE1 and HCT116 derived aneuploid cell lines compared to the diploid cell lines.

Gene name	Protein name
PLAUR	Urokinase plasminogen activator surface receptor
RAB27B	Ras-related protein Rab-27B
P4HA2	Prolyl 4-hydroxylase subunit alpha-2
FRY	Furry homolog (Drosophila)
BDKRB1	B1 bradykinin receptor
HOXB5	Homeobox protein Hox-B5
GDF15	Growth/differentiation factor 15
OASL	highly similar to Homo sapiens 2'-5'-oligoadenylate synthetase-like (OASL)
SERPINE2	Glia-derived nexin; Protease nexin I
IFI44	Interferon-induced protein 44;Microtubule-associated protein 44
AMDHD1	Probable imidazolonepropionase; Amidohydrolase domain-containing protein 1
TMEM171	Transmembrane protein 171
TMEM169	Transmembrane protein 169
GLRX	Glutaredoxin-1;Thioltransferase-1
DMBT1	Deleted in malignant brain tumors 1 protein
COL13A1	Collagen alpha-1(XIII) chain;COLXIIIA1;COL13A1 protein; Type XIII collagen
SH2D1B	SH2 domain-containing protein 1B
MIA	Melanoma-derived growth regulatory protein; Melanoma inhibitory activity protein

Separate analysis of overlapping up- and down- regulated genes for the RPE1 and HCT116 derived aneuploid cell lines resulted in many more gene entries. For the RPE1 derived aneuploid cell lines 607 highly up- and 606 highly down- regulated genes overlap in their expression. These gene entries were clustered in the DAVID tool in 151 and 130 clusters, respectively. The three top hits defined by the up-regulated genes were extracellular region part, extracellular matrix and plasma membrane part. For the down-regulated gene, I identified following clusters: transcription, positive regulation of transcription and RNA metabolic process and GTPase activity.

Similar analysis of the HCT116 derived aneuploid cell lines, excluding the post- tetraploid aneuploids, resulted in 372 overlapping up- regulated gene entries and 805 down- regulated gene entries. The three gene clusters with the highest enrichment score for the up- regulated genes were extracellular region, membrane fraction and vesicle related annotations. For the down- regulated genes, DAVID analysis revealed gene clusters with the annotations membrane- enclosed lumen (organelle, nuclear), non- membrane- bounded organelle and ribosome biogenesis/ rRNA processing. Interestingly, extracellular proteins seem to be up- regulated in all aneuploid cells independent of the cell line. Besides that, it is difficult to make conclusions from the information of single deregulated genes.

3.1.2.5. Gene Enrichment Analysis of Post- Tetraploid Cell Lines

The post- tetraploid cell lines were derived from unstable tetraploid cells. Tetraploidy was induced by cytokinesis failure and consequently chromosomal instability might give rise to the complex aneuploid cells, called post- tetraploid. This adaption is a hypothesized mechanism leading to complex aneuploid cancer cells. Analysis of the transcriptome in HCT116 derived post- tetraploid cells, HPT1 and HPT2, is not only of interest because of the response to complex aneuploidy but also because of its CIN induced nature, which is very close to what we expect in aneuploid cancer cells.

Filtering of the gene expression data of HPT1 and HPT2 for genes present in both cell lines resulted in a list of 1229 genes with a log2 fold change of at least 0.5. These genes are in their expression more than 1.4 fold up- regulated compared to the diploid cell line. Functional gene clustering resulted in 216 clusters with the top hits indicated by a high enrichment score. The three top clusters included genes annotated with extracellular region, peptidase/ enzyme/ endopeptidase inhibitor activity and lysosome/ lytic vacuole/ vacuole activity. KEGG pathway analysis gave a better idea of the relationship between the genes in these clusters. The top hits chosen for a closer investigation were “pathways in cancer”, “lysosomes” and “p53 signaling”. As an example, the “p53 signaling” pathway results are depicted in Figure 12. Interestingly, the gene expression of p53 target genes like p21, BAX, PUMA, p48 is up- regulated. These genes are involved in p53 dependent cell cycle arrest and apoptosis pathways in response to stress and also in CIN. In contrast, the expression of MDM2 responsible for p53 inhibition in a negative feedback loop is also upregulated.

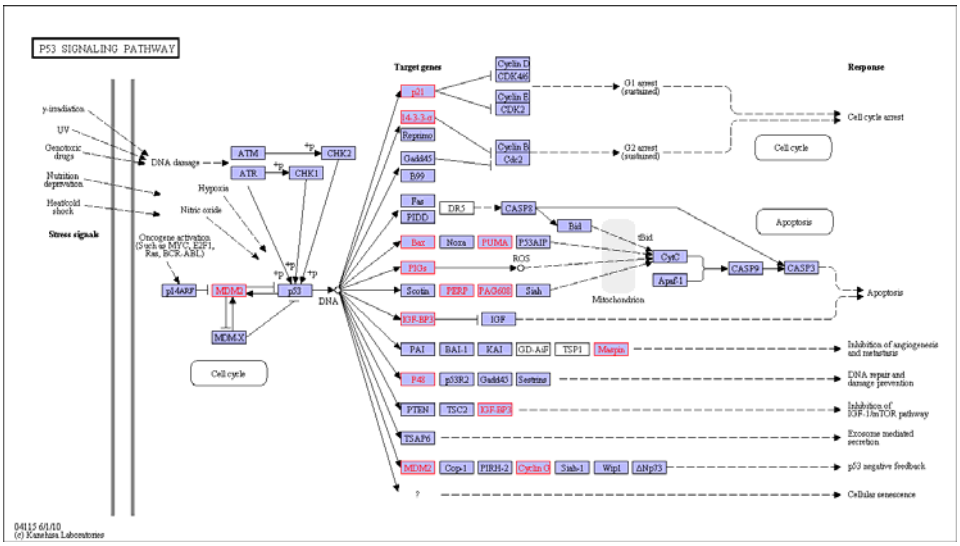

Figure 12: p53 signaling pathway. Genes for which an upregulation with a more than 1.4 fold change in expression was observed are colored in red.

Genes with more than 1.4 fold down- regulated expression present in both HPT1 and HPT2 made up a list of 593 genes. Top hits of the functional gene clustering were: DNA metabolic process/ response to DNA damage stimulus/ cellular response to stress/DNA repair; chromosome/ cytoskeleton and cell cycle/ mitosis/ cell division/ chromosome segregation/ M phase/ organelle fission. Analysis of the KEGG pathway results provided more detailed information about the genes whose transcription is down- regulated and annotated with cell cycle (Figure 13). Downregulation of gene expression can be mainly observed for transcripts of the MCM (Mini- Chromosome Maintenance) complex, as well as for some Cdc (cell- division cycle) proteins, which are important during the S-Phase of the cell cycle. This downregulation of genes functioning in the cell cycle progression and upregulation of genes related to the cell cycle arrest and apoptosis is an interesting observation given that the post-tetraploid cells were derived from chromosomally unstable tetraploid cells.

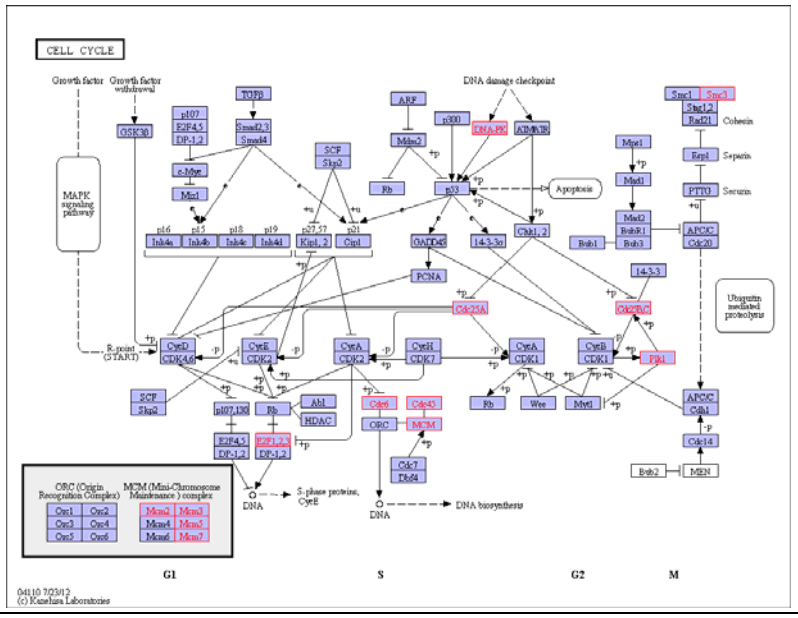

Figure 13: KEGG cell cycle pathways. Genes for which a downregulation with a more than 1.4 fold change in expression was observed are colored in red.

3.1.3.2D Annotation Enrichment Analysis

3.1.3.1. Comparison of HCT116 and RPE1 derived Cell Lines

To investigate the global properties of the transcriptional response to aneuploidy, I performed functional annotation enrichment. Thereby, an overall response of transcription on pathway levels could be assessed. A score ranging from -1 and 1 was built within the Perseus algorithm based on the fold change of the genes within each annotation. This score represents the overall up- or downregulation of a particular annotation. Using R, the annotation scores for each cell line were plotted in a scatter plot. For visualization, the annotations were clustered in R in larger categories (DNA, RNA, spliceosome, membrane, oxid metabolism, ER, anabolic metabolism, lysososome, carbohydrate and Golgi network) and colored according to the categories. Figure 14 shows annotation enrichment plots between the aneuploid cell lines HCT116 5/4, HCT116 3/3 and HCT116 H2B-GFP 5/4. Annotations which are plotted in the left lower and right upper quarter of the plot are similar up- or down- regulated. Data points in the other two quarters of the plot are not correlating in their up- or downregulation between the two compared cell lines.

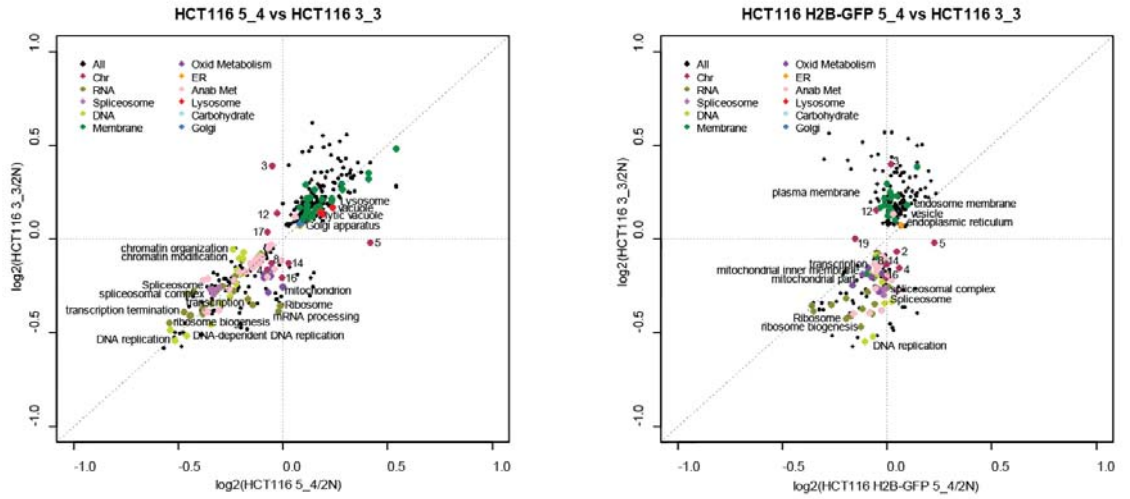

Figure 14: 2D annotation enrichment plots of the cell lines HCT116 5/4, HCT116 3/3 and HCT116 H2B-GFP 5/4. Data points were colored according to general categories (plot legend) in which the pathways were organized.

As a control for correct annotation enrichment in aneuploid cell lines serves the "chromosome" category. Cell lines with known whole chromosome aneuploidy should reveal an up- or downregulation in the entries linked to this chromosome. The annotation enrichment of the cell lines HCT116 5/4, HCT116 3/3 and HCT116 H2B-GFP 5/4 shows the expected up- regulated transcription for chromosome 3 and chromosome 5, respectively. In addition, other chromosomes are deregulated. In HCT116 3/3, the annotation for chromosome 12 is slightly up- regulated, whereas the annotations for chromosome 8, 16, 14, 4 and 2 are slightly down- regulated. In the cell line HCT116 5/4, the annotations for chromosome 17, 12 and 8 are enriched, but not strongly deregulated. Interestingly, the annotation of chromosome 19 is clearly down- regulated for HCT116 H2B-GFP 5/4.

The 2D annotation enrichment for HCT116 3/3 and HCT116 5/4 results in enrichment of similarly deregulated annotations. For both cell lines the transcription for genes annotated with DNA, thus transcription of genes involved in DNA replication and DNA organization processes and pathways, is down- regulated. Further, annotations related to the transcriptional processes are down-regulated in both cell lines, as well as annotations for genes involved in splicing processes. Moreover, mitochondria annotations are enriched, but although they are down- regulated in HCT116 3/3, only a minor downregulation for HCT116 5/4 can be observed. Besides similarities in down- regulated annotations, the enrichment indicates a similar transcriptional upregulation in enriched pathways. For both cell lines, membrane associated annotations are up- regulated. In addition, the Golgi apparatus associated annotations are enriched, as well as annotations for lysosome structures and processes.

The transcriptional deregulation of HCT116 H2B-GFP 5/4 shows the same trend as HCT116 5/4 and HCT116 3/3. However, the extent of the deregulation seems to be lesser for DNA and membrane associated annotations. Interestingly, spliceosome processes and pathways are not deregulated in this cell line.

In the following analysis, the complex aneuploid cell lines HPT1 and HPT2 were compared to the above described tri- and tetrasomic cell lines. As depicted in the representative plots in Figure 15 the deregulated transcription of HPT1 and HPT2 demonstrate a similar annotation enrichment as the cell lines HCT116 5/4, HCT116 H2B-GFP 5/4 and HCT 116 3/3. Consistent with the above described enriched annotations, membrane, lysosome, Golgi and endoplasmatic reticulum (ER) associated annotations are up- regulated. Further, DNA replication and organization, transcriptional processes and spliceosomal annotations are strongly down- regulated. An exception to the consistent transcriptional response in enriched annotations is that the mitochondria associated annotations are not deregulated in HPT1 and in contrast to HCT116 3/3 up- regulated in HPT2 (Appendix Figure 43).

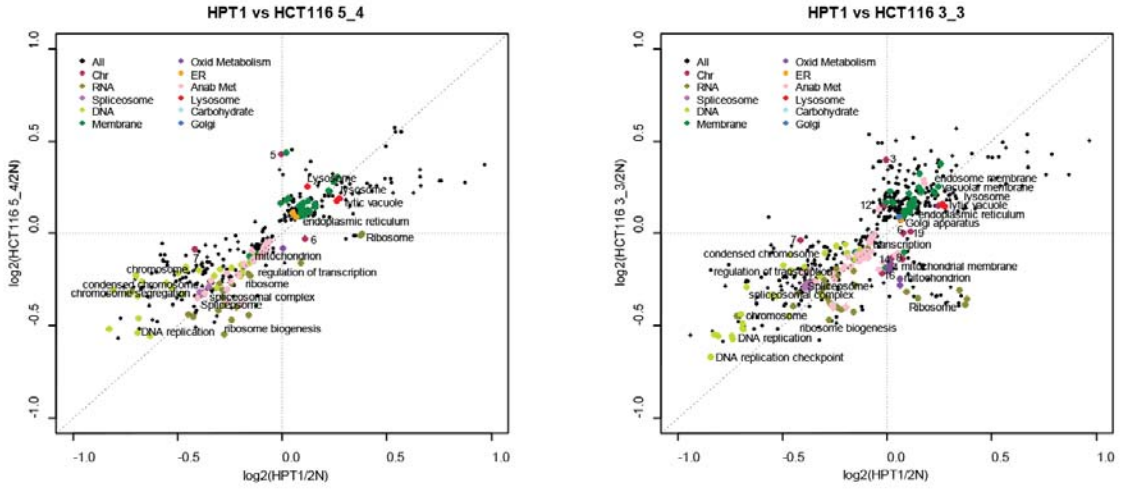

Figure 15: 2D annotation enrichment plots of HPT1 in comparison to HCT116 5/4 and HCT116 3/3. Data points were colored according to general categories (plot legend) in which the pathways were organized.

The visualization of the 2D annotation enrichment of the post- tetraploid cell line itself proves the observation of a similar transcriptional response of aneuploid cell lines on pathway level (Figure 16). For instance, an upregulation of lysosome and membrane associated annotations can be observed, as well as a downregulation for spliceosome, transcription and DNA processing related annotations. The comparison of the post- tetraploid cell lines indicates a different response of mitochondria related pathways to complex aneuploidy, as for HPT1 mitochondria related annotation are not deregulated and for HPT2 up- regulated. In addition, the ribosome related annotation is for HPT1 not deregulated, but for HPT2, as for the other aneuploid cell lines, down- regulated. Interestingly, for this cell lines with complex aneuploidy the enrichment of several chromosome annotations can be observed. In HPT1 transcription of chromosome 6 and 19 is up- regulated and for chromosome 7 strongly down-regulated. As for HPT2 a downregulation of transcription on chromosome 19 can be observed.

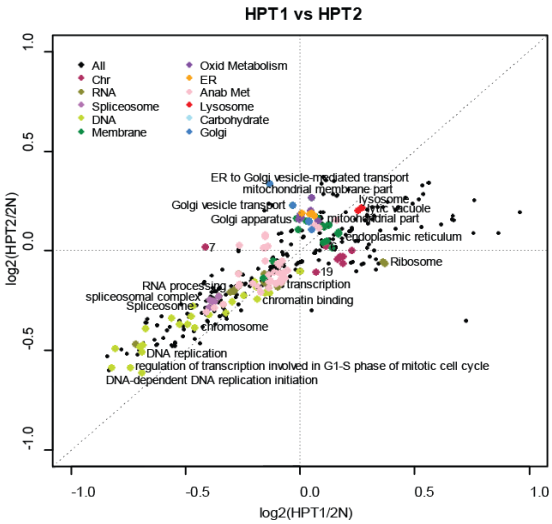

Figure 16: 2D annotation enrichment of the post- tetraploid cell lines HPT1 and HPT2. Data points were colored according to general categories (plot legend) in which the pathways were organized.

To investigate how different cell lines response to aneuploidy on the level of pathways, 2D annotation enrichment of fold change ratios of RPE1 12/3 5/3 and RPE1 H2B-GFP 21/3 was performed. As depicted in Figure 17, comparing those two RPE1 derived cell lines in 2D annotation enrichment revealed similar enriched pathways as for HCT116 derived cell lines. In line with the above described results, Golgi and ER related pathways are up- regulated. Transcription and DNA associated annotations are down- regulated. Notably, spliceosome and RNA related annotations are only down- regulated in RPE1 H2B-GFP 21/3 as observed in HCT116. For RPE1 12/3 5/3 gene expression annotated with spliceosome and mitochondria is up- regulated.

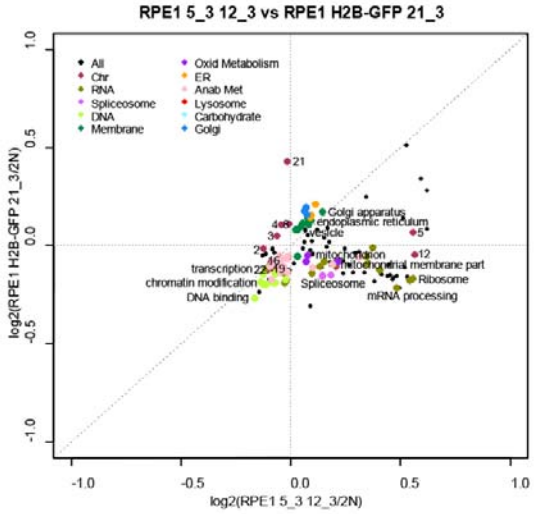

Figure 17: 2D annotation enrichment of RPE1 12/3 5/3 and RPE1 H2B-GFP 21/3. Data points were colored according to general categories (plot legend) in which the pathways were organized.

Comparison of enriched pathways between RPE1 and HCT116 derived cell lines revealed also an upregulation of the lysosome and membrane annotated gene expression (Figure 18). Also, the downregulation of DNA and transcription associated genes can be observed.

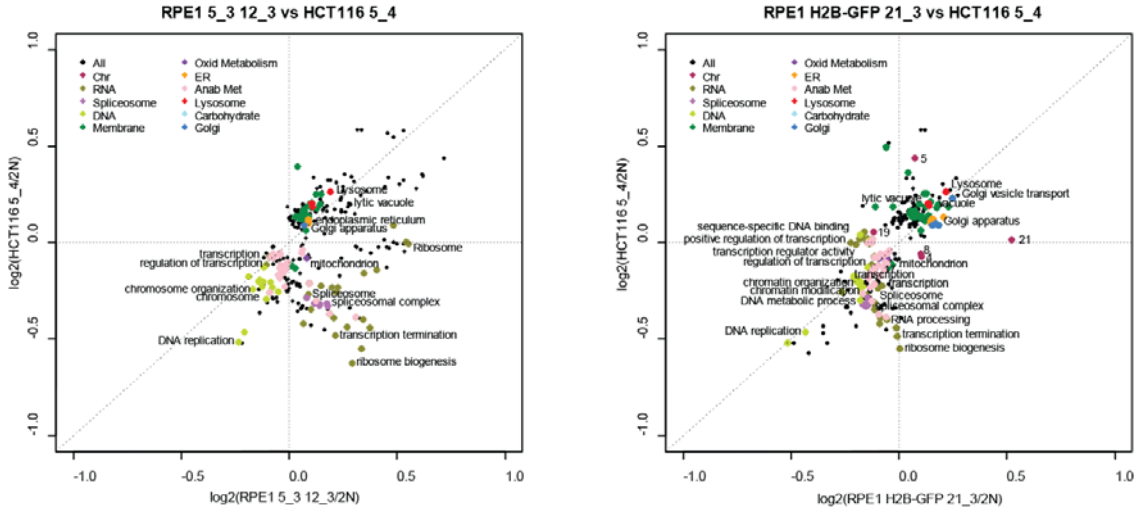

Figure 18: Representative 2D annotation enrichments between RPE1 derived aneuploid cell lines and HCT116 5/4, as representative for aneuploid HCT116 derived cell lines. Data points were colored according to general categories (plot legend) in which the pathways were organized.

To summarize, the comparison of RPE1 and HCT116 derived cell lines with different aneuploidies shows a similar transcriptional response on a pathway level. In all cell lines, DNA and RNA related annotations are down- regulated and lysosome, membrane, Golgi as well as ER associated annotations are up- regulated. Spliceosomal and mitochondrial pathways are not consistently deregulated between the cell lines.

3.1.3.2. Comparison of Published Transcriptome Data of Aneuploid Cell Lines

In addition to the transcriptional analysis of the RPE1 and HCT116 derived cell lines, gene expression of two other cell lines, namely colorectal cancer cell line (DLD1) and human embryonic cells (HE35), was analyzed. Expression data on DLD1 with the trisomies of chromosome 7, 3 and 13 was available. Upregulation of the corresponding chromosome annotations as validates the 2D annotation enrichment (Figure 19, Appendix Figure 44). In line with the results on HCT116 and RPE1, the same pathways are enriched and deregulated for DLD1 3/3 and 13/3. In fact, annotations for vacuole, Golgi and membranes are up- regulated, whereas DNA, spliceosome, mitochondria and RNA associated annotations are down- regulated. Only DLD1 7/3 shows no deregulation of ribosomal and mitochondria related annotation.

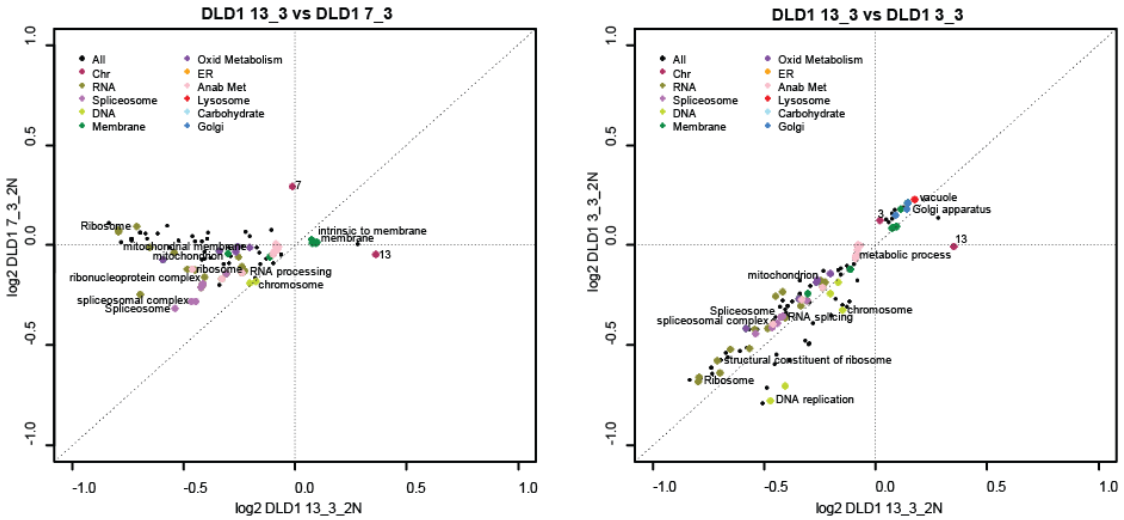

Figure 19: 2D annotation enrichment of DLD1 derived trisomic cell lines of chromosome 13, 3 and 7.

The analysis of the HE35 derived cell line with trisomy of chromosome 8 further confirmed that there is a global response to aneuploidy, which is independent of the specific cell line. As shown in Figure 20 in comparison to aneuploid HCT116 derived cell lines, the enriched annotations are the same as described for the pathway analysis on RPE1, HCT116 and DLD1 derived aneuploid cell lines. For instance, upregulation of lysosome, Golgi and ER annotations and down- regulated gene expression for DNA related processes and pathways are observed. Also in comparison with RPE1 derived cell lines, HE35 8/3 shows the characteristic pattern of enriched annotations (Appendix Figure 45). Despite this consistent results, the deregulation of gene expression related to mitochondrial and spliceosomal pathways is not consistent between the different aneuploid cell lines and can be observed as up- regulated for HE35 8/3.

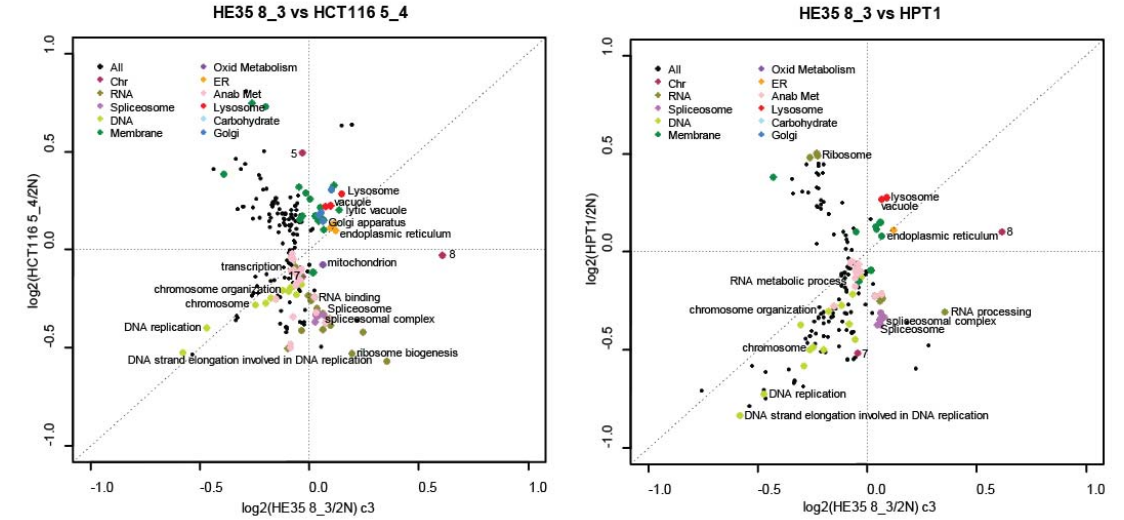

Figure 20: 2D annotation enrichment of HE35 8/3 in comparison with the cell lines HCT116 3/3, HCT116 5/4 and HPT1. For 2D enrichment with HCT116 3/3 see Appendix Figure 46.

3.1.4. Comparison of Transcriptional Aneuploidy Response to Stress Response

3.1.4.1. Comparison of Transcriptional Aneuploidy Response to Inflammatory Stress Response

To exclude that the global transcriptional response to aneuploidy on pathway level is due to a higher level of cellular stress in aneuploid cell lines, I analyzed mRNA expression data of HCT116 derived cell lines after various stress treatments. mRNA expression data of HCT116 after treatment with nitrogen oxide, hydrogen peroxide, hydroxyl urea and hypoxia were obtained from the omnibus database. These compounds are known to be cytotoxic and cause DNA damage or DNA replication arrest.

The 2D annotation enrichment analysis was performed by comparing stress-treated HCT116 with aneuploid HCT116 derived cell lines. Representative plots of the comparison between HCT116 5/4 and HCT116 expression data after treatment with hydrogen peroxide or growth under hypoxic conditions is shown in Figure 21. Whereas lysosome, Golgi, ER and membrane associated annotations are up- regulated for HCT116 5/4, these pathways are down- regulated in oxygen stressed HCT116 cells. In contrast to the downregulation of DNA, RNA, spliceosomal and mitochondrial related annotations terms for HCT116 5/4, the same pathways are enriched but up- regulated in response to oxygen stress. The same can be observed in comparison to post- tetraploid and other HCT116 derived aneuploid cell lines. HCT116 cells treated with nitrogene oxide and hydroxyurea are compared to HPT1 in the representative plot of Figure 21. As for the comparison of the transcriptional response to nitrogen oxide, enriched annotations are up- or down- regulated without any correlation to the response to aneuploidy. Expression response to hydroxyurea shows only the ribosome annotation up- regulated as it is for HPT1, but not for the other aneuploid cell lines. Thus it appears that the expression response to inflammatory stress shows no correlation to the response to aneuploidy.

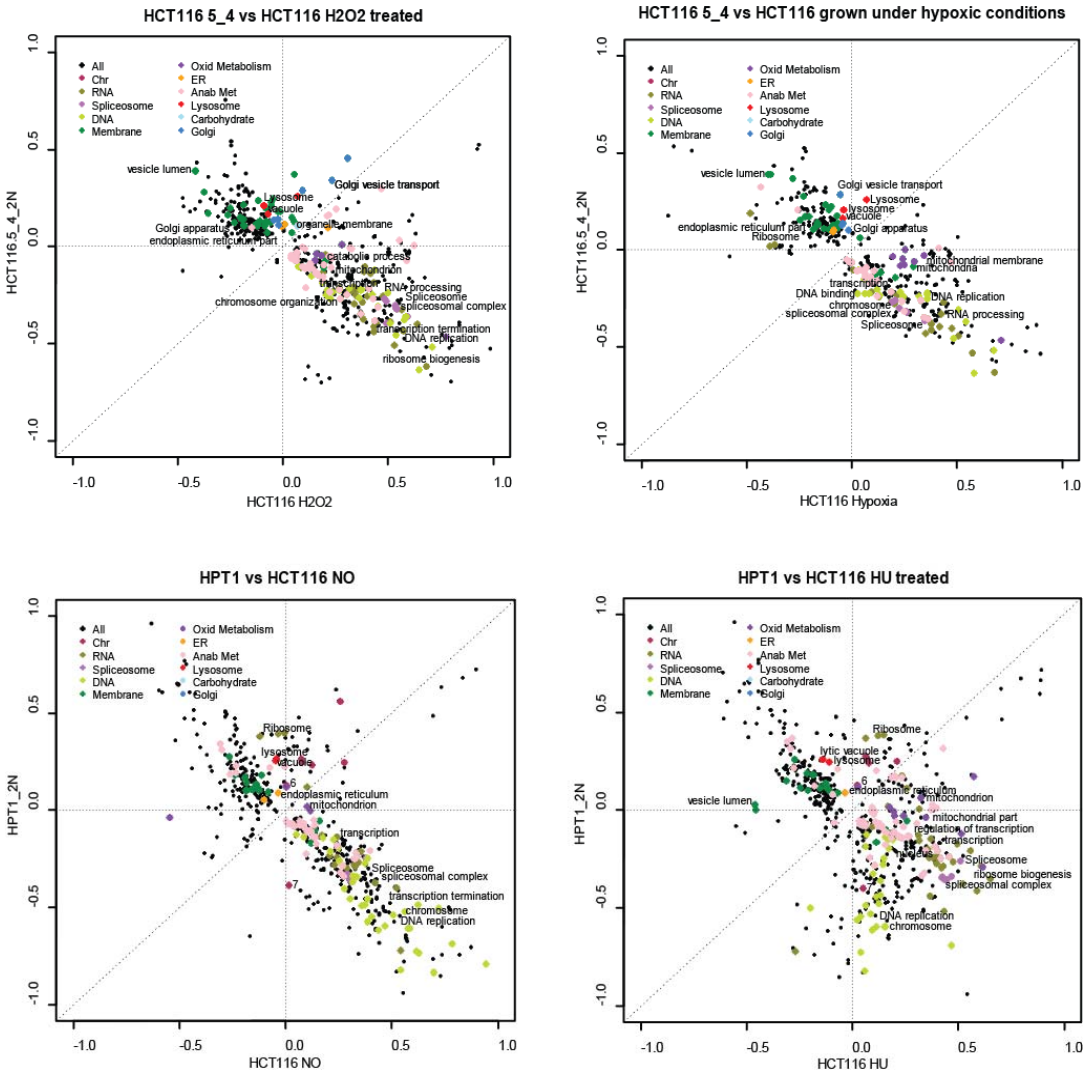

Figure 21: Representative 2D annotation enrichment plots between HCT116 treated with different compounds (NO, H_2O_2, HU and hypoxia) and HCT116 5/4 (as representative for aneuploid HCT116 derived cell lines) as well as HPT1 (representative for post- tetraploid cell lines).

To summarize the correlation of the transcriptional response in aneuploid cell lines and in stressed HCT116 cell lines a Spearman correlation coefficient was calculated in R. The calculated distances of the mRNA expression data between HCT116 5/4, 3/3, HCT116 H2B-GFP 5/4, HPT1, HPT2, RPE1 H2B-GFP 21/3, RPE1 12/3 5/3 and the HCT116 cell lines treated with nitrogen oxide, hydrogen peroxide, hydroxylurea and grown under hypoxic conditions were visualized in a correlation matrix map (Figure 22). The correlation from 1, high correlation, to 0, no correlation, is indicated by a color spectrum from blue via white to dark brown. The correlation matrix is clearly divided in a blue part, which represents the high correlation between the aneuploid cell lines, and a brown part, which indicates a low correlation between. No correlation can be observed for the nitrogen oxide treated HCT116 expression in comparison to the RPE1 and HCT116 derived aneuploid cell lines. Dark blue to light blue in the lower right of the correlation matrix represents the correlation of the expression patterns between the stress treated cell lines.

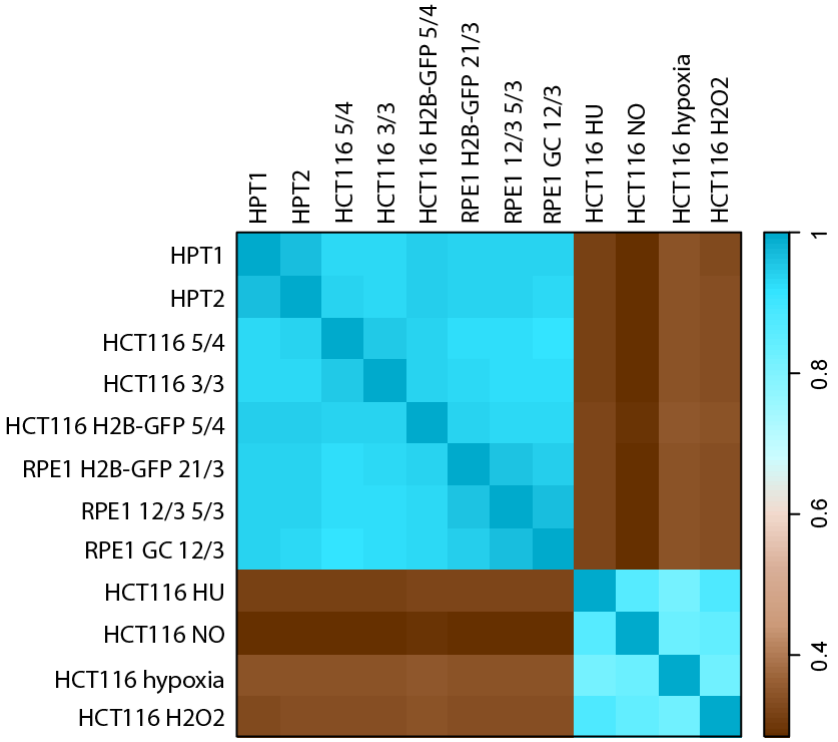

Figure 22: Correlation matrix map between the HCT116 and RPE1 derived aneuploid cell lines and the stress treated HCT116 cell lines. Correlation ranges from 1 to 0 indicating a high correlation (blue) and no correlation (dark brown).

3.1.4.2. Comparison of Transcriptional Aneuploidy Response to the Nutrition Stress Response

In addition to cellular stress responses described above, transcriptional response to nutrition stress was assessed. Therefore, I performed a 2D annotation enrichment analysis to compare the aneuploid cell lines and HCT116 grown under high or low glucose conditions. For both stress responses, a high number of enriched pathways could be observed. The pathways in response to high glucose levels are not strongly up- or down- regulated, but rather the values can be found near zero (Figure 23). Up- regulated pathways are DNA processes, spliceosome, and transcription related annotations, which is in contrast to the observed regulation of these pathways in aneuploid cell lines. some membrane related annotations are up- regulated, but not to the extent as observed in aneuploid cell lines. Furthermore, lysosome, Golgi and ER associated annotations are observed as down-regulated in contrast to their upregulation in response to aneuploidy.

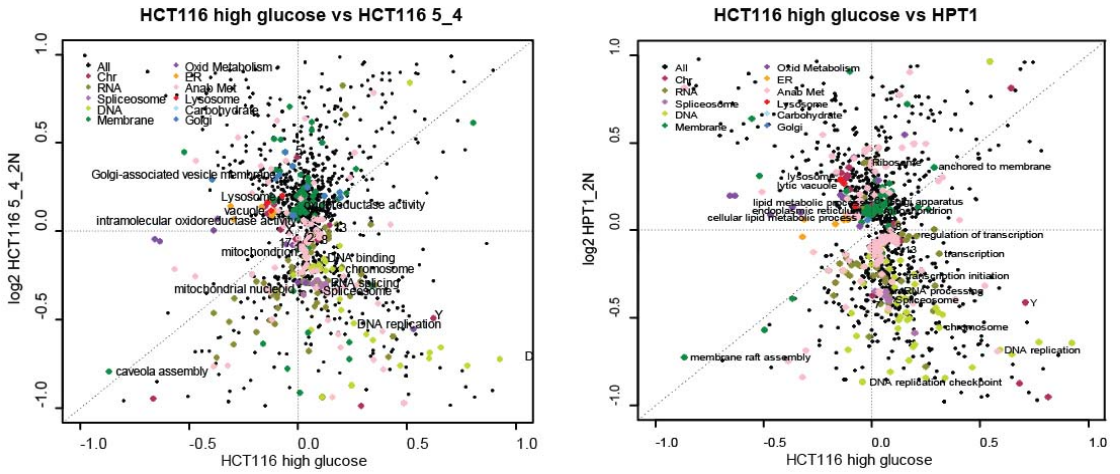

Figure 23: Representative 2D annotation enrichment plots of HCT116 mRNA expression grown on high glucose medium and HCT116 5/4 as well as HPT1. For 2D enrichment plot with HCT116 3/3 see Appendix Figure 47.

The response of HCT116 cells grown in media with low glucose was found to be more similar to the response to aneuploidy. As given in the representative plots in Figure 24, lysosome, Golgi, ER and membrane related pathways can be identified as up- regulated. Moreover, pathways related to DNA metabolism as well as transcription and spliceosome related annotation are similarly down-regulated.

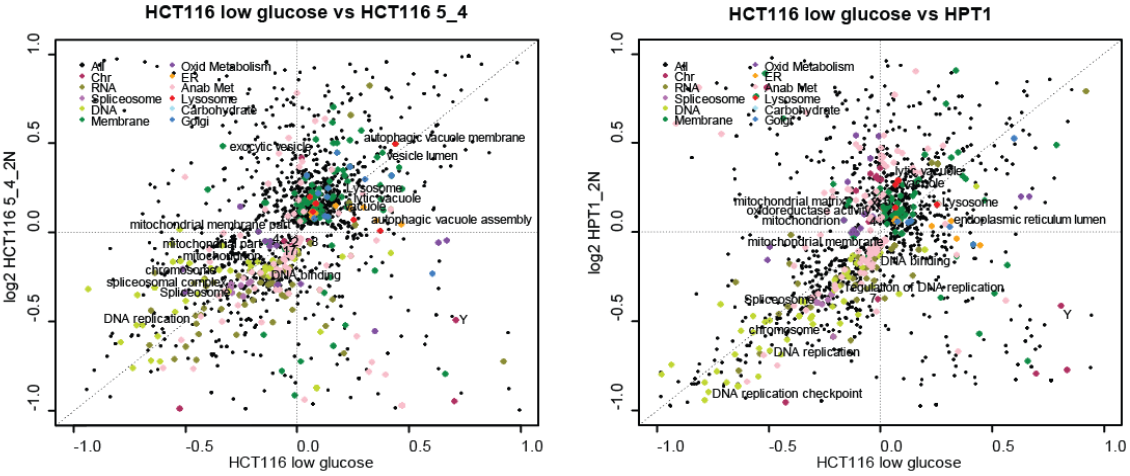

Figure 24: Representative 2D annotation enrichment plots of HCT116 mRNA expression grown on low glucose and HCT116 5/4 as well as HPT1. For 2D enrichment plot with HCT116 3/3 see Appendix Figure 47

Figure 25 presents the correlation matrix map between RPE1 and HCT116 derived aneuploid cell lines and HCT116 grown under low and high glucose conditions. Spearman correlation calculation underlines the low correlation between transcriptional response to high glucose and the response to aneuploidy. Surprisingly, the response to low glucose shows a low correlation to the response to aneuploidy as well. The 2D enrichment shows similarities between the transcriptional response to low glucose and to aneuploidy. But this was calculated on the level of significantly enriched pathways, whereas the Spearman coefficient is calculated from all gene entries. Thus, the

correlation matrix demonstrates a low correlation between the overall transcriptome of cells grown in media with low glucose and aneuploid cells

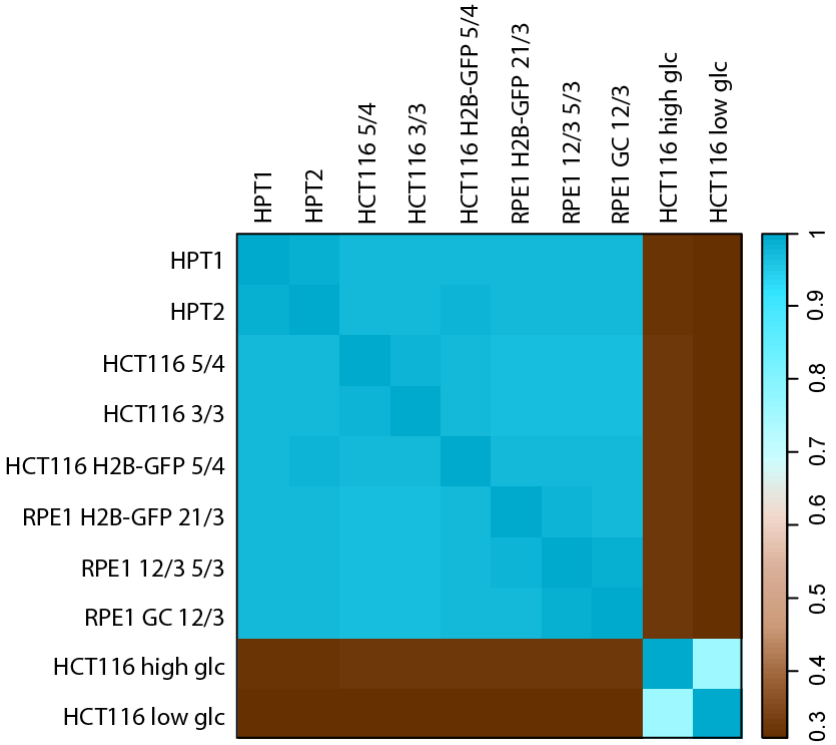

Figure 25: Correlation matrix map of HCT116 and RPE1 derived aneuploid cell lines and HCT116 cell lines grown under high and low glucose conditions. Correlation ranges from 1 to 0 indicating a high correlation (blue) and no correlation (dark brown).

3.2. Physiological Response to Aneuploidy

3.2.1. Autophagy in Aneuploid Cell Lines

3.2.1.1. p62 and LC3-II Levels

Pathway enrichment analysis revealed a global upregulation for lysosome and vesicle metabolism. This observation might reflect activation of the autophagy pathway, which was suggested to balance the proteotoxic stress in aneuploid cells. To monitor autophagy in HCT116 and RPE1 derived aneuploid cell lines, LC3-II and p62 levels were detected by immunoblotting of cell lysates. Microtubule- associated protein light chain 3 (LC3) is a component of the autophagic machinery involved in the formation of the autophagosome (Mizushima et al. 2010). The isoform LC3-II is conjugated with phophatidylethanolamine and found at the autophagosomal membrane. Sequestosome-1 (p62) is a signaling adapter which binds to LC3, thereby playing a role in packing and delivering polyubiquitinated proteins to the autophagic pathway. Both proteins are widely used markers for autophagy. Cell lysates of cell cultures treated with bafilomycin A1 for 16 hrs and corresponding controls were separated by SDS- Page followed by western blot procedure (Figure 26). p62 was detected with a size of 62 kDa, GAPDH (loading control) at 38 kDa and LC3-II at 18 kDa. The cell lysates after bafilomycin treatment show an increase for the LC3-II levels in all cell lines.

This indicates the inhibition of the fusion between lysosomes and autophagosomes and is an important control for the experiment. Accumulation of autophagy markers alone does not always indicate a higher autophagic activity. It could also reflect an induction and/or a block in downstream steps of autophagosome maturation. Consequently, the differences in the levels of the marker in the bafilomycin treated control cells and untreated cells represent the amount of autophagosomes delivered for lysosomal degradation (autophagic flux). Comparing the LC3 levels, an increase of LC3-II in HCT116 H2B-GFP 5/4 compared to HCT116 H2B-GFP can be observed. For HPT1 and HPT2 an increase in LC3-II levels compared to HCT116 diploid cell line can be hardly seen. In comparison of RPE1 and the post- tetraploid cell line RPT1, no increase in the LC3-II can be observed.

The p62 levels show an increase in bafilomycin treated cells similarly as for the LC3-II levels, with exception of the RPT1 cell line. In comparison of the aneuploid cell lines with the diploid cell line, an obvious increase for HCT116 H2B-GFP 5/4 can be observed. For HPT1 and HPT2, a light p62 signal indicates a small increase in p62. No difference can be observed comparing RPE1 to RPT1 p62 levels. The p62 level indicates a higher level of autophagy in HCT116 5/4 and no increase in autophagy for the post- tetraploid cell lines. In contrast, the LC3-II only mirrors partly these observations, as an increase of LC3-II is very small for HCT116 H2B-GFP 5/4.

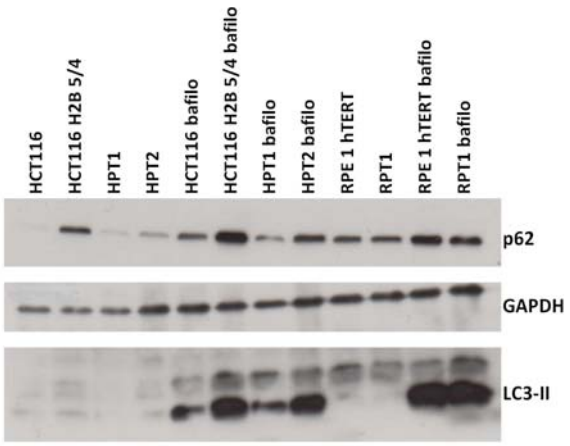

Figure 26: Representative western blot of HCT116 and RPE1 cell lysates. Cells were treated with 50pmol bafilomycin for 16h prior to cell lysis for with "bafilo" marked samples. Two cell extracts were analyzed (biological replicates).

For further investigation of the p62 level in aneuploid cell lines, I performed immunofluorescence detection of p62 in fixed cells. In addition, I analyzed cellular ubiquitin distribution in order to detect differences in the amount of poly- ubiquitinated protein aggregates and their targeting by p62. As depicted in Figure 27, bright speckles of p62 and ubiquitin indicated the successful immunofluorescence staining.

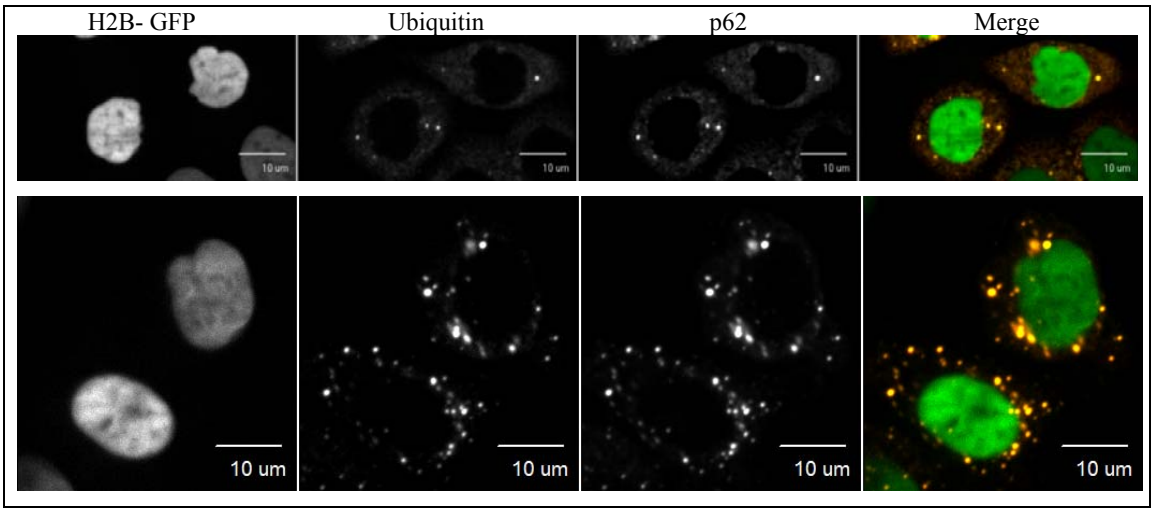

Figure 27: Representative immunostaining of p62 and ubiquitin in HCT116 H2B-GFP (above) and HCT116 H2B-GFP 5/4 below.

Speckles were counted by the Cell Profiler software. I normalized the p62 and ubiquitin levels to the corresponding diploid cell line by subtracting the median count and dividing by the median average deviation of the diploid cell line. The resulted z*- scores were plotted as bar plots with their mean of three replicates and standard error of the mean (Figure 28). After bafilomycin treatment the p62 counting shows a significant increase in p62 speckles. The only exception is HCT116 H2B-GFP 5/4, where no significant change in p62 levels can be observed. With no exception this is also true for the counting of the ubiquitin speckles. An accumulation of p62 after bafilomycin treatment indicates a successful inhibition of the autophagosome/ lysosome fusion and an otherwise efficient autophagic flux.

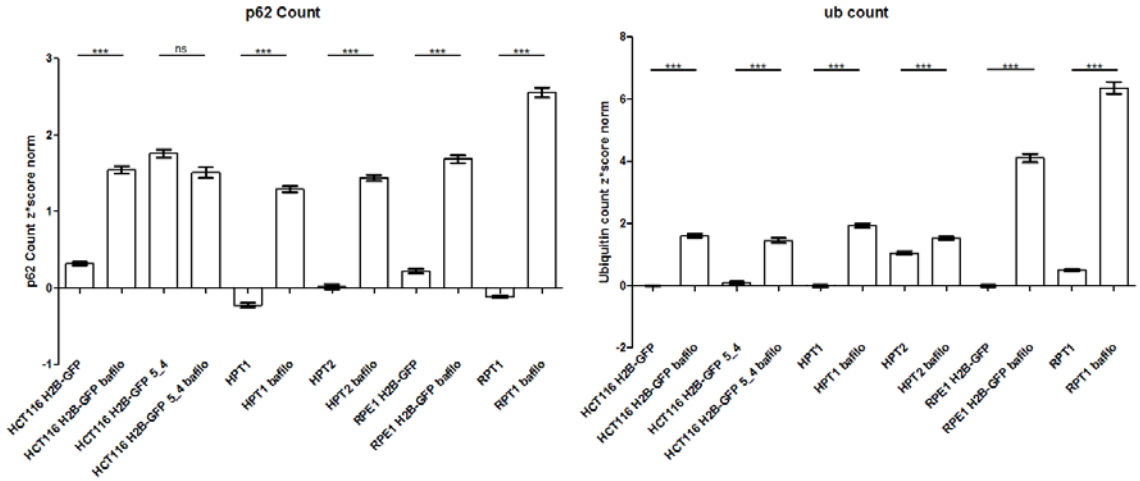

Figure 28: p62 and ubiquitin count after immunofluorescent detection in three experiments. Count was z*score normalized to the diploid cell line by subtracting the median count and dividing by the median average deviation of the diploid cell line. Bafilomycin treated cells were incubated for 16h with 50pmol bafilomycin prior to cell lysis.

In comparison of the untreated aneuploid cell lines against the diploid untreated cell line, a significant increase in p62 levels for HCT116 H2B-GFP 5/4, but a significant decrease for the post-tetraploid cell lines can be observed (Figure 29). The counting of the ubiquitin foci shows a different

result than the p62 counting. This is, only a small increase can be observed for HCT116 H2B-GFP 5/4. Surprisingly, HPT2 as well as RPT1 show a strong significant increase of the ubiquitin level.

The detected p62 levels are in line with the results from the western blot. Accumulation of p62 for HCT116 H2B-GFP 5/4 might present an increased autophagic activity. Post- tetraploid cells seem to exhibit no higher level of autophagy. However, the results for the ubiquitin detection are not in agreement with the p62 results. As illustrated in Figure 27, microscopy pictures show mostly a high colocalization of ubiquitin and p62. This can be explained by technical artifacts such as a spectral bleed through artifact. Neither the images nor the Cell Profiler quantification allow a conclusion about the ubiquitin concentrations in the cell lines.

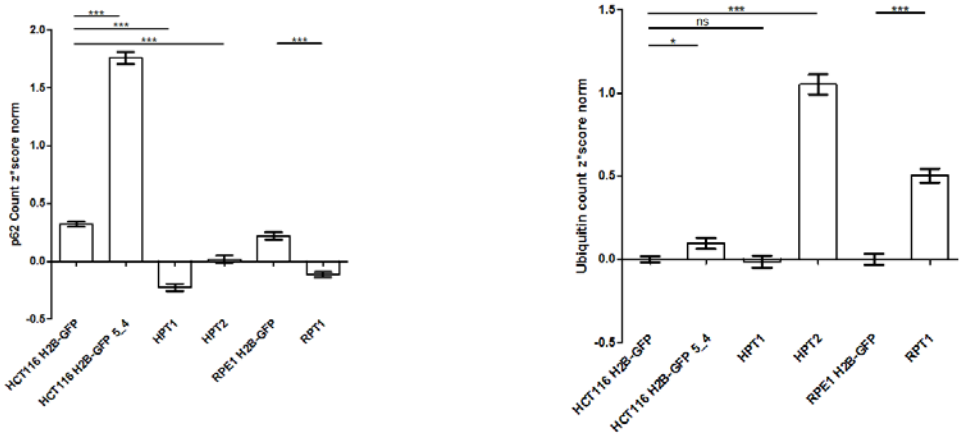

Figure 29: p62 and ubiquitin count after immunofluorescent detection in three experiments. Count was z*score normalized to the diploid cell line by subtracting the median count and dividing by the median absolute deviation of the diploid cell line.

3.2.1.2. Quantitative Changes of Lysosomes in Response to Aneuploidy

Microarray pathway and gene enrichment analysis revealed an upregulation of gene expression associated with lysosomes, lytic vacuoles and vacuoles. To quantitatively determine the changes between the diploid and aneuploid cell lines, I stained lysosomes on fixed cell slides followed by microscopy (Figure 30).

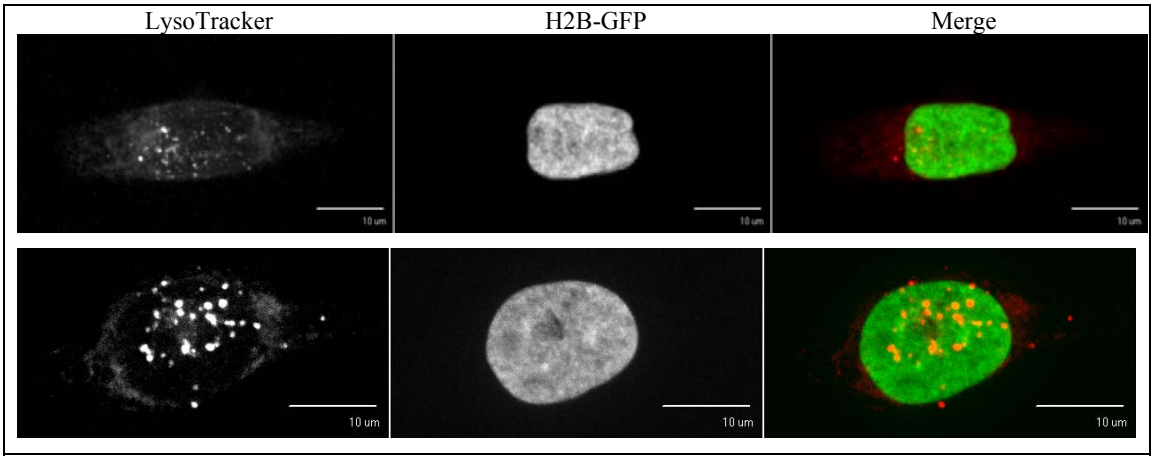

Figure 30: Representative LysoTracker staining of active and acidic lysosomes of HCT116 H2B-GFP (above) and HCT116 H2B-GFP 5/4 (below).

Lysosome speckles were counted by the Cell Profiler software. Due to different cell and nuclei sizes of the cell lines, I normalized the lysosome foci count to the cell area. Figure 31 provides information on the lysosome level per µm in four biological replicates. The result indicates a significant change in number of lysosomes for HCT116 H2B-GFP 5/4 compare to the diploid cell line, which is also visualized in the representative pictures in Figure 30. For the post- tetraploid cell lines no significant difference in comparison to the diploid cell line can be observed. This observation is surprising given that lysosome associated pathways were up- regulated in the gene expression analysis. On the other hand, the higher number of lysosomes in HCT116 H2B-GFP 5/4 and the unchanged number in the post- tetraploid cells reflects the autophagy level observed in other experiments.

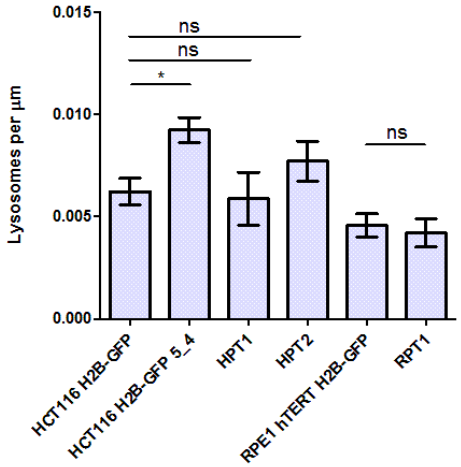

Figure 31: Lysosome count per µm of four biological replicates.

3.2.2. Quantitative Differences in Processing Bodies

Annotation enrichment analysis showed the expression of genes associated with transcriptional activities down- regulated in all aneuploid cell lines. Despite the similar down- regulated annotations related to transcription, analysis on single gene entries revealed that this is due to different deregulated genes. Only a few identical genes are transcriptionally deregulated in all HCT116 and RPE1 derived cell lines. As a global approach I assessed the level of processing bodies (P-bodies) in response to aneuploidy, which was shown to be proportional to the level of untranslated mRNA (Balagopal and Parker 2009). P-bodies are structures consisting out of proteins important for mRNA decay (Balagopal and Parker 2009). They are especially important for mRNA turnover and storage of translationally silenced mRNA. Together with stress granules, P-bodies are linked to translational quality control and regulation of gene expression (Buchan and Parker 2009; Mao et al. 2011).

I identified the P-bodies by immunostaining of LSM4, a part of the LSM1-7 complex, which is as decapping activator predominantly found in P-bodies. The bright stained dots in the representative picture (Figure 32) show the success of the immunostaining procedure.

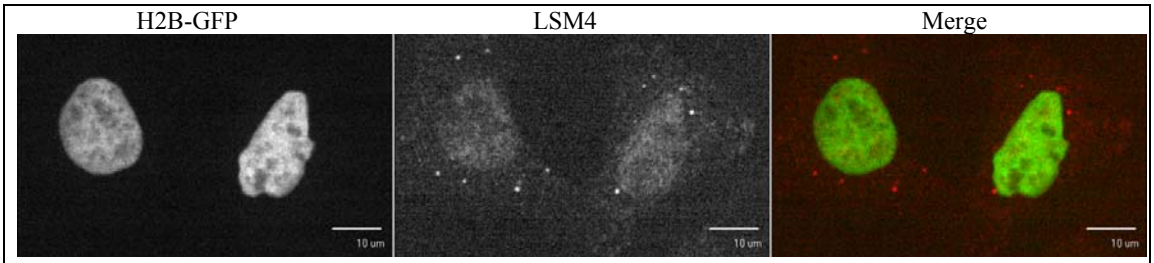

Figure 32: Representative immunostaining of Lsm4 which is predominantly found in P-bodies.

Counting of P-bodies using the Cell Profiler Software resulted in no differences between the number of P-bodies for each cell line in three biological replicates. Due to that, I assessed the percentage of cells which possess no, up to three or more than four P-bodies (Figure 33). Around 60% of the cells hold no staining for LSM4, which was true for all analyzed cell lines. 30% of the cells possess one to three P-bodies and 10% showed more than 4 P-bodies. Comparing the aneuploid cell lines to the diploid cell line, no differences in the P-bodies count could be observed. The difference in gene expression annotated with transcription is therefore not reflected in the quantity of P-bodies.

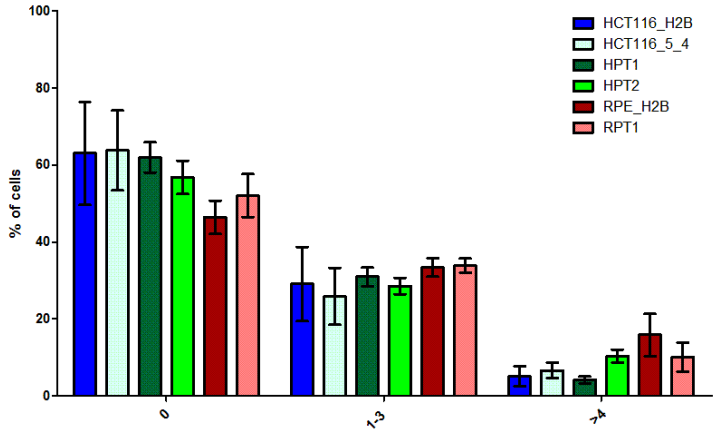

Figure 33: Percentage of cells with no, one to three or more than 4 P-bodies. Immunostaining of Lsm4 was carried out in three biological replicates.

3.2.3. Mitochondria Content and Morphology in Response to Aneuploidy

mRNA expression analysis revealed an enrichment of mitochondrial annotations. But together with the results on the gene level, it seemed for each cell line transcription of different mitochondria related genes is deregulated. Thus, we choose a microscopy approach to elucidate differences regarding mitochondria content and morphology between the aneuploid cell lines and the diploid cell lines. I stained the mitochondria with a chemical dye which is oxidized in active mitochondria and thereby becoming a fluorophore. Using Cell Profiler, a mean intensity of MitoTracker staining per cell was analyzed. Comparing the different cell lines, no differences in the mitochondria content could be observed. However, analysis of the images led to the observation that there are differences in the morphologies between the cell lines and between bafilomycin treated and untreated cells. Consequently, I assessed mitochondria morphology by categorizing the cells. The categories round

(fission), tubules (fusion) and an intermediate state were defined. Figure 34 provides the percentage of cells in each morphology category. Interestingly, all analyzed diploid HCT116 cells show a round morphology of the mitochondria, whereas the trend for bafilomycin treated cells is towards the tubule morphology (fusion). This was also observed for the other HCT116 derived aneuploid cell lines. Comparing the diploid HCT116 H2B-GFP cell line with HCT116 H2B-GFP 5/4 and HPT1, a general trend to more fusion of mitochondria can be observed. Nevertheless, the majority of cells possess round mitochondria morphology. For HPT2 the majority of the cells showed an intermediate morphology between fission and fusion.

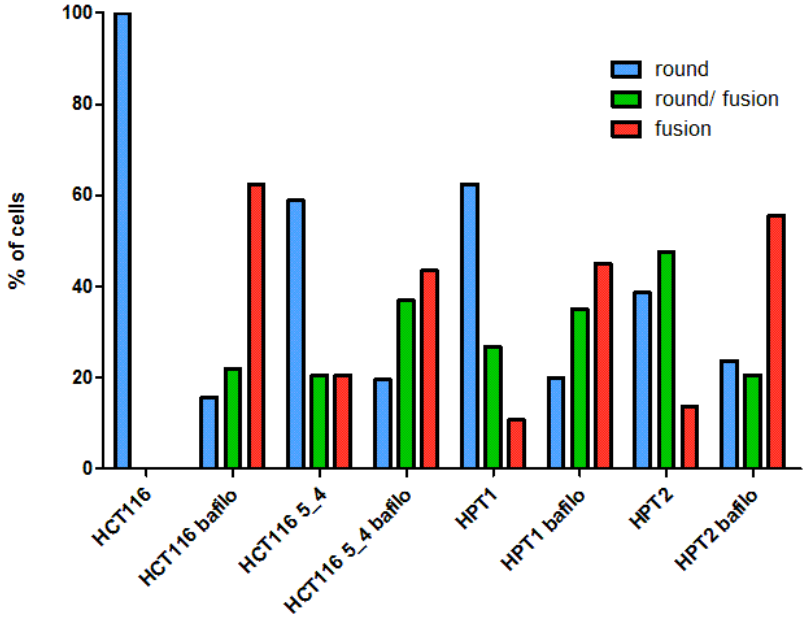

Figure 34: Percentage of cells with round, fusion or intermediate mitochondria morphology.

Representative images of mitochondria staining show HCT116 H2B-GFP with round mitochondria morphology and fusion morphology after bafilomycin treatment (Figure 35). The lower images depict HCT116 H2B-GFP 5/4 cells with round mitochondria morphology. It can be observed that the round mitochondria morphology is not as clearly structured as in the diploid cell line. Nevertheless, it can be distinguished from the fusion morphology of the bafilomycin treated HCT116 H2B-GFP 5/4 cells.

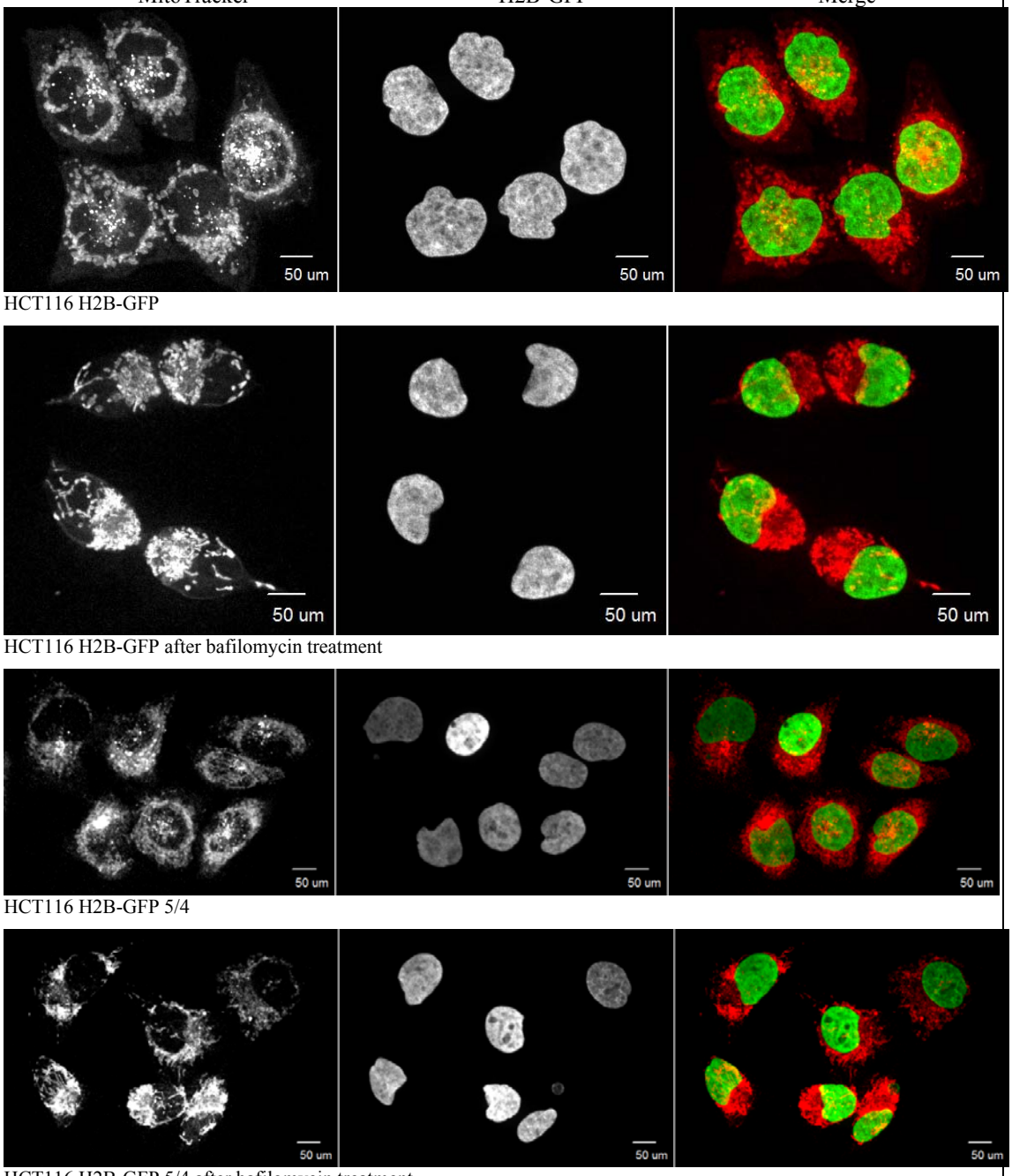

Figure 35: Mitochondria staining in HCT116 H2B-GFP and HCT116 H2B-GFP 5/4 cells, each untreated and after bafilomycin treatment. Tubule morphology of mitochondria after bafilomycin treatment can be observed, as well as a difference between the round morphology of HCT116 H2B-GFP and HCT116 H2B-GFP 5/4 cells.

Mitochondrial morphology reflects the stress level experienced by the cells. The altered morphology in the aneuploid cells towards fusion mitochondria indicates a higher metabolic or environmental stress in these cells. The trend towards fusion morphology after bafilomycin treatment might be due to the accumulation of proteins. As the autophagic pathway is inhibited by bafilomycin, proteins targeted for degradation accumulate. Hence, the different morphologies are due to different

causes, on the one hand it reflects the high stress level in aneuploid cells and on the other hand a stress caused by autophagy inhibition in bafilomycin treated cells.

3.2.4. DNA Damage

3.2.4.1. γH2AX Levels in Aneuploid Cells

Annotation enrichment analysis of mRNA expression data in response to aneuploidy revealed a downregulation of DNA, DNA replication and cell cycle associated pathways. This downregulation could reflect activation of checkpoint pathways in response to DNA damage. Therefore, it was of interest to assess the DNA damage level in aneuploid cells. Especially, observations of DNA damage in post- tetraploid cells were interesting, as they were derived from unstable tetraploid cell lines with high levels of CIN.

Phosphorylated histone H2AX (γH2AX) is a well-known marker of DNA double strand breaks. To assess the levels of DNA double strand breaks I performed γH2AX immunostaining. γH2AX foci were counted using Cell Profiler software with a custom made script. I applied z*-score normalization to the γH2AX foci count and median of three biological replicates was plotted in a bar plot (Figure 36). As a positive control I used cells treated with doxorubicin to induce DNA damage. Comparing untreated and treated cells in the right bar plot of Figure 36, a clear increase in γH2AX foci quantity can be observed in control cells treated with a DNA damaging agent. In comparison of the aneuploid cell lines with the diploid cell line, only for HCT116 H2B-GFP 5/4 and increase in γH2AX foci can be observed. The post- tetraploid cell lines possess no enhanced level of DNA damage marked by γH2AX.

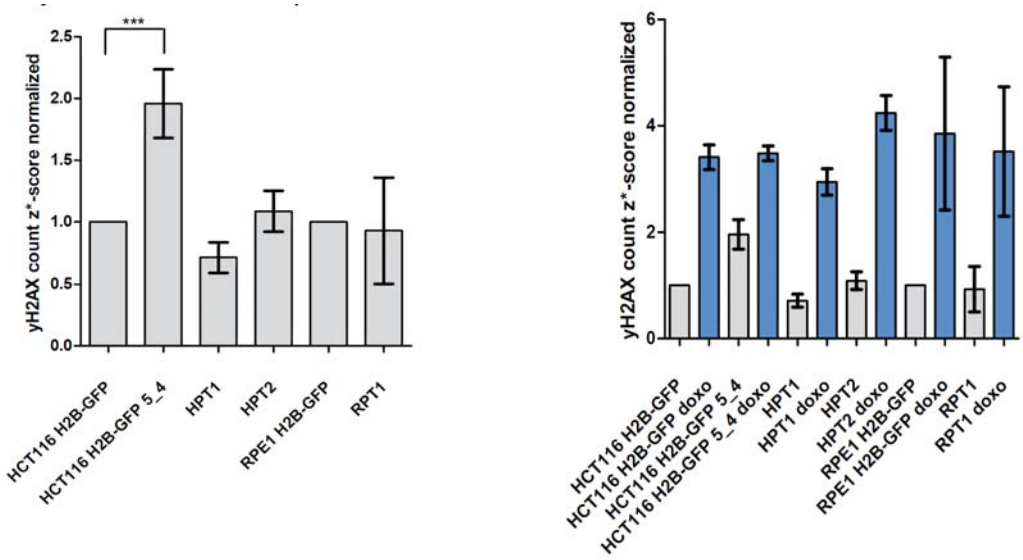

Figure 36: γH2AX foci count normalized to median and median absolute deviation of diploid cell line. Immunofluorescent experiments was repeated in three biological replicates.

Representative γH2AX immunostaining images for HCT116 H2B-GFP and HCT116 H2B-GFP 5/4 indicate the higher level of γH2AX in the aneuploid cell line (Figure 37).

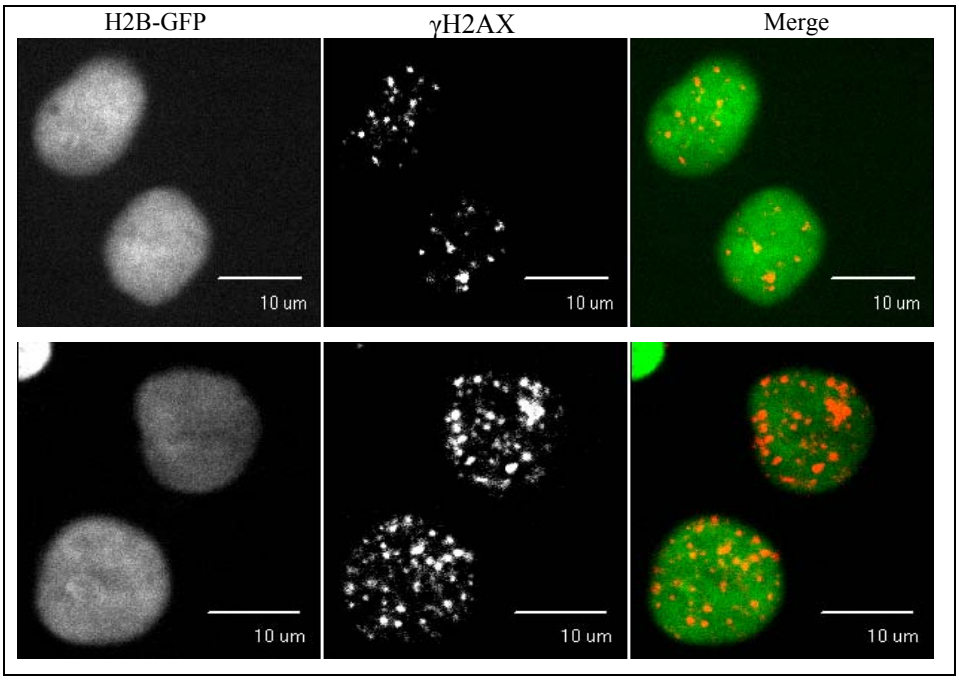

Figure 37: Representative images of γH2AX immunostaining for HCT116 H2B-GFP (above) and HCT116 H2B-GFP 5/4 (lower image).

3.2.4.2. RPA Immunofluorescence Experiments

Replication protein A (RPA) has an important function in DNA replication, repair, recombination and damage response pathway. RPA binds single- stranded DNA and its nuclear foci formation is strongly related to the DNA double- strand repair. I assessed RPA foci formation in aneuploid cells via immunostaining of RPA, followed by microscopy imaging with a 40x objective. As can be observed in Figure 38, RPA staining resulted in small high intensity speckles in the nucleus with a background staining.

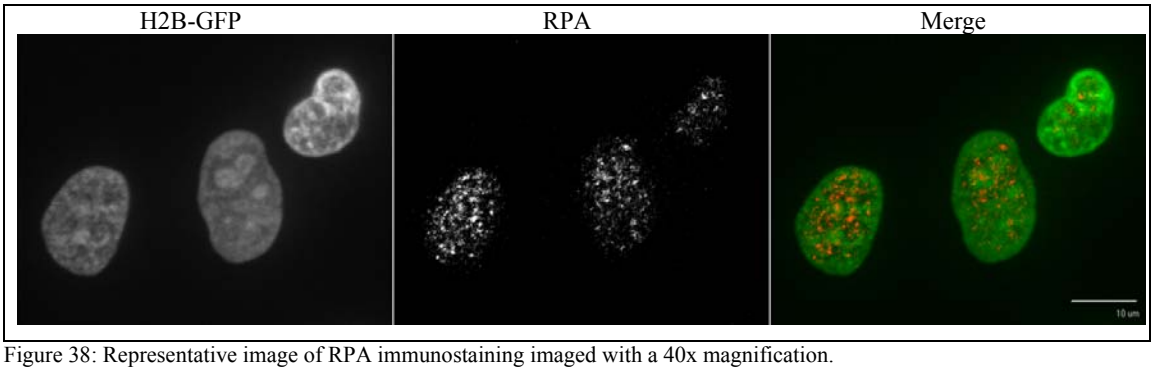

Figure 38: Representative image of RPA immunostaining imaged with a 40x magnification.

As it was not possible to clearly identify the RPA foci in the background noise, I analyzed the mean intensity of RPA immunostaining in the nucleus. For three biological replicates, mean and standard deviation of the mean intensity signal was plotted as depicted in Figure 39. In the right plot,

foci quantification in untreated cells can be compared to the foci count in doxorubicin treated cells. In the HCT116 H2B-GFP, cell line an increasing number of foci in the treated cells can be observed. But for the other cell lines no significant difference between untreated and treated cells was detected. Comparing the untreated cell lines HCT116 H2B-GFP and the aneuploid HCT116 H2B-GFP 5/4, HPT1 and HPT2 as well as the RPE1 H2B-GFP and RPT1, no differences in RPA foci count was observed. Since the DNA damage induced positive control shows no increase in RPA foci, it is not possible to validate the experiment and draw any conclusions. The experimental conditions have to be changed to observe a clear RPA response to DNA damage.

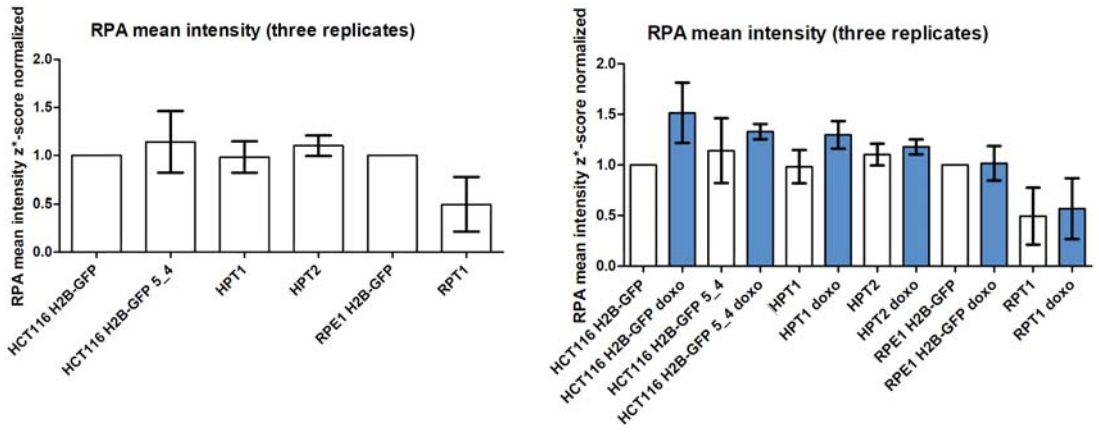

Figure 39: Mean intensity of RPA immunostaining with median and standard deviation plotted for three biological replicates. In the right blot, blue bars represent the mean intensity RPA signal of doxorubicin treated cells.

3.2.5. Lipid Droplets

Proteome analysis of HCT116 derived cell lines in response to bafilomycin treatment revealed an increase in protein levels associated with lipid metabolism (unpublished data). It was reported that turnover of intracellular deposits of lipid esters, lipid droplets (LD), is regulated by autophagy in a process called lipophagy. To investigate quantitative changes of LDs, I performed chemical staining followed by microscopy. LDs were counted using Cell Profiler software and the count was normalized to the cell area. Mean lipid droplet count of each cell lines for untreated and bafilomycin treated cells were visualized in a bar chart (Figure 40). For the cell lines HCT116 H2B-GFP and HCT116 H2B-GFP 5/4 no significant difference between the untreated and treated cells in lipid droplet number can be observed, whereas for the other cell lines HPT1, HPT2, RPE1 H2B-GFP and RPT1 a difference in lipid droplet count after bafilomycin treatment can be observed. Looking at the differences between the untreated cell lines, only for HCT116 H2B-GFP 5/4 a higher number of lipid droplets was counted. Between the diploid cell lines and the post- tetraploid cell lines no difference in lipid droplet counting was observed.

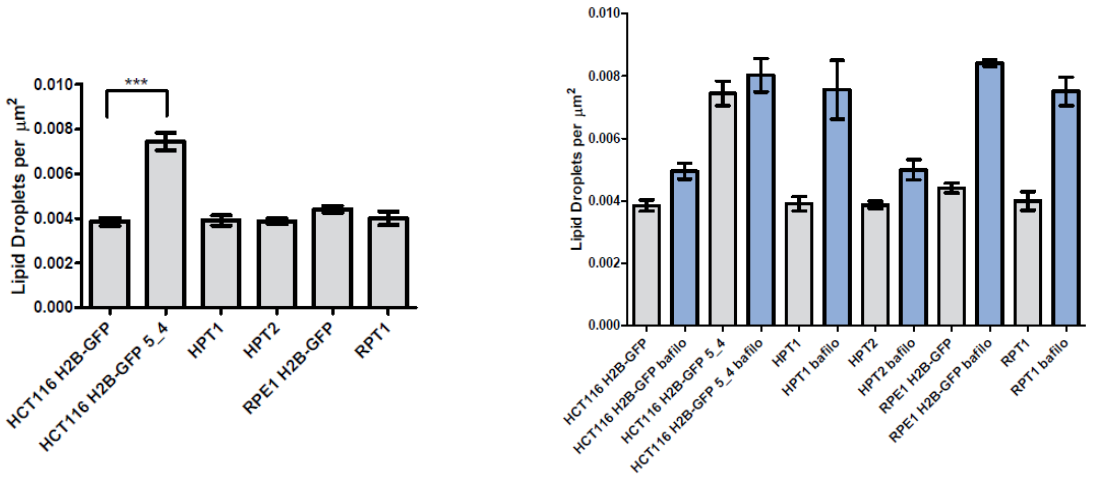

Figure 40: Lipid Droplets counting per µm comparing different aneuploid cell lines on the left. On the right: Comparison between Lipid Droplets amount in untreated and after 16h bafilomycin (50pmol) treatment.

Figure 41 shows representative images of the LD staining. A quantitative difference in LD between the diploid cell line HCT116 H2B-GFP and HCT116 H2B-GFP 5/4 can be observed.

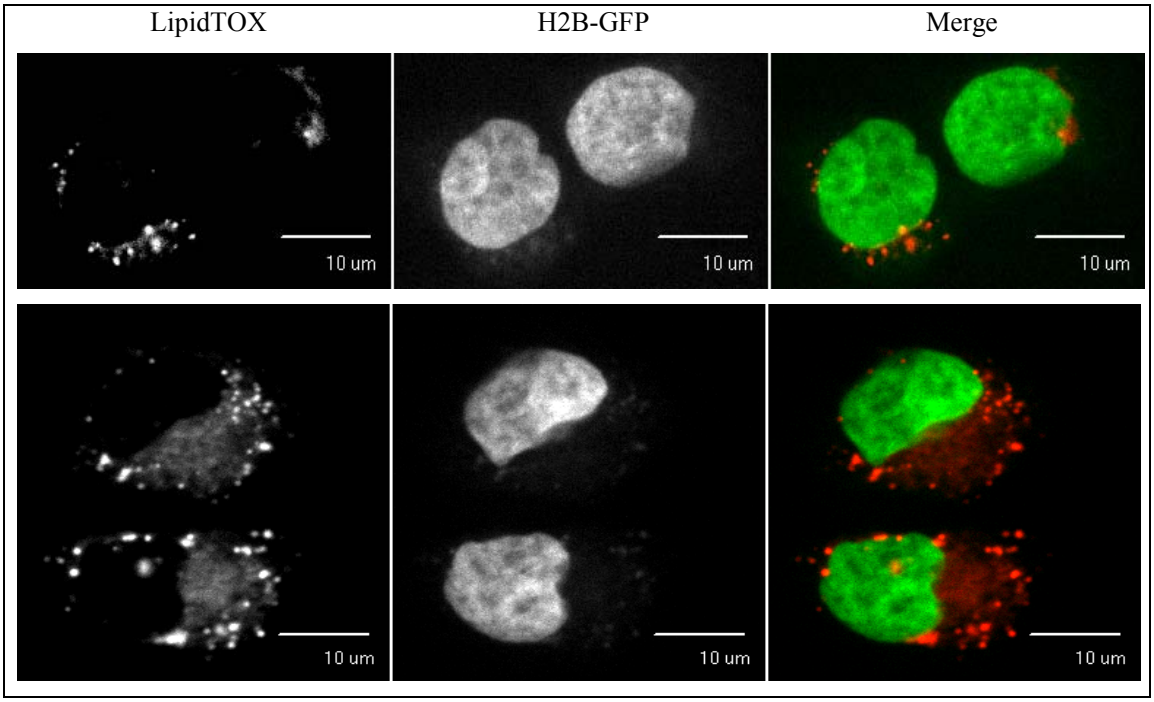

Figure 41: Representative staining of neutral lipids of HCT116 H2B-GFP (above) and HCT116 H2B-GFP 5/4 (lower picture).

An autophagy inhibition is expected to result in an increase of LD. As this is not true for HCT116 H2B-GFP and HCT116 H2B-GFP 5/4, the validation of the experiment is questionable. Besides that, the observed increase in LDs for HCT116 H2B-GFP 5/4 and the unchanged levels for the post-tetraploid cell lines is consistent with the autophagy levels observed in previous experiments.

4. Discussion

4.1. A Global Transcriptional Response to Aneuploidy

The mechanisms underlying the consequences of aneuploidy on cell physiology are poorly understood. To address this issue the alteration of gene expression in human trisomic cells was investigated in the past (Upender et al. 2004; Nawata et al. 2011). My master thesis provides a more complete understanding of the transcriptional consequences across different aneuploid cell lines. The aim was to investigate whether there is a global response to aneuploidy. I found that there is a distinct number of pathways consistently deregulated independently of the cell line and type of aneuploidy.

Transcriptome analysis on pathway level revealed a downregulation of annotations related to DNA and RNA metabolism pathways in all analyzed cell lines. These annotations can be linked to the progression of the cell cycle and may reflect cause or the consequence of the proliferation defects commonly found in aneuploid cells. This is in line with the recently published observations of transcriptional consequences of aneuploidy and moreover found to be conserved between species (Sheltzer et al. 2012). However, it is important to note that not all aneuploid cell lines show a prominent growth defect (unpublished work). Since these pathways are strongly down- regulated in all analyzed cell lines, it questions the proliferation defect as a putative cause of the observed down-regulated pathways.

I identified several enriched pathways globally up- regulated in response to aneuploidy, as For instance, annotation terms for lysosomes and lytic vacuoles. This finding adds weight to the notion that autophagy is activated in aneuploid cells to balance the protein overload caused by higher genome content (Stingele et al. 2012; Tang et al. 2011) reviewed in (Siegel and Amon 2012). Additionally, I found membrane, Golgi and ER associated annotations consistently up- regulated. Upregulation of these pathways likely reflects a general stress response in aneuploid cells which includes proteotoxic stress, energy stress and oxidative stress (Fulda et al. 2010). Perturbance of the energy metabolism in special disturbance of the Ca^{2+} homeostasis, oxygen or glucose deprivation can lead to ER stress (Malhotra and Kaufman 2011; Gorman et al. 2012). Both ER stress and proteotoxic stress lead to an accumulation of unfolded proteins and trigger the unfolded protein response pathway. The Golgi apparatus is closely linked to ER functions, thus the upregulation of these pathways might counterbalance cellular stresses in aneuploid cells.

We were interested whether the response to aneuploidy is a novel transcriptional response, or whether it triggers some previously recognized stress response pathway. Therefore, I compared the transcriptional response of aneuploidy to the responses to cellular stresses. I found that induced inflammatory and nutrition stress does not mimic the response to aneuploidy. However, closer inspection of the pathway enrichment between low glucose and aneuploidy revealed that a subset of pathways is similarly enriched. I found lysosomal and vesicle associated annotations both up-regulated. This finding can be attributed to a similar level of autophagy activation, as starvation is known to induce autophagy as an intracellular energy source (Altman and Rathmell 2012). Hence, it

further supports that up- regulated lysosome pathways can be linked to autophagy. Interestingly, also DNA replication and chromosome related annotations are similar down- regulated. Despite these similarities in some enriched pathways, the overall transcriptional response to the tested stress factors does not correlate with the response to aneuploidy. It seems likely that the stresses analyzed in my thesis are not similar to the stress caused by the unbalanced genome content in aneuploid cells. An additional explanation might be that aneuploidy results in multiple various stress types, which affects the cell physiology in a different way than a defined stress by treatment with one compound.

Although these analyses provide deep insights into the gene expression of aneuploid cells, no final conclusion of the translation to the protein level can be made. Regulatory effects such as proposed dosage compensation mechanisms can influence the response to aneuploidy on protein level (Stingele et al. 2012). However, pathways which are found globally up- or down- regulated in my studies were also found deregulated on proteome level (Stingele et al. 2012). In agreement with findings in my thesis, pathways associated with DNA and RNA metabolism were found down-regulated and membrane biogenesis, ER, Golgi and lysosome annotated pathways were found up-regulated.

In addition to the pathway analysis of the transcriptome data, my master thesis provides information on the deregulated transcription on single gene entries. I could show that different genes in the different aneuploid cell lines were responsible for up- or downregulation of an annotated pathway. In other words, overlap of gene entries between the aneuploids derived from RPE1 and HCT116 was found with only a few genes in common. I have shown that the up- regulated genes are predominantly transmembrane, plasma membrane or extracellular associated genes. In contrast down-regulated genes don´t fit into distinct groups. Nevertheless, these identified single genes could present useful markers for aneuploid cells. Further studies should confirm their altered expression by other methods such as real time PCR or immunofluorescence detection of corresponding proteins. It would be interesting to test the expression of those genes in even a wider range of aneuploid cell lines and also in cancer cells

4.2. Transcriptome of Post- Tetraploid Cells

This study describes the transcriptome of a human model cell line with complex aneuploidy. Due to their complex aneuploid genomic state it was interesting to observe, which chromosomes are predominantly altered in their expression. I found that both analyzed post- tetraploid cell lines show different chromosomes for which the gene expression was dysregulated. These findings further imply that the global transcriptional response on pathway level is not due to the specific chromosome aneuploidy but rather results from an altered genomic state per se. Beside the global pathway response, few enriched pathways differed in their deregulation between the two post- tetraploid cell lines. For instance, Golgi metabolism pathways were shown down- regulated in HPT1 and up-regulated in HPT2. Also the mitochondrial metabolism is deregulated to different extends. These

discrepancies in the pathway response can be caused by the different chromosomes which are deregulated in their expression.

One of the most interesting but also controversial finding is the regulation of the cell cycle progression and apoptosis related pathways. The transcriptional pathway analysis revealed downregulation of DNA and RNA metabolism, which is linked to phenotypic proliferation defects of aneuploid cell lines (Stingele et al. 2012). In post- tetraploid cells this is supported by the analysis on gene level, which demonstrated the downregulation of the expression of genes important for the cell cycle progression especially in the S- phase. Further, the upregulation of several target genes of the tumor suppressor p53 adds weight to this interpretation. These genes are known for their negative regulation of the cell cycle and apoptosis pathway activation (Giono and Manfredi 2006). However, unpublished experiments observed a rather minor growth delay of the post- tetraploids compared to the diploid cell lines. A hypothesis explaining this, is that during the in vitro evolution from the unstable tetraploid cells to the post- tetraploid cells darwinion selection would favor the predominance of those cells that managed to overcome the negative effects on proliferation. Importantly, MDM2 expression is up- regulated, which promotes p53 degradation. This might be a mechanism by which post- tetraploid cells attenuate the p53 dependent cell cycle arrest. One can speculate that in a selective process MDM2 overexpression served as an advantage over the cells with p53 limited proliferation. Nevertheless, this rise the question, why genes for negative regulation of the cell cycle and apoptosis are still up- regulated in their transcription. It would be interesting to further elucidate the mechanism by which the post- tetraploid cells adapt to the proliferation defects.

Post- tetraploid cells with their complex aneuploid genomic state provides a model for the aneuploid cells commonly found in cancer. Since the chromosomal instability driven variability and adaption of aneuploid cells is hypothesized to be important for tumorigenesis and cancer development, the evolution of aneuploid cells is of central interest. In this study transcriptome analysis of the post- tetraploid cell lines provides evidence for an evolution of these aneuploid cells. Thus, future studies with the focus on the evolutionary aspect of post- tetraploid cell lines would help to uncover the important players in a selection process of complex aneuploid cells.

4.3. Physiological Response to Aneuploidy in Cellular Assays

In this study, I investigated different biological aspects of aneuploidy in cellular assays.

Autophagy in aneuploid cell lines Since the transcriptome studies revealed a global upregulation for lysosome associated annotations, autophagy activity was investigated by western blot, immunofluorescence experiments and quantitative changes of lysosome structures. I found that autophagy is activated in the whole chromosome aneuploid cell line. This was indicated by a higher amount of lysosomal structures and increased levels of p62 in immunofluorescence experiments and western blot analysis. LC3 as an important autophagy marker showed in western blot analysis also a minor increased level compared to the diploid control cell line. These results are in line with previous findings suggesting activation of autophagy in HCT116 derived whole chromosome aneuploid cell

lines (Stingele et al. 2012). Conversely, the results of my studies suggest that in post- tetraploid cells autophagy is not prominently activated. In post- tetraploid cells not only the lysosomal content showed no significant increase, but also p62 was not found to be increased in immunofluorescence experiments. In the western blot analysis minor increase in p62 for the HCT116 derived post-tetraploids but not for the RPE1 derived post- tetraploid cell line indicates that the autophagy is not clearly activated. This discrepancy to the results from the pathway enrichment suggests a translational regulation of the autophagy pathway activation. There are several possible explanations why post-tetraploid cells don´t show activated autophagy. First, proteotoxic stress might be not as high as in the whole chromosome aneuploid cell lines. It is suggested that autophagy activation in aneuploid cells helps to balance protein overload resulting from the additional chromosome. But as post- tetraploids derived in a highly selective process from the unstable tetraploid cells- that is most of the subclones underwent apoptosis- these survived cells show probably a lower level of proteotoxic stress. On the other hand a post- tetraploid genomic state would rather suggest an even higher protein overload. Second, autophagy is also known as intracellular energy source and is activated as consequence of the high energy demand of aneuploid cells. In contrast, cancer cells express oncogenic kinases to stimulate intrinsic growth signals which in term facilitate nutrient uptake and aerobic glycolysis (DeBerardinis et al. 2008). As complex aneuploidy is often observed in cancer cells, it might be that the unstable post- tetraploid aneuploids adapt to a similar glycolytic metabolism and therefore don´t show autophagy activity.

Quantitative investigation of lipid droplets The turnover of intracellular deposits of lipid esters is associated with the activation of the autophagy pathway in whole chromosome aneuploid cell lines (Singh and Cuervo 2012). Previous proteome analysis showed an increase in proteins of the lipid metabolism after inhibition of autophagy with bafilomycin. In my thesis I found, that inhibition of the basal autophagy with bafilomycin in diploid and post- tetraploid cell lines indeed lead to an increase in lipid droplets. But important for the physiological characterization of the post- tetraploid cell lines, I found no differences in lipid deposits amount compared to the diploid cell line. Nevertheless, for the whole chromosome cell line HCT116 H2B-GFP 5/4 this study demonstrated a significant higher amount of lipid droplets. However, bafilomycin inhibition of autophagy does not lead to an additional increased accumulation of the lipid deposits in this cell line. It might be that this is a chromosome specific effect. This means that the four copies of chromosome 5 affect the lipid metabolism in a way that the turnover is not blocked by autophagy or explaining the increase of the lipid storage. To make further conclusions future studies should investigate the lipid droplets in other aneuploid cell lines.

DNA damage in aneuploid cell lines To investigate the link between globally down-regulated DNA metabolism in transcriptome studies, proliferation defects of aneuploid cells and CIN, DNA damage was assessed in the aneuploid cell lines. Interestingly, I demonstrated that post-tetraploid cell lines do not show an enhanced level of DNA double strand breaks compared to the diploid cells. In contrast, the whole chromosome aneuploid HCT116 H2B-GFP 5/4 was found with a

significant increase of DNA double strand breaks. Accumulation of DNA damage is known to induce cell cycle arrest pathways in a p53 dependent manner, resulting in proliferation defects (Li et al. 2010). The observation in post- tetraploid cells is in line with unpublished work in the laboratory of Anastasia Kuznetsova on CIN in tetraploid and post- tetraploid cells. In accordance no DNA damage could be observed in the post- tetraploid cell lines, but rather increased rates of chromosome segregation errors. Key aspects of the hypothesis are that CIN in post- tetraploid cells rather results from increased rates of chromosome segregation errors than from accumulation of DNA damage. High rates of CIN results in limited growth by p53 dependent cell cycle arrest (Fujiwara et al. 2005; Li et al. 2010). However, previous work demonstrated an attenuated p53 arrest in post- tetraploid cells. The mechanism by which p53 pathway is attenuated in the post- tetraploids remained so far elusive. Possibly the up- regulated expression Mdm2 (described above) could present a link in these speculations.

Quantitative difference in p-bodies Global downregulation of pathways related to transcriptional annotations made it interesting to investigate this processes. P- bodies are important in mRNA decay and store untranslated mRNA. The accumulation of p-bodies would be a first link to the down- regulated transcriptional metabolism. However, I found no quantitative differences in the number of p-bodies between the cell lines. Another class of mRNA foci are stress granules (Thomas et al. 2011). Assembly of these cytoplasmic aggregates is induced upon cellular stress and plays an important role of transcriptional regulation under such conditions (Kedersha and Anderson 2007; Hofmann et al. 2012). Future investigations focusing on the abundance of stress granules in aneuploid cell lines would be of interest.

Mitochondria in aneuploid cell lines In my master thesis annotation enrichment resulted in enriched and mostly down- regulated mitochondria annotations. I was able to show that not the mitochondrial content, but the morphology is different in the aneuploid cell lines compared to the diploid cell line. For the whole chromosome aneuploid cell line HCT116 H2B-GFP 5/4 I found a higher percentage of cells with fusion morphology of mitochondria. The dynamic of mitochondrial morphology plays an important role in the quality control of mitochondria in response to metabolic and environmental stress (Youle and van der Bliek 2012). Mitochondria with damaged DNA or proteins fuse to compensate for the defects. Fusion is also enhanced by activated autophagy in order to protect the mitochondria for autophagic clearance and support the higher demand for oxidative phosphorylation through the metabolism of lipids and proteins (Rossignol 2004; Rambold et al. 2011). Thus, fusion morphology of mitochondria in whole chromosome aneuploid cells may be caused by the high levels of metabolic and energetic stress as well as increased autophagic activity. In the post-tetraploid cell lines the morphology of the mitochondria was not found with a clear trend to fusion, but rather a mixture of different fusion and fission. This would add weight to previous evidence that post- tetraploid show lower level of cellular stress than whole chromosome aneuploids. Further it indicates, that the mitochondria metabolism is deregulated in complex way in post- tetraploid cells.

The mitochondria dynamics in cancer cells remain so far unclear (Zhao et al. 2012). Two mitochondrial properties are found in cancer. First, the Warburg effect which describes an increased dependency on the aerobic glycolysis as energy source and a negligible role of the mitochondrial oxidative phosphorylation (Scatena 2012). Changes in mitochondrial morphology are likely involved in the regulation of the cellular energy metabolism. Second, mitochondria play a central role in the induction of apoptosis by release of apoptosis inducing proteins. In cancer this processes are often compromised due to the activity the of oncogenic BCL2- family. Fission morphology of mitochondria is linked to extensive apoptosis and inhibition was shown to contribute to cancer cell resistance to chemotherapy. These findings demonstrate the importance of mitochondrial function and related morphology in cancer. Insight into the involvement of mitochondria functions in aneuploidy, especially in complex aneuploidy, presents an important field for further research.

In summary, there is a general physiological response to aneuploidy. But within this response the assays demonstrate that the response of the post- tetraploid aneuploid cell lines differs from the cell line with whole chromosome aneuploidy. Most of the phenotypes of whole chromosome aneuploid cell lines are likely caused by the metabolic and proteotoxic stress resulting from the unbalanced genome content. The results of my studies suggest that the post- tetraploid cell line shows reduced levels of cellular stresses. This can be explained by the origin of these aneuploid cells. Whole chromosome aneuploid cells have an artificial aneuploidy, which the cells are not adapted to. In contrast, the complex aneuploidy derived from a selective process, in which most of the unstable tetraploid cells underwent apoptosis. Only cells which adapted in a way, tolerating the altered genome content with minor negative effects on cell physiology, could outgrow and survive.

Appendix

Supplementary Figures

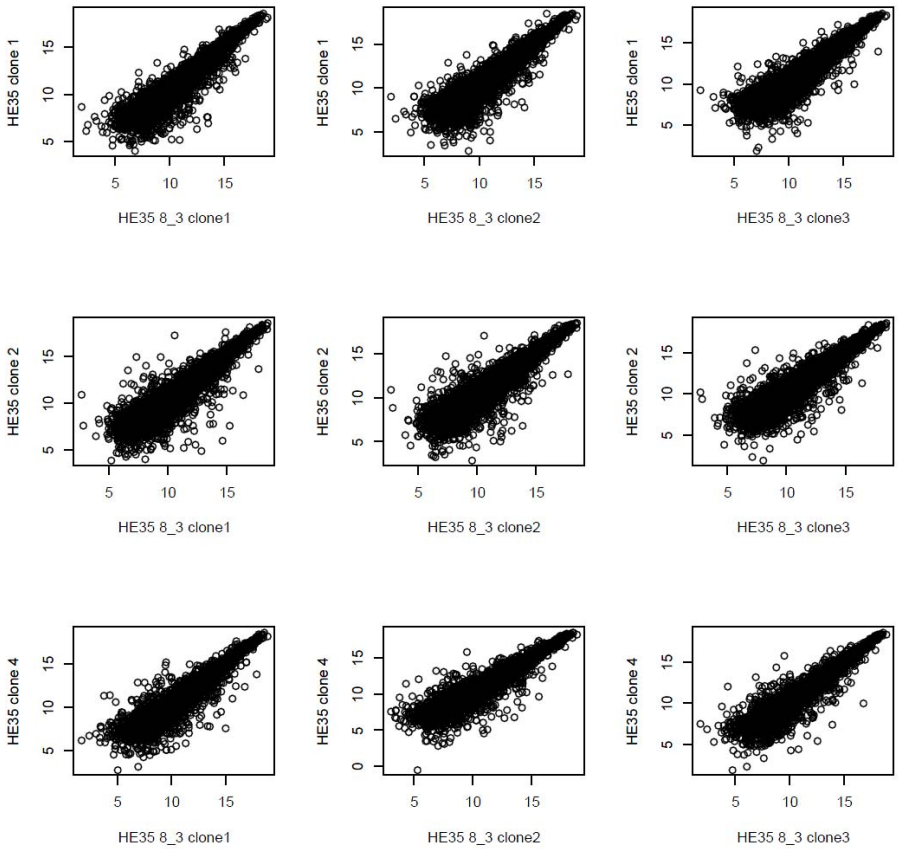

Figure 42: Scatterplot analysis of the three clones for the diploid HE35 cell line and the HE35 cell line trisomic in chromosome 8.

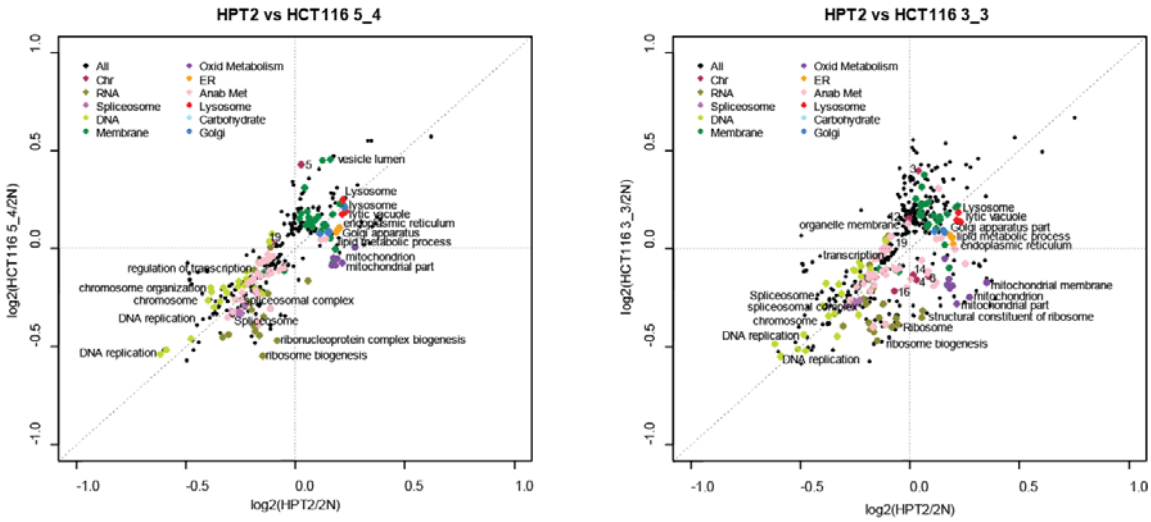

Figure 43: 2D annotation enrichment plots of HPT2 in comparison to HCT116 5/4 and HCT116 3/3. Data points were colored according to general categories (plot legend) in which the pathways were organized

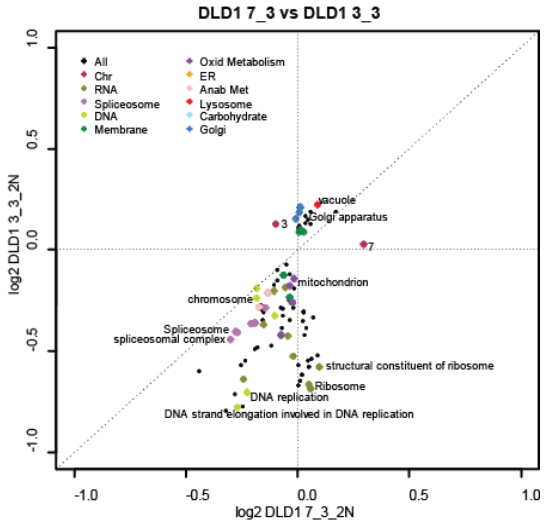

Figure 44: 2D annotation enrichment of DLD1 derived trisomic cell lines of chromosome 3 and 7.

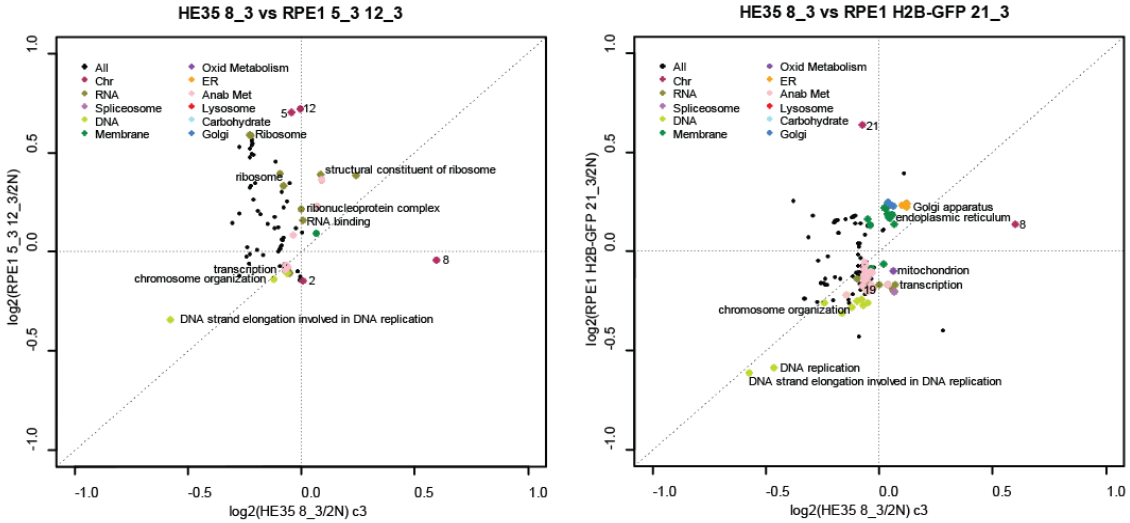

Figure 45: 2D annotation enrichment of HE35 8/3 and the cell lines RPE1 5/3 12/3 and RPE1 H2B-GFP 21/3.

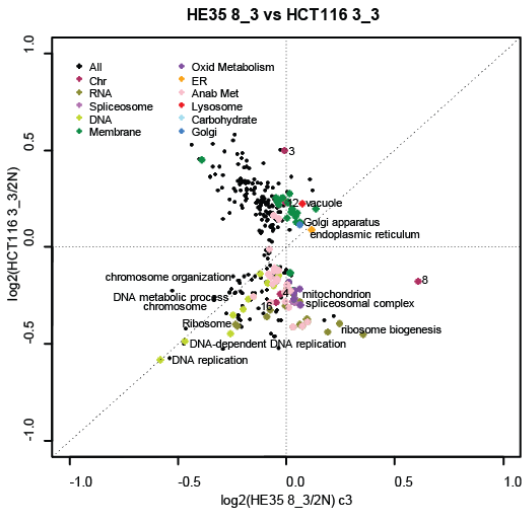

Figure 46: 2D annotation enrichment of HE35 8/3 and HCT116 3/3

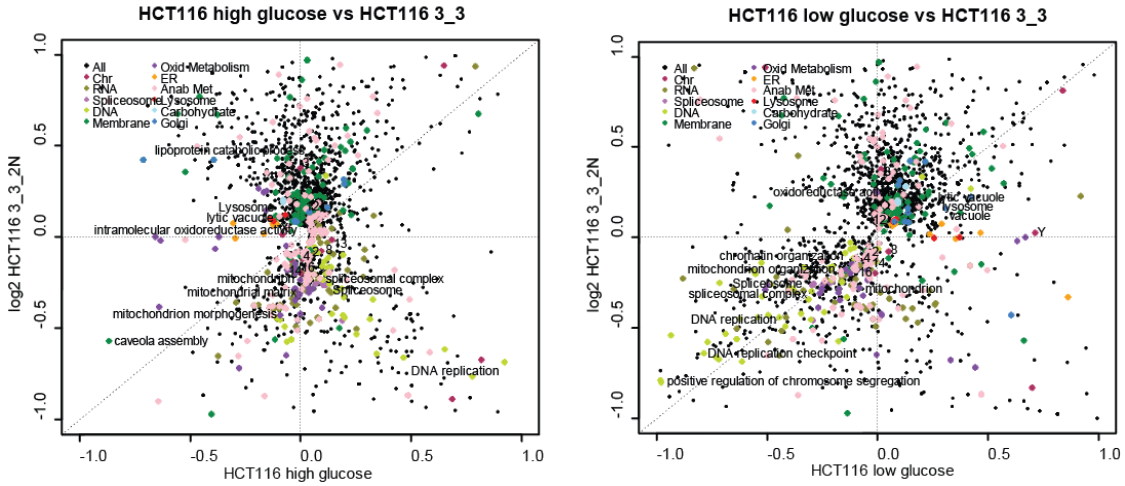

Figure 47: 2D annotation enrichment plots of HCT116 mRNA expression grown on high or low glucose medium and HCT116 3/3.

List of Figures

List of Tables

Abbreviations

Anaphase- Promoting Complex	APC
Centromere Protein E	CenpE
Chromosomal Instability	CIN
Copy Number Variations	CNV
Database for Annotation, Visualization and Integrated Discovery	DAVID
Diploid Colorectal Cancer Cell Line	DLD1
Endoplasmatic Reticulum	ER
Gene Ontology	GO
Golgi Apparatus	Golgi
Hour	H
HCT116 H2B-GFP derived post- tetraploid cell line	HPT1
Human Embryonic Cell Line	HE35
Human Colorectal Carcinoma Cell Line	HCT116
Kyoto Encyclopedia of Genes and Genomes	KEGG
Microtubule- associated protein light chain	LC3
Minutes	Min
Mouse Embryonic Fibroblasts	MEFs
Mosaic Variegated Aneuploidy	MVA
Nanometer	Nm
Non- Homologous End- Joining	NHEJ
Processing Bodies	p-bodies
Reactive Oxygen Species	ROS
Retinal Pigment Epithelial Cell Line	RPE1-hTERT (RPE1)
RPE1-hTERT H2B-GFP derived post- tetraploid cell line	RPT1
Spindle Assembly Checkpoint	SAC

References

'World Health Statistics 2012' http://www.who.int/gho/publications/world_health_statistics/EN_WHS2012_Part2.pdf>, updated 7 May 2012, accessed 27 Sep 2012.

Alberts, B. (2002), *Molecular biology of the cell* (4th edn., New York: Garland Science).

Albertson, D. G., Collins, C., McCormick, F. et al. (2003), 'Chromosome aberrations in solid tumors', *Nat Genet*, 34/4: 369–376.

Altman, B. J., and Rathmell, J. C. (2012), 'Metabolic Stress in Autophagy and Cell Death Pathways', *Cold Spring Harbor Perspectives in Biology*, 4/9: a008763.

Baker, D. J., Jin, F., Jeganathan, K. B. et al. (2009), 'Whole chromosome instability caused by Bub1 insufficiency drives tumorigenesis through tumor suppressor gene loss of heterozygosity', *Cancer Cell*, 16/6: 475–486.

Balagopal, V., and Parker, R. (2009), 'Polysomes, P bodies and stress granules: states and fates of eukaryotic mRNAs', *Current Opinion in Cell Biology*, 21/3: 403–408.

Barber, T. D., McManus, K., Yuen, K. W. Y. et al. (2008), 'Chromatid cohesion defects may underlie chromosome instability in human colorectal cancers', *Proceedings of the National Academy of Sciences*, 105/9: 3443–3448.

Benjamini, Y., and Hochberg, Y. (1995), 'Controlling the False Discovery Rate: A Practical and Powerful Approach to Multiple Testing'

Bolstad, B., Irizarry, R., Astrand, M. et al. (2003), 'A comparison of normalization methods for high density oligonucleotide array data based on variance and bias', *Bioinformatics*, 19/2: 185–193.

Bradford, M. M. (1976), 'A rapid and sensitive method for the quantitation of microgram quantities of protein utilizing the principle of protein-dye binding', *Anal Biochem*, 72: 248–254.

Brown, S. (2008), 'Miscarriage and its associations', *Semin Reprod Med*, 26/5: 391–400.

Buchan, J. R., and Parker, R. (2009), 'Eukaryotic Stress Granules: The Ins and Outs of Translation', *Molecular Cell*, 36/6: 932–941.

Burnette, W. N. (1981), '"Western blotting": electrophoretic transfer of proteins from sodium dodecyl sulfate--polyacrylamide gels to unmodified nitrocellulose and radiographic detection with antibody and radioiodinated protein A', *Anal Biochem*, 112/2: 195–203.

Callier, P., Faivre, L., Cusin, V. et al. (2005), 'Microcephaly is not mandatory for the diagnosis of mosaic variegated aneuploidy syndrome', *Am J Med Genet A*, 137/2: 204–207.

Cheadle, C., Vawter, M. P., Freed, W. J. et al. (2003), 'Analysis of microarray data using Z score transformation', *J Mol Diagn*, 5/2: 73–81.

Chen, G., Rubinstein, B., and Li, R. (2012), 'Whole chromosome aneuploidy: Big mutations drive adaptation by phenotypic leap', *Bioessays*, 2012: n/a.

Cimini, D., Howell, B., Maddox, P. et al. (2001), 'Merotelic kinetochore orientation is a major mechanism of aneuploidy in mitotic mammalian tissue cells', *J Cell Biol*, 153/3: 517–527.

Cleveland, W. S. (1979), 'Robust Locally Weighted Regression and Smoothing Scatterplots', *Journal of the American Statistical Association*, 74/368: 829–836.

Cleveland, W. S., and Devlin, S. J. (1988), 'Locally Weighted Regression: An Approach to Regression Analysis by Local Fitting', *Journal of the American Statistical Association*, 83/403: 596–610.

Colnaghi, R., Carpenter, G., Volker, M. et al. (2011), 'The consequences of structural genomic alterations in humans: genomic disorders, genomic instability and cancer', *Semin Cell Dev Biol*, 22/8: 875–885.

Cox, J., and Mann, M. (2008), 'MaxQuant enables high peptide identification rates, individualized p.p.b.-range mass accuracies and proteome-wide protein quantification', *Nat Biotechnol*, 26/12: 1367–1372.

Crasta, K., Ganem, N. J., Dagher, R. et al. (2012), 'DNA breaks and chromosome pulverization from errors in mitosis', *Nature*, 482/7383: 53–58.

Dai, W., Wang, Q., Liu, T. et al. (2004), 'Slippage of mitotic arrest and enhanced tumor development in mice with BubR1 haploinsufficiency', *Cancer Res*, 64/2: 440–445.

DeBerardinis, R. J., Lum, J. J., Hatzivassiliou, G. et al. (2008), 'The biology of cancer: metabolic reprogramming fuels cell growth and proliferation', *Cell Metab*, 7/1: 11–20.

Dennis, G., JR, Sherman, B. T., Hosack, D. A. et al. (2003), 'DAVID: Database for Annotation, Visualization, and Integrated Discovery', *Genome Biol*, 4/5: P3.

Draghici, S. (2002), 'Statistical intelligence: effective analysis of high-density microarray data', *Drug Discov Today*, 7/11: S55-63.

Duggan, D. J., Bittner, M., Chen, Y. et al. (1999), 'Expression profiling using cDNA microarrays', *Nat Genet*, 21/1 Suppl: 10–14.

Edgar, R. (2002), 'Gene Expression Omnibus: NCBI gene expression and hybridization array data repository', *Nucleic Acids Research*, 30/1: 207–210.

Emmert-Streib, F., and Dehmer, M. (2008), *Analysis of microarray data*: *A network-based approach* (Weinheim ;, Chichester: Wiley-VCH).

Fang, X., and Zhang, P. (2011), 'Aneuploidy and tumorigenesis', *Semin Cell Dev Biol*, 22/6: 595–601.

Farcomeni, A. (2008), 'A review of modern multiple hypothesis testing, with particular attention to the false discovery proportion', *Stat Methods Med Res*, 17/4: 347–388.

Fenech, M., Kirsch-Volders, M., Natarajan, A. T. et al. (2010), 'Molecular mechanisms of micronucleus, nucleoplasmic bridge and nuclear bud formation in mammalian and human cells', *Mutagenesis*, 26/1: 125–132.

Fujiwara, T., Bandi, M., Nitta, M. et al. (2005), 'Cytokinesis failure generating tetraploids promotes tumorigenesis in p53-null cells', *Nature*, 437/7061: 1043–1047.

Fulda, S., Gorman, A. M., Hori, O. et al. (2010), 'Cellular stress responses: cell survival and cell death', *Int J Cell Biol*, 2010: 214074.

Ganem, N. J., Godinho, S. A., and Pellman, D. (2009), 'A mechanism linking extra centrosomes to chromosomal instability', *Nature*, 460/7252: 278–282.

Ganem, N. J., Storchova, Z., and Pellman, D. (2007), 'Tetraploidy, aneuploidy and cancer', *Curr Opin Genet Dev*, 17/2: 157–162.

Gene Ontology Consortium (2004), 'The Gene Ontology (GO) database and informatics resource', *Nucleic Acids Research*, 32/90001: 258D.

Giono, L. E., and Manfredi, J. J. (2006), 'The p53 tumor suppressor participates in multiple cell cycle checkpoints', *J Cell Physiol*, 209/1: 13–20.

Gordon, D., Resio, B., and Pellman, D. (2012), 'Causes and consequences of aneuploidy in cancer', *Nat Rev Genet*, 13/3: 189–203.

Gorman, A. M., Healy, S. J. M., Jager, R. et al. (2012), 'Stress management at the ER: regulators of ER stress-induced apoptosis', *Pharmacol Ther*, 134/3: 306–316.

Graffelman, J., and van Eeuwijk, F. (2005), 'Calibration of Multivariate Scatter plots for Exploratory Analysis of Relations Within and Between Sets of Variables in Genomic Research', *Biom. J.*, 47/6: 863–879.

Gregory R. Warnes (2012), 'gplots: various R programming tools for plotting data', 2012.

Guo, Z., Kozlov, S., Lavin, M. F. et al. (2010), 'ATM activation by oxidative stress', *Science*, 330/6003: 517–521.

Gupta, S. (2000), 'Hepatic polyploidy and liver growth control', *Semin Cancer Biol*, 10/3: 161–171.

Hanks, S., Coleman, K., Reid, S. et al. (2004), 'Constitutional aneuploidy and cancer predisposition caused by biallelic mutations in BUB1B', *Nat Genet*, 36/11: 1159–1161.

Hanks, S., and Rahman, N. (2005), 'Aneuploidy-cancer predisposition syndromes: a new link between the mitotic spindle checkpoint and cancer', *Cell Cycle*, 4/2: 225–227.

Hassold, T., Abruzzo, M., Adkins, K. et al. (1996), 'Human aneuploidy: incidence, origin, and etiology', *Environ Mol Mutagen*, 28/3: 167–175.

Hassold, T., Hall, H., and Hunt, P. (2007), 'The origin of human aneuploidy: where we have been, where we are going', *Hum Mol Genet*, 16 Spec No. 2: R203-8.

Hekstra, D., Taussig, A. R., Magnasco, M. et al. (2003), 'Absolute mRNA concentrations from sequence-specific calibration of oligonucleotide arrays', *Nucleic Acids Res*, 31/7: 1962–1968.

Hofmann, S., Cherkasova, V., Bankhead, P. et al. (2012), 'Translation suppression promotes stress granule formation and cell survival in response to cold shock', *Mol Biol Cell*, 23/19: 3786–3800.

Hofmann, W.-K. (2006), *Gene expression profiling by microarrays*: *Clinical implications* (Cambridge: Cambridge University Press).

Holland, A. J., and Cleveland, D. W. (2009), 'Boveri revisited: chromosomal instability, aneuploidy and tumorigenesis', *Nat Rev Mol Cell Biol*, 10/7: 478–487.

Holland, A. J., and Cleveland, D. W. (2012), 'Losing balance: the origin and impact of aneuploidy in cancer', *EMBO Rep*, 13/6: 501–514.

Irizarry, R. A., Chi Wang, Yun Zhou et al. (2009), 'Gene set enrichment analysis made simple', *Statistical Methods in Medical Research*, 18/6: 565–575.

Iwanaga, Y., Chi, Y.-H., Miyazato, A. et al. (2007), 'Heterozygous deletion of mitotic arrest-deficient protein 1 (MAD1) increases the incidence of tumors in mice', *Cancer Res*, 67/1: 160–166.

Janssen, A., van der Burg, M., Szuhai, K. et al. (2011), 'Chromosome Segregation Errors as a Cause of DNA Damage and Structural Chromosome Aberrations', *Science*, 333/6051: 1895–1898.

Jemal, A., Bray, F., Center, M. M. et al. (2011), 'Global cancer statistics', *CA: A Cancer Journal for Clinicians*, 61/2: 69–90.

Jones, T. R., Kang, I., Wheeler, D. B. et al. (2008), 'CellProfiler Analyst: data exploration and analysis software for complex image-based screens', *BMC Bioinformatics*, 9/1: 482.

Kedersha, N., and Anderson, P. (2007), 'Mammalian stress granules and processing bodies', *Methods Enzymol*, 431: 61–81.

Kingsbury, M. A., Friedman, B., McConnell, M. J. et al. (2005), 'Aneuploid neurons are functionally active and integrated into brain circuitry', *Proc Natl Acad Sci U S A*, 102/17: 6143–6147.

Kops, G. J. P. L., Weaver, B. A. A., and Cleveland, D. W. (2005), 'On the road to cancer: aneuploidy and the mitotic checkpoint', *Nat Rev Cancer*, 5/10: 773–785.

Korn, E., Habermann, J., Upender, M. et al. (2004), 'Objective method of comparing DNA microarray image analysis systems', *Biotechniques*, 36/6: 960–967.

Kreil, D. P., and Russell, R. R. (2005), 'There is no silver bullet--a guide to low-level data transforms and normalisation methods for microarray data', *Brief Bioinform*, 6/1: 86–97.

Li, M., Fang, X., Baker, D. J. et al. (2010), 'The ATM-p53 pathway suppresses aneuploidy-induced tumorigenesis', *Proc Natl Acad Sci U S A*, 107/32: 14188–14193.

Long, A. D. (2001), 'Improved Statistical Inference from DNA Microarray Data Using Analysis of Variance and A Bayesian Statistical Framework. Analysis of global gene expression in escherichia coli k12', *Journal of Biological Chemistry*, 276/23: 19937–19944.

Mah, N., Thelin, A., Lu, T. et al. (2004), 'A comparison of oligonucleotide and cDNA-based microarray systems', *Physiol Genomics*, 16/3: 361–370.

Malhotra, J. D., and Kaufman, R. J. (2011), 'ER stress and its functional link to mitochondria: role in cell survival and death', *Cold Spring Harb Perspect Biol*, 3/9: a004424.

Mao, R., Zielke, C. L., Zielke, H. R. et al. (2003), 'Global up-regulation of chromosome 21 gene expression in the developing Down syndrome brain', *Genomics*, 81/5: 457–467.

Mao, Y. S., Zhang, B., and Spector, D. L. (2011), 'Biogenesis and function of nuclear bodies', *Trends in Genetics*, 27/8: 295–306.

Margaritis, T., Lijnzaad, P., van Leenen, D. et al. (2009), 'Adaptable gene-specific dye bias correction for two-channel DNA microarrays', *Mol Syst Biol*, 5: 266.

McClelland, S. E., Burrell, R. A., and Swanton, C. (2009), 'Chromosomal instability: a composite phenotype that influences sensitivity to chemotherapy', *Cell Cycle*, 8/20: 3262–3266.

Mitelman, F., Johansson, B., and Mertens, F. (2012), 'Mitelman Database of Chromosome Aberrations and Gene Fusions in Cancer', http://cgap.nci.nih.gov/Chromosomes/Mitelman, 2012.

Mizushima, N., Yoshimori, T., and Levine, B. (2010), 'Methods in Mammalian Autophagy Research', *Cell*, 140/3: 313–326.

Nadon, R., and Shoemaker, J. (2002), 'Statistical issues with microarrays: processing and analysis', *Trends Genet*, 18/5: 265–271.

Naef, F., and Magnasco, M. O. (2003), 'Solving the riddle of the bright mismatches: labeling and effective binding in oligonucleotide arrays', *Phys Rev E Stat Nonlin Soft Matter Phys*, 68/1 Pt 1: 11906.

Nawata, H., Kashino, G., Tano, K. et al. (2011), 'Dysregulation of gene expression in the artificial human trisomy cells of chromosome 8 associated with transformed cell phenotypes', *PLoS One*, 6/9: e25319.

Nishioka, T., Eustace, A., and West, C. (2012), 'Lysyl oxidase: from basic science to future cancer treatment', *Cell Struct Funct*, 37/1: 75–80.

Ogata, H., Goto, S., Sato, K. et al. (1999), 'KEGG: Kyoto Encyclopedia of Genes and Genomes', *Nucleic Acids Research*, 27/1: 29–34.

Pfau, S. J., and Amon, A. (2012), 'Chromosomal instability and aneuploidy in cancer: from yeast to man', *EMBO Rep*, 13/6: 515–527.

Plaja, A., Vendrell, T., Smeets, D. et al. (2001), 'Variegated aneuploidy related to premature centromere division (PCD) is expressed in vivo and is a cancer-prone disease', *Am J Med Genet*, 98/3: 216–223.

Prestel, M., Feller, C., and Becker, P. B. (2010), 'Dosage compensation and the global re-balancing of aneuploid genomes', *Genome Biol*, 11/8: 216.

Quackenbush, J. (2002), 'Microarray data normalization and transformation', *Nat Genet*, 32: 496–501.

Quintana, F. J. (2004), 'Functional immunomics: Microarray analysis of IgG autoantibody repertoires predicts the future response of mice to induced diabetes', *Proceedings of the National Academy of Sciences*, 101/suppl_2: 14615–14621.

R Development Core Team (2009), *R: A language and environment for statistical computing* (Vienna, Austria: R Foundation for Statistical Computing).

R. Gentleman and V. Carey and W. Huber and F. Hahne, 'genefilter: methods for filtering genes from from microarray experiments'.

Rajagopalan, H., and Lengauer, C. (2004), 'Aneuploidy and cancer', *Nature*, 432/7015: 338–341.

Rambold, A. S., Kostelecky, B., Elia, N. et al. (2011), 'Tubular network formation protects mitochondria from autophagosomal degradation during nutrient starvation', *Proceedings of the National Academy of Sciences*, 108/25: 10190–10195.

Rehen, S. K., McConnell, M. J., Kaushal, D. et al. (2001), 'Chromosomal variation in neurons of the developing and adult mammalian nervous system', *Proc Natl Acad Sci U S A*, 98/23: 13361–13366.

Ricke, R. M., van Ree, J. H., and van Deursen, J. M. (2008), 'Whole chromosome instability and cancer: a complex relationship', *Trends Genet*, 24/9: 457–466.

Rossignol, R. (2004), 'Energy Substrate Modulates Mitochondrial Structure and Oxidative Capacity in Cancer Cells', *Cancer Research*, 64/3: 985–993.

Sarkar, D. (2008), *Lattice*: *Multivariate data visualization with R* (New York ;, London: Springer Science+Business Media).

Satge, D., Sommelet, D., Geneix, A. et al. (1998), 'A tumor profile in Down syndrome', *Am J Med Genet*, 78/3: 207–216.

Scatena, R. (2012), 'Mitochondria and cancer: a growing role in apoptosis, cancer cell metabolism and dedifferentiation', *Adv Exp Med Biol*, 942: 287–308.

Schena, M. (1999), *DNA microarrays*: *A practical approach* (Oxford;, New York: Oxford University Press).

Schena, M., Shalon, D., Davis, R. W. et al. (1995), 'Quantitative monitoring of gene expression patterns with a complementary DNA microarray', *Science*, 270/5235: 467–470.

Schuster, E. F., Blanc, E., Partridge, L. et al. (2007), 'Correcting for sequence biases in present/absent calls', *Genome Biol*, 8/6: R125.

Schvartzman, J.-M., Duijf, P. H. G., Sotillo, R. et al. (2011), 'Mad2 is a critical mediator of the chromosome instability observed upon Rb and p53 pathway inhibition', *Cancer Cell*, 19/6: 701–714.

Sebastiani, P., Gussoni, E., Kohane, I. S. et al. (2003), 'Statistical Challenges in Functional Genomics', *Statist. Sci.*, 18/1: 33–70.

Sheltzer, J. M., Torres, E. M., Dunham, M. J. et al. (2012), 'Transcriptional consequences of aneuploidy', *Proc Natl Acad Sci U S A*, 109/31: 12644–12649.

Siegel, J. J., and Amon, A. (2012), 'New Insights into the Troubles of Aneuploidy', *Annu Rev Cell Dev Biol*, 2012.

Singh, R., and Cuervo, A. M. (2012), 'Lipophagy: Connecting Autophagy and Lipid Metabolism', *International Journal of Cell Biology*, 2012: 1–12.

Solomon, D. A., Kim, T., Diaz-Martinez, L. A. et al. (2011), 'Mutational Inactivation of STAG2 Causes Aneuploidy in Human Cancer', *Science*, 333/6045: 1039–1043.

Sotillo, R., Schvartzman, J.-M., Socci, N. D. et al. (2010), 'Mad2-induced chromosome instability leads to lung tumour relapse after oncogene withdrawal', *Nature*, 464/7287: 436–440.

Stafford, P., and Brun, M. (2007), 'Three methods for optimization of cross-laboratory and cross-platform microarray expression data', *Nucleic Acids Res*, 35/10: e72.

Stankiewicz, P., and Lupski, J. R. (2010), 'Structural Variation in the Human Genome and its Role in Disease', *Annu. Rev. Med.*, 61/1: 437–455.

Stenman, G., Andersson, M. K., and Andren, Y. (2010), 'New tricks from an old oncogene: gene fusion and copy number alterations of MYB in human cancer', *Cell Cycle*, 9/15: 2986–2995.

Stingele, S., Stoehr, G., Peplowska, K. et al. (2012), 'Global analysis of genome, transcriptome and proteome reveals the response to aneuploidy in human cells', *Mol Syst Biol*, 8.

Storchova, Z. (2012) (ed.), *The Causes and Consequences of Aneuploidy in Eukaryotic Cells* (InTech).

Storchova, Z., and Kuffer, C. (2008), 'The consequences of tetraploidy and aneuploidy', *J Cell Sci*, 121/Pt 23: 3859–3866.

Strimmer, K. (2008a), 'A unified approach to false discovery rate estimation', *BMC Bioinformatics*, 9: 303.

Strimmer, K. (2008b), 'fdrtool: a versatile R package for estimating local and tail area-based false discovery rates', *Bioinformatics*, 24/12: 1461–1462.

Sussan, T. E., Yang, A., Li, F. et al. (2008), 'Trisomy represses Apc(Min)-mediated tumours in mouse models of Down's syndrome', *Nature*, 451/7174: 73–75.

Tamari, M., Daigo, Y., Ishikawa, S. et al. (1998), 'Genomic structure of a novel human gene (XYLB) on chromosome 3p22--p21.3 encoding a xylulokinase-like protein', *Cytogenet Cell Genet*, 82/1-2: 101–104.

Tang, Y.-C., Williams, B. R., Siegel, J. J. et al. (2011), 'Identification of aneuploidy-selective antiproliferation compounds', *Cell*, 144/4: 499–512.

Tarca, A. L., Romero, R., and Draghici, S. (2006), 'Analysis of microarray experiments of gene expression profiling', *Am J Obstet Gynecol*, 195/2: 373–388.

Thomas, M. G., Loschi, M., Desbats, M. A. et al. (2011), 'RNA granules: The good, the bad and the ugly', *Cellular Signalling*, 23/2: 324–334.

Thompson, S. L., and Compton, D. A. (2010), 'Proliferation of aneuploid human cells is limited by a p53-dependent mechanism', *J Cell Biol*, 188/3: 369–381.

Thompson, S., Bakhoum, S., and Compton, D. (2010), 'Mechanisms of chromosomal instability', *Curr Biol*, 20/6: R285-95.

Tighe, A., Johnson, V. L., Albertella, M. et al. (2001), 'Aneuploid colon cancer cells have a robust spindle checkpoint', *EMBO Rep*, 2/7: 609–614.

Torres, E., Sokolsky, T., Tucker, C. et al. (2007), 'Effects of aneuploidy on cellular physiology and cell division in haploid yeast', *Science*, 317/5840: 916–924.

Upender, M., Habermann, J., McShane, L. et al. (2004), 'Chromosome transfer induced aneuploidy results in complex dysregulation of the cellular transcriptome in immortalized and cancer cells', *Cancer Res*, 64/19: 6941–6949.

van Iterson, M., Duijkers, F. A. M., Meijerink, J. P. P. et al. (2012), 'A novel and fast normalization method for high-density arrays', *Stat Appl Genet Mol Biol*, 11/4.

Wang, J., Tan, A. C., and Tian, T. (2012), *Next generation microarray bioinformatics*: *Methods and protocols* (New York: Humana Press).

Weaver, B. A. A., and Cleveland, D. W. (2006), 'Does aneuploidy cause cancer?', *Curr Opin Cell Biol*, 18/6: 658–667.

Weaver, B. A. A., and Cleveland, D. W. (2007), 'Aneuploidy: instigator and inhibitor of tumorigenesis', *Cancer Res*, 67/21: 10103–10105.

Weaver, B. A. A., Silk, A. D., Montagna, C. et al. (2007), 'Aneuploidy acts both oncogenically and as a tumor suppressor', *Cancer Cell*, 11/1: 25–36.

Williams, B. R., Prabhu, V. R., Hunter, K. E. et al. (2008), 'Aneuploidy Affects Proliferation and Spontaneous Immortalization in Mammalian Cells', *Science*, 322/5902: 703–709.

Xiao, J., Lucas, A., DÁndrade, P. et al. (2006), 'Performance of the Agilent Microarray Platform for One-Color Analysis of Gene Expression'.

Yang, Y. H., Dudoit, S., Luu, P. et al. (2002), 'Normalization for cDNA microarray data: a robust composite method addressing single and multiple slide systematic variation', *Nucleic Acids Res*, 30/4: e15.

Youle, R. J., and van der Bliek, A. M. (2012), 'Mitochondrial fission, fusion, and stress', *Science*, 337/6098: 1062–1065.

Zhang, N., Ge, G., Meyer, R. et al. (2008), 'Overexpression of Separase induces aneuploidy and mammary tumorigenesis', *Proceedings of the National Academy of Sciences*, 105/35: 13033–13038.

Zhao, J., Lendahl, U., and Nister, M. (2012), 'Regulation of mitochondrial dynamics: convergences and divergences between yeast and vertebrates', *Cell Mol Life Sci*, 2012.

Zusammenfassung

Aneuploidie ist eine häufig vorkommende genetische Variation in Tumorzellen. Der Begriff Aneuploidie beschreibt einen Chromosomensatz, der sich von seinen multiplen des haploiden Chromosomensatzes unterscheidet. Diese genomischen Veränderungen haben erhebliche Auswirkungen auf die Zellphysiologie. Die Mechanismen durch welche Aneuploidie die Tumorgenese und die Tumorentwicklung fördert sind bis heute noch nicht vollständig bekannt. Um die Auswirkungen von Aneuploidie aufzudecken, sind Transkriptomanalysen hilfreich, da diese es erlauben Veränderungen der Genexpression global zu erfassen.

In der vorliegenden Masterarbeit wurden bioinformatische Methoden entwickelt und angewendet, um die von Aneuploidie verursachten transkriptionellen Veränderungen zu untersuchen. Um allgemeine Muster in der deregulierten Genexpression zu finden, wurden Daten von verschiedenen aneuploiden Zelllinien mit einfacher Aneuploidie dh. Aneuploid in einem Chromosom und mit komplexer Aneuploidie untersucht. Es konnte gezeigt werden, dass es unabhängig von der Zelllinie und dem Typus der Aneuploidie ein einheitliches Muster an deregulierten Signalwegen gibt. So waren Annotationen für den DNS und RNA Metabolisums global herab reguliert. Hingegen sind Lysosomen, Membranen, Golgi Apperat und ER assoziierte Signalwege hoch reguliert. Des Weiteren wurde in dieser Arbeit gezeigt, dass diese transkriptionelle Antwort auf Aneuploidie nicht mit der Antwort auf inflammatorischen oder metabolischen Stress korreliert. Darüber hinaus konnte durch die Analyse von Genen, die in allen analysierten Zelllinien differentiell expremiert waren, potentielle Marker für Aneuploidie identifiziert werden.

Trotz den bemerkenswerten Übereinstimmungen zwischen den verschiedenen aneuploiden Zelllinien, zeigt die vorgelegte Arbeit Unterschiede zwischen Zelllinien mit einer einfachen Aneuploidie und den Zelllinien mit komplexer Aneuploidie (post- tetraploide Zelllinien) auf. In zellulären Experimenten konnte gezeigt werden, dass post- tetraploide Zellen keine erhöhte Autophagie aufweisen, wie es für die Zellen mit Aneuploidie in einem Chromosom gezeigt wurde. Des Weiteren, zeigten post- tetraploide Zellen keine Akkumulation von Lipid Ablagerungen oder eine veränderte mitochondriale Morphologie. Darüber hinaus bestätigt diese Arbeit, dass post- tetraploide Zelllinien keine erhöhten DNS Schäden aufweisen, obwohl aneuploide Zellen als chromosomal instabil gelten. Schliesslich, führte die Transkriptomanalyse zu interessanten Ergebnissen hinsichtlich der Deregulation in der Expression von p53 abhängigen Zellzyklusarrest und Apoptose Signalwegen. Es konnte gezeigt werden, dass die Expression von p53 aktivierten Genen erhöht ist. Zugleich ist aber auch die Expression von Mdm2, welches die Funktion des Tumorsupressors p53 inhibiert, erhöht. Dies liefert einen ersten Hinweis durch welchen Meachnismus post- tetraploide Zellen den p53 Signalweg abschwächen könnten, der als Grund für die Proliferationsdefekte in Zellen mit Aneuploidie in einem Chromosome angenommen wird.

Selbständigkeitserklärung

Ich erkläre, dass ich die Arbeit selbständig und nur mit den angegebenen Hilfsmitteln angefertigt habe und das alle Stellen, die dem Wortlaut oder dem Sinne nach anderen Werken entnommen sind, durch Angabe der Quellen als Entlehnung kenntlich gemacht worden sind. Die Arbeit wurde weder ganz noch teilweise für eine Prüfung an einer anderen Hochschule eingereicht.

München, 16. Oktober 2012

Milena Dürrbaum

Acknowledgement

I express my gratitude to my supervisor Prof. Torres for his guidance in this master thesis.

I thank Zuzana for her supervision throughout the master thesis. I am grateful for her active support during the last months and I appreciate the effort, motivation and feedback. I am thankful that she gave me the opportunity for this thesis in her research group.

I wish to thank the whole lab for welcome me warmly and a good working atmosphere. Especially, I want to thank Anastasia for her support and fruitful discussions. Also I thank Chris, who never became tired of helping and sharing his knowledge and experience.

Big thanks also to Gabi, who answered all my questions about Perseus and gave me a starting script for the 2D enrichment visualization.

The visit of the bioinformatic group of Bianca Habermann in cologne was a great experience. Thank you for hosting me one week and introducing me to DAVID and other tools.

I am grateful for the support from my family. Jürgen, I thank you very much for supporting my education and your help in all questions of live. Thank you, Daniel, for all your support, encouragement and understanding.

Finally, I like to thank Betty for all the supporting phone calls and friendship throughout the whole time of our study.